AD-A129 604 DEVELOPMENT OF AUTOMATED DETECTION AND DISCRIMINATION TECHNIQUES FOR USE A..(U) INSTITUTE FOR THE STUDY OF EARTH AND MAN DALLAS TX GEOPHYSICA.. E HERRIN ET AL. 1/2

UNCLASSIFIED 14 OCT 82 AFOSR-TR-83-0528 F49620-81-C-0010 F/G 8/11 NL

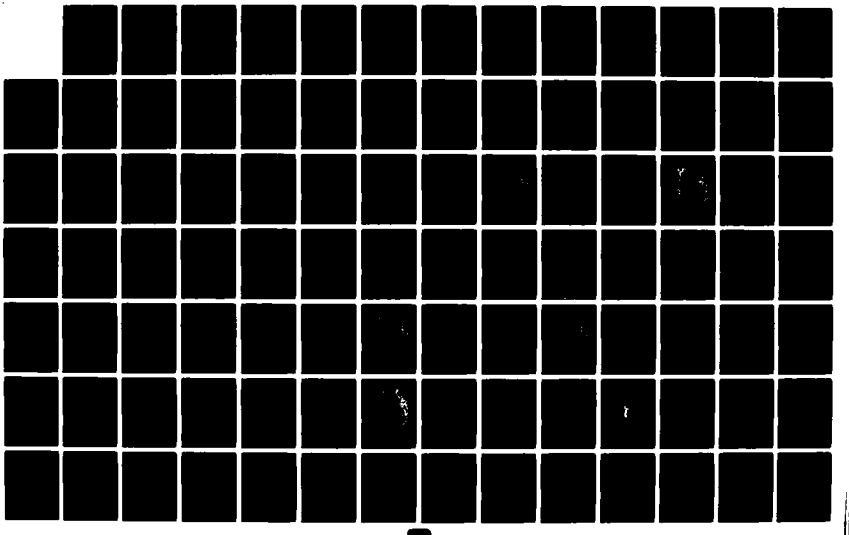

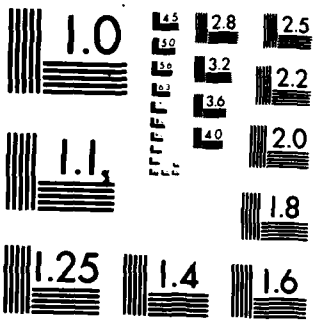

AFOSR-TR- 83-0528



FINAL TECHNICAL REPORT

to the

AIR FORCE OFFICE OF SCIENTIFIC RESEARCH

Geophysical Laboratory
Institute for the Study of Earth and Man
Southern Methodist University
Dallas, Texas 75275



Effective Date of Contract: 15 October 1980
Contract Expiration Date: 14 October 1982
Total Amount of Contract: $513,548
Contract Number: F49620-81-C-0010

Principal Investigators and Phone Number: Eugene Herrin
Tom Goforth
AC 214-692-2760

Program Manager and Phone Number: Mildred Haenel, Director
of Research Administration
AC 214-692-2033

Title of Work: Development of Automated Detection and Discrimination Techniques for Use at Regional to Teleseismic Distances.



Sponsored by
Defense Advanced Research Projects Agency

UNCLASSIFIED

SECURITY CLASSIFICATION OF THIS PAGE (When Data Entered)

| REPORT DOCUMENTATION PAGE | | READ INSTRUCTIONS BEFORE COMPLETING FORM |
|---|---|---|
| 1. REPORT NUMBER<br>AFOSR-TR- 83-0528 | 2. GOVT ACCESSION NO. | 3. RECIPIENT'S CATALOG NUMBER |
| 4. TITLE (and Subtitle)<br>DEVELOPMENT OF AUTOMATED DETECTION AND DISCRIMINATION TECHNIQUES FOR USE AT REGIONAL TO TELESEISMIC DISTANCES | | 5. TYPE OF REPORT & PERIOD COVERED<br>FINAL<br>15 Oct 80 - 14 Oct 82<br>6. PERFORMING ORG. REPORT NUMBER |
| 7. AUTHOR(s)<br>Eugene Herrin<br>Tom Goforth | | 8. CONTRACT OR GRANT NUMBER(s)<br>F49620-81-C-0010 |
| 9. PERFORMING ORGANIZATION NAME AND ADDRESS<br>Geophysical Laboratory<br>Institute for the Study of Earth and Man<br>Southern Methodist University<br>Dallas, Texas 75275 | | 10. PROGRAM ELEMENT, PROJECT, TASK AREA & WORK UNIT NUMBERS<br>61102F<br>2309/A1 |
| 11. CONTROLLING OFFICE NAME AND ADDRESS<br>AFOSR/NP<br>Buidling 410<br>Bolling AFB DC 20332 | | 12. REPORT DATE<br>14 Oct 82<br>13. NUMBER OF PAGES<br>147 |
| 14. MONITORING AGENCY NAME & ADDRESS(if different from Controlling Office) | | 15. SECURITY CLASS. (of this report)<br>UNCLASSIFIED<br>15a. DECLASSIFICATION/DOWNGRADING SCHEDULE |

16. DISTRIBUTION STATEMENT (of this Report)

Approved for public release; distribution unlimited.

17. DISTRIBUTION STATEMENT (of the abstract entered in Block 20, if different from Report)

18. SUPPLEMENTARY NOTES

19. KEY WORDS (Continue on reverse side if necessary and identify by block number)

20. ABSTRACT (Continue on reverse side if necessary and identify by block number)

The resolution of the seismic sensors discussed in this report is limited either by the self-noise of the system or the ambient ground noise at the observing site. The resolution limits of a particular system are frequency-dependent. A major objective of the designer is to insure that seismic sensors are available which will be limited in resolution only by the ambient background noise at the quietest sites over the frequency band of interest in treaty verification research. This report presents a review of the data currently available on the limiting resolution of the most advanced instruments used in this research program.

DD FORM 1 JAN 73 1473 EDITION OF 1 NOV 65 IS OBSOLETE UNCLASSIFIED



SECURITY CLASSIFICATION OF THIS PAGE (When Data Entered)

UNCLASSIFIED

SECURITY CLASSIFICATION OF THIS PAGE (When Data Entered)

| REPORT DOCUMENTATION PAGE | | READ INSTRUCTIONS BEFORE COMPLETING FORM |
|---|---|---|
| 1. REPORT NUMBER<br>AFOSR-TR- 83-0528 | 2. GOVT ACCESSION NO. | 3. RECIPIENT'S CATALOG NUMBER |
| 4. TITLE (and Subtitle)<br>DEVELOPMENT OF AUTOMATED DETECTION AND DISCRIMINATION TECHNIQUES FOR USE AT REGIONAL TO TELESEISMIC DISTANCES | | 5. TYPE OF REPORT & PERIOD COVERED<br>FINAL<br>15 Oct 80 - 14 Oct 82<br>6. PERFORMING ORG. REPORT NUMBER<br>- |
| 7. AUTHOR(s)<br>Eugene Herrin<br>Tom Goforth | | 8. CONTRACT OR GRANT NUMBER(s)<br>F49620-81-C-0010 |
| 9. PERFORMING ORGANIZATION NAME AND ADDRESS<br>Geophysical Laboratory<br>Institute for the Study of Earth and Man<br>Southern Methodist University<br>Dallas, Texas 75275 | | 10. PROGRAM ELEMENT, PROJECT, TASK AREA & WORK UNIT NUMBERS<br>61102F<br>2309/A1 |
| 11. CONTROLLING OFFICE NAME AND ADDRESS<br>AFOSR/NP<br>Buidling 410<br>Bolling AFB DC 20332 | | 12. REPORT DATE<br>14 Oct 82<br>13. NUMBER OF PAGES<br>147 |
| 14. MONITORING AGENCY NAME & ADDRESS(if different from Controlling Office) | | 15. SECURITY CLASS. (of this report)<br>UNCLASSIFIED<br>15a. DECLASSIFICATION/DOWNGRADING SCHEDULE |

16. DISTRIBUTION STATEMENT (of this Report)

Approved for public release; distribution unlimited.

17. DISTRIBUTION STATEMENT (of the abstract entered in Block 20, if different from Report)

18. SUPPLEMENTARY NOTES

19. KEY WORDS (Continue on reverse side if necessary and identify by block number)

20. ABSTRACT (Continue on reverse side if necessary and identify by block number)

The resolution of the seismic sensors discussed in this report is limited either by the self-noise of the system or the ambient ground noise at the observing site. The resolution limits of a particular system are frequency dependent. A major objective of the designer is to insure that seismic sensors are available which will be limited in resolution only by the ambient background noise at the quietest sites over the frequency band of interest in treaty verification research. This report presents a review of the data currently available on the limiting resolution of the most advanced instruments used in this research program

DD FORM 1 JAN 73 1473 EDITION OF 1 NOV 65 IS OBSOLETE UNCLASSIFIED

SECURITY CLASSIFICATION OF THIS PAGE (When Data Entered)

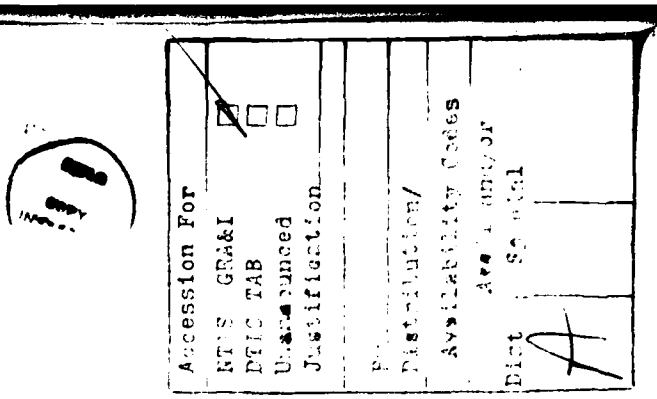


CONTENTS

# VARIATIONS IN BODY WAVE MAGNITUDE FOR YUCCA FLAT, NEVADA EXPLOSIONS

JOHN F. FERGUSON

## ABSTRACT

This paper is an investigation of teleseismic body wave amplitude anomalies caused by near source scattering. A profile in the central portion of Yucca Flat was selected for two dimensional seismic response calculation. The subsurface control on the model structure is excellent and variation in the strike direction is minimal. There are thirteen nuclear shots arrayed on the profile in a reasonably uniform manner. A network of six seismic stations was selected and the P-wave amplitude was calculated at five frequency values uniformly spaced between 0.8 and 1.2 Hz for each shot-station pair. These spectral values were reduced to magnitude by Bache's $\hat{m}_b$ estimator. The theoretical magnitudes can be compared to the observed magnitudes which have been adjusted to a common magnitude by a scaling relationship. The resulting pattern of magnitude deviation compares very favorably with observations by Alewine (personal communication). The best test of this prediction would be to obtain seismograms from the shot and station pairs used in this report and compute $\hat{m}_b$ for each pair.

# INTRODUCTION

A systematic variation in body wave magnitude has been discovered at Yucca Flat, Nevada, through an analysis by Alewine (personal communication) of the yield-magnitude relationship for nuclear explosions. Comparison of the expected magnitude for explosions of known yield, derived from scaling laws similar to those of Mueller and Murphy (1971) and Murphy and Mueller (1971), and observed magnitudes at teleseismic distances reveals a decrease in magnitude from west to east of over 0.3 magnitude units. The pattern of deviation is correlative with the local geologic structure, which is a Cenozoic graben with an axial trend roughly north to south. The basin is filled with low velocity alluvium and volcanic rocks, which contrast with the surrounding higher velocity Paleozoic sediments. Previous studies by Ferguson (1981, 1982) and Hart, et al (1979) support the hypothesis, that the amplitude deviation is due to scattering in the near-source structure.

The previous results discussed by Ferguson (1981, 1982) were limited in that both the wavefield and structure were modelled in two dimensions. The two dimensionality assumption is valid for the structure, at least in selected regions of Yucca Flat, but it limits the location of receiver locations to a great circle containing the model profile. In a two dimensional structure the scattering interaction is limited to the model plane, and good qualitative agreement with observations was found by averaging over incidence angle. Attempts to model specific shots have been thwarted by an inability to recreate the station network and averaging process used to reduce

the magnitude observations. Considerable bias results from azimuthal effects and receiver site-dependent effects. The experiment presented in this paper endeavors to overcome both of these obstacles. A network of six stations was selected along with a profile through the center of Yucca Flat. The stations are representative of those used to monitor nuclear explosions (Bache, personal communication), and the profile was selected on the basis of structural uniformity and shot distribution.

## THE MODELING TECHNIQUE

The model is defined to have two dimensional structural variation with homogeneous regions of variable vertical thickness separation by non-planar interfaces. A numerical approach is necessary to solve the wave equation in models of this type. All calculations performed for this study make use of the Aki-Larner method (Aki and Larner, 1970) as described in Ferguson (1981). The solution to the wave equation is expanded in a series of plane waves within each homogeneous region. At each interface the boundary conditions of continuous normal displacement and stress are satisfied in at least squares sense at a finite set of points. In this manner the frequency-wavenumber spectrum of each wave type (P, SV, or SH-waves) is produced in each layer. The derivation of the method is contained in Larner (1970) and Bouchon and Aki (1977).

A large set of equations must be solved at each interface for each frequency component. The computational effort is substantial even for modern computing machines and is the primary limitation in the large scale application of the technique. Due to this fact, only two dimensional structures are practical although the wave field is specified in three dimensions. Another factor of some importance is the Rayleigh ansatz error which results from a incomplete description of the wave field in the vicinity of the boundary. This can be overcome by use of the extended boundary condition of Waterman (Bates, 1980), however the present program does not contain this improvement. The boundary errors in normal diplacement and traction

are carefully monitored and have not been observed to be a problem. The statistics of the error magnitude in displacement and traction were computed and a histogram plotted for each interface calculation. In addition a plot of error magnitude versus horizontal location was plotted so that correlation with interface shape could be detected. A discussion of many practical considerations for basin response calculations can be found in Bard and Bouchon (1980a, 1980b).

The source contribution to the wavefield can be applied in two ways; the source spectrum can be added to the response directly or the reciprocity theorem can be used to generate the far field response from that of an incident plane wave (Bouchon, 1976). The second approach was chosen for this study due to the large saving in computer time that was anticipated. Essentially each station defines a plane P-wave, with azimuth and incidence angle appropriate to the ray path from Yucca Flat to the station. The P-wave response at the station from any number of shot locations within the model can be obtained from the single response calculation for the incident wave.

The source must be specified in the frequency domain. In the calculations presented here, source was represented by the spectral seismic moment for a Heavyside unit step. The more realistic Von Seggern and Blandford (1972) source function was also tried, but the resulting pattern of magnitude deviations was unaffected.

## THE EXPERIMENTAL PLAN

The locations of the six seismic observatorys simulated in these calculations are shown in Figure 1. They were chosen to be representative of those stations used for routine nuclear explosion monitoring. Figure 2 is a map of the Yucca Flat, Nevada, area, with the basin outlined in bold lines and the structural contours on top of the Paleozoic shown as light lines. The structure is derived from seismic reflection, gravity and borehole data in Ferguson (1981). The selected profile is drawn from A to A' and the locations of explosions within 1600m of the line are presented as dots. The bearings of the six stations are depicted on the map border. The station locations are given in Table I and data on the shots are tabulated in Table II. With these shot-station pairs it is possible to compare the results of this numerical experiment directly to observation without the intermediate averaging process associated with the reduced magnitude deviations.

Due to the expense involved in synthesis of time domain signals when using a frequency domain technique, it was decided to use a frequency domain magnitude formula to compare the theoretical and observational data. In addition it has been demonstrated that spectral based magnitude estimates are more stable and reliable than the traditional time domain methods. The Bache (1981) estimator, $\hat{m}_b$, was chosen for this application. This technique was designed to use spectral amplitudes produced by the MARS program. MARS is based on an analytic signal decomposition and

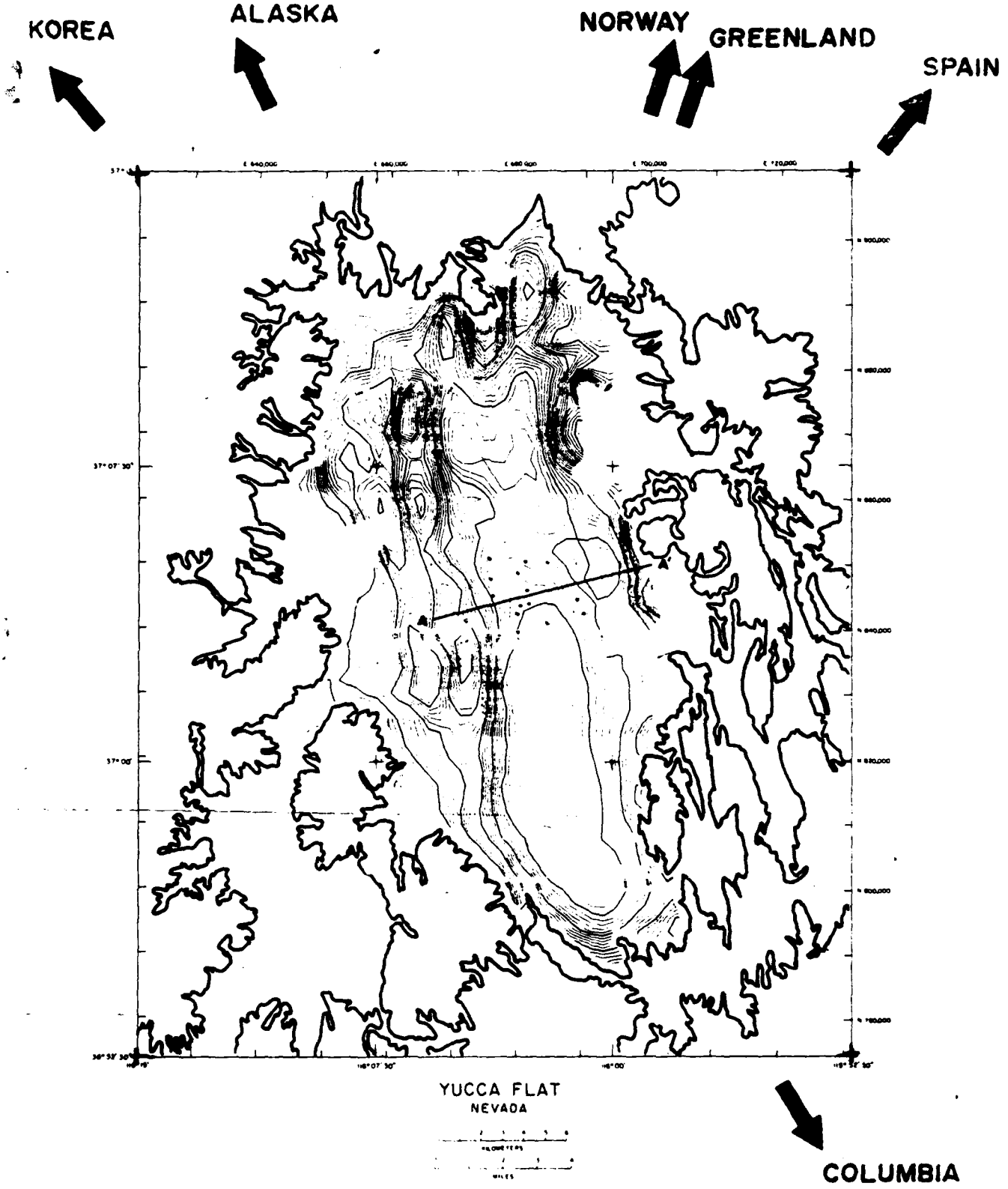


Figure 2. The bold outline delineates Yucca Flat with the lighter contours showing the depth to the Paleozoic basement in 50m increments. The profile A to A' was studied in this report along with the 13 shots illustrated as black dots.

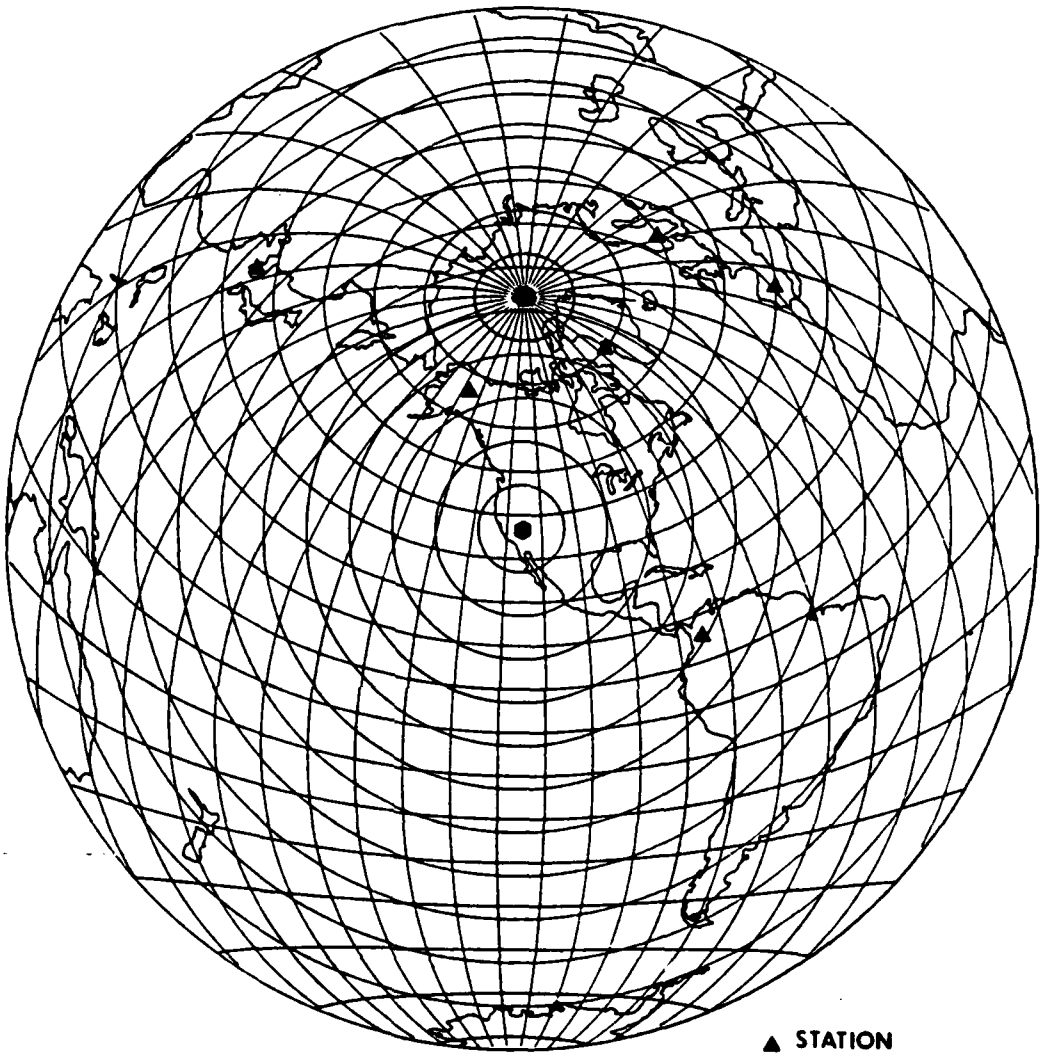


Figure 1. This map displays the location of Yucca Flat, Nevada as a hexagon in the center and the locations of the six seismic stations as triangles. The lines of latitude, longitude and range are graduated in ten degree units.

TABLE II

EXPLOSIONS

| Name | Latitude (deg min sec) | Longitude (deg min sec) | Depth (m) | Date (yr mo day) | GMT Origin (hr min sec) | Yield* (kt) |
|---|---|---|---|---|---|---|
| Sandreef | 37 4 20 | 116 03 00 | 600(est) | 77 11 09 | 22 00 00 | $m_b = 5.7^+$ |
| Rummy | 37 4 47 | 116 03 05 | 600(est) | 78 09 27 | 17 20 00 | $m_b = 5.9^+$ |
| Algodones | 37 03 26 | 116 02 11 | 527 | 71 08 18 | 14 00 00 | 66 |
| Wagtail | 37 03 52 | 116 02 14 | 749 | 65 03 03 | 19 13 00 | 65 |
| Tan | 37 04 06 | 116 02 07 | 560 | 66 06 03 | 14 00 00 | 140 |
| Oscuro | 37 04 55 | 116 02 12 | 560 | 72 09 21 | 15 30 00 | 130 |
| Keelson | 37 04 09 | 116 01 49 | 640 | 76 02 04 | 14 20 00 | 200 |
| Escabosa | 37 04 30 | 116 01 55 | 675(est) | 74 07 10 | 16 00 00 | 170 |
| Piranha | 37 05 13 | 116 02 00 | 548 | 66 05 13 | 13 30 00 | 100 |
| Bilby | 37 03 38 | 116 01 18 | 714 | 63 09 13 | 17 00 00 | 235 |
| Shaper | 37 05 10 | 116 01 16 | 560 | 70 03 23 | 23 05 00 | 93 |
| Tijeras | 37 04 14 | 116 00 18 | 560 | 70 10 14 | 14 30 00 | 94 |
| Monero | 37 03 53 | 116 00 06 | 537 | 72 05 19 | 17 00 00 | 7 |

* Estimates from Dahlman Israelson (1977), except Bilby which was announced.

\+ From PDE published by USGS.

produces a rather smooth spectral estimate. Bache selected five frequency samples between 0.8 and 1.2 Hz and smoothed these by fitting a second degree polynomial by least squares. The logarithm of the polynomial evaluated at 1 Hz is used to estimate the magnitude. The paths between each station and all shots are essentially the same, so that further corrections for path effects are unnecessary because only the difference between shots or stations is all that is required.

The basin was modelled by four layers representing dry Quaternary alluvium, dry Tertiary volcanic rocks, saturated volcanic rocks and Paleozoic basement, which is mostly limestone, quartzite and other high velocity sedimentary rocks. The properties of these materials were selected from an analysis of well logs and are presented in Table III.

In addition to the velocities a Q of 50 was specified for the entire model. This is necessary to insure numerical stability and is also within the expected Q range for this region. The depths of each of the three interfaces, as determined from borehole and the gravity model of Ferguson (1981), and shown in Figure 3. The gravity model was produced by a three dimensional inversion technique and is indicated by a dashed line. The solid line is the interface actually used in the calculations. The interface depths from well logs are projected orthogonally into the profile and are displayed on the cross section. It is seen that the structure in this part of Yucca Flat is satisfactorily controlled by subsurface information. Reference to structure contours on the

TABLE III

VELOCITY STRUCTURE OF YUCCA FLAT, NEVADA

| Stratagraphic Unit | P-Wave Velocity | S-Wave Velocity | Poisson's Ratio | Density |
|---|---|---|---|---|
| QAL | 1.34 | 0.64 | 0.35 | 1.80 |
| TV (Dry) | 2.14 | 1.14 | 0.30 | 1.80 |
| TV (Wet) | 3.00 | 1.60 | 0.30 | 1.80 |
| PZ | 4.57 | 2.64 | 0.25 | 2.50 |

Units are km/sec and gm/cc.

top of the Paleozoic in Figure 2 provides support for the assumption that the basin structure is uniform along strike for several kilometers on either side of A-A' (approximately the first Fresnel zone).

The wave field is expanded in 35 discrete horizontal wavenumber components in the direction normal to strike. The response for incident P-waves from each of the six stations were computed at frequencies of 0.8 to 1.2 Hz at 0.1 Hz intervals. The shot locations are taken to be those of the 13 shots in Table II projected along strike into the profile. The amplitude responses were reduced in the manner of the Bache $\hat{m}_b$ estimator for a total of 78 magnitude estimates.

## RESULTS

The statistics for the magnitudes at each shot point are printed in Table IV. The distribution has a nearly coincident mean, median and midrange for each shot and is thus nearly symmetric. The range is 0.3 to 0.4 $m_b$ units and the standard deviation is near 0.1 $m_b$ units. There is an undetermined additive constant for each shot, which is proportional to the moment and hence the yield of the explosion. The mean of each shot and limits corresponding to one standard deviation are plotted as a function of horizontal position in Figure 3. Also plotted in the same figure are the actual observed $m_b$ deviations (Alewine, personal communication). The magnitude level was adjusted so that the theoretical and observed values matched on the average over the entire data set. The pattern of west to east decrease in magnitude is fit extremely well by the calculations in spite of the in station network and magnitude formula used in the calculation were different from that used to find the observed magnitudes (Alewine, personal communication). It is interesting to note that the dispersion of the estimates increases to the east as the deviation decreases. With the increasing dispersion a large bias due to network differences would be expected and may be observed in the fit. The only shot to fall outside of the one standard deviation limit is Bilby. This is the earliest and largest shot and may be effected by a network bias or difficiences in the yield scaling laws.

Two other calculations were performed with the same parameters and model, but different source distributions. The sources were

Table IV
Deviation Statistics of $m_b$ for Each Shot

| Name | Mean | Median | Midrange | Standard Deviation | Range |
|---|---|---|---|---|---|
| Sandreef | 0.076 | 0.063 | 0.057 | 0.133 | 0.365 |
| Rummy | 0.045 | 0.004 | 0.005 | 0.145 | 0.343 |
| Algodones | 0.091 | 0.105 | 0.054 | 0.102 | 0.252 |
| Wagtail | 0.185 | 0.170 | 0.193 | 0.080 | 0.203 |
| Tan | 0.178 | 0.126 | 0.210 | 0.081 | 0.209 |
| Oscuro | 0.225 | 0.209 | 0.231 | 0.103 | 0.306 |
| Keelson | 0.233 | 0.201 | 0.262 | 0.096 | 0.289 |
| Escabosa | 0.231 | 0.194 | 0.266 | 0.093 | 0.275 |
| Piranha | 0.178 | 0.154 | 0.211 | 0.091 | 0.264 |
| Bilby | 0.145 | 0.101 | 0.191 | 0.090 | 0.252 |
| Shaper | 0.038 | 0.035 | 0.040 | 0.264 | 0.766 |
| Tijeras | -0.055 | -0.159 | 0.061 | 0.189 | 0.496 |
| Monero | -0.140 | -0.190 | -0.059 | 0.189 | 0.523 |

The levels were adjusted by an arbitrary constant to fit the observations, which have been reduced to a common yield. The statistics are based on the distributions for the six stations in figure 1. The shots are ordered according to occurrence in figure 3 from west to east.

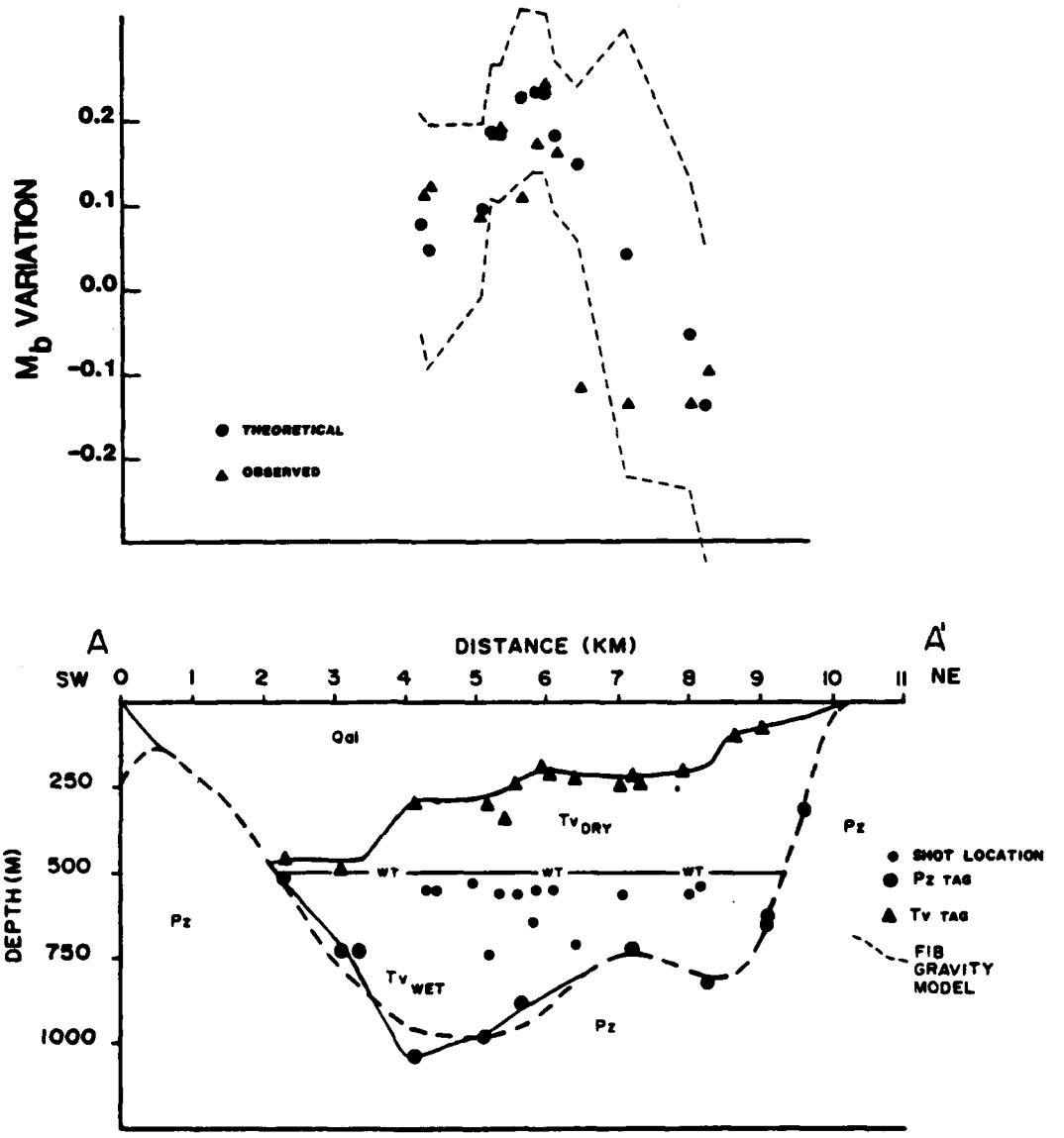


Figure 3. The lower part ot this figure shows the geologic structure on profile A to A' in figure 2. The triangles are depths to the Tertiary volcanics and the circles are depths to the Paleozoic sediments, both as determined in boreholes. The open circles are the projections of the shot locations into the profile. The upper part of the figure illustrates the correlation of magnitude deviation with the structure. The black circles were calculated for this report for the shot locations shown. The dashed lines are $\pm$ 1$\sigma$ as determined for the network of figure 1. The triangles are actual observations from Alewine (personal communication).

arrayed on planes just below the water table at 550m and 600m depths. There was no significant effect on the pattern in either case when compared to the source distribution in Figure 3.

The convergence of the Fourier series in wavenumber was tested by a run with 53 rather than 35 wavenumber samples for station 6. The results were very similar to the original calculation so that it is concluded that satisfactory convergence is obtained with the shorter series. There is a tendency to ill conditioning in the boundary value equations with the addition of the higher wavenumbers and the inhomogeneous waves they represent.

A final calculation on a model lacking the water table interface was performed. This interface has the lowest impedance contrast of the three originally present. The pattern of deviation completely changed on the eastern end of the profile. An increase from west to east in magnitude was found with no appreciable decline on the eastern end as observed in the actual measurements. Based on this experience, it is felt that the four layer model is close to the minimum complexity necessary to explain the observations.

# CONCLUSIONS

The Yucca Flat geophysical model utilized in this calculation was derived from abundant geologic and geophysical data and is quite detailed. The Aki-Larner technique has been effective in computing the plane wave response of two dimensional cross sections taken from the geophysical model. The plane wave response was used in a reciprocity relationship in order to obtain the far field P-wave response at a selected set of six stations due to a set of thirteen explosions in the cross section. A frequency domain body wave magnitude formula due to Bache, was used to reduce these calculations to a profile of magnitude deviation versus horizontal location on the model. These predictions agree with the observations of magnitude deviation for the same shot points. The best test of the predictions would be to use the Bache magnitude formula on the actual seismograms from the same shots and stations.

## REFERENCES


Aki, K. and K. L. Larner, (1970), Surface Motion of a Layered Medium Having an Irregular Interface due to Incident Plane SH Waves, J. Geophys. Res., V. 75, p. 933-954.

Bache, T. C., (1981), Definitions of Body Wave Magnitude, in A Technical Assesment of Seismic Yield Estimation, Appendix, DARPA-NMR-81-01.

Bard, P-Y. and M. Bouchon, (1980a), The Seismic Response of Sediment-Filled Valleys, Part I., The Case of Incident SH Waves, Bull. Seis. Soc. Am., V. 70, p. 1263-1286.

Bard, P-Y. and M. Bouchon, (1980b), The Seismic Response of Sediment-Filled Valleys. Part 2. The Case of Incident P and SV Waves, Bull. Seis. Soc. Am., V 70, p. 1921-1941.

Bates, R., (1980), General Introduction to the Extended Boundary Condition, in Acoustic, Electromagnetic and Elastic Wave Scattering Focus on the T-Matrix Approach, V.K. Varadan and V.V. Varadan, eds, Pergamon Press, New York.

Bouchon, M. and K. Aki, (1977), Near-Field of a Seismic Source in a Layered Medium with Irregular Interfaces, Geophys. J.R. Astr. Soc., V 50, p. 669-684.

Bouchon, M., (1976), Teleseismic Body Wave Radiation from a Seismic Source in a Layered Medium, Geophy. J.R. Astr. Soc., V 47, p. 515-530.

Dahlman, O. and M. Israelson, (1977), Monitoring Underground Nuclear Explosions, Elsevier, New York.

Ferguson, J., (1981), Geophysical Investigations of Yucca Flat, Nevada, Ph. D. Thesis, Southern Methodist University.

Ferguson, J., (1982), The Effect of Near Source Scattering on Teleseismic P-waves from Yucca Flat, Nevada, abstract DARPA Symposium on Seismic Detection, Analysis, Discrimination, Yield Determination, Hampton Va., May 25-27, 1982.

Hart, R. S., D. M. Hadley, G. R. Mellman and R. Butler, (1979), Seismic Amplitude and Waveform Research, Sierra Geophysics report SGI-R-79-012 submitted to DARPA, 99p.

Larner, K., (1970), Near-Receiver Scattering of Teleseismic Body Waves in Layered Crust-Mantle Models Having Irregular Interfaces, Ph. D. Thesis, Massachusetts Institute of Technology.

Mueller, R. and J. Murphy, (1971), Seismic Characteristics of Underground Nuclear Detonations, Part I., Seismic Spectrum Scaling, Bull. Seis. Soc. Am., V 61, p. 1675-1692.

Murphy, J. and R. Mueller, (1971), Seismic Characteristics of Underground Nuclear Detonations, Part II., Elastic Energy and Magnitude Determinations, Bull. Seis. Soc. Am., V 61, p. 1693-1704.

Von Seggern, D. and R. Blandford, (1972), Source Time Functions and Spectra for Underground Nuclear Explosions, Geophys. J. R. Astr. Soc., V 31, p. 83-97.

# GEOPHYSICAL INVESTIGATIONS

# OF

# YUCCA FLAT, NEVADA

JOHN F. FERGUSON

CONTENTS

# ILLUSTRATIONS

# TABLES

## ACKNOWLEDGEMENTS

This research would not have been possible without the cooperation of many people. I would like to acknowledge the contributions of my professors and collaborators Eugene Herrin, Wayne Peeples, Tom Goforth and David Blackwell of Southern Methodist University and Carlos Aiken of the University of Texas at Dallas. The free exchange of data and ideas between Roger Felch and myself while he worked on his Masters degree at Texas Christian University and Los Alamos National Laboratory greatly improved the early phases of this project. I would also like to thank Alan Cogbill and his colleages at LANL who supplied a great deal of otherwise difficult to obtain information. Many of the ideas embodied in this dissertation have benefitted from a long standing dialog with my fellow student, John Ziagos. Mike Sorrells of Teledyne-Geotech, Inc. has extended his support to me numerous times in the course of this work.

My deepest appreciation is expressed to my parents, Ruth and Frank Ferguson and to Margaret Olwell, who have loved, supported and encouraged me through the years. A special acknowledgement is due John Harrington for helping me to find the way on more than one occasion.

This work was supported by Defense Advanced Research Projects Agency contracts F49620-76-0030 and F49620-77-0126 monitored by William Best.

# PART I

## INTRODUCTION

In recent years it has become evident that lateral variations in geologic structure at Yucca Flat, Nevada, exert controls over the far field waveforms from explosions detonated there. A marked correlation was observed between structural contour, Bouguer gravity, and normalized body wave magnitude maps. This correlation suggested that a deterministic geophysical model based on an accurately defined geologic structure could be used to predict far-field body wave amplitude variations. When the examination of existing structural interpretations proved to be deficient, it was decided to obtain modern seismic reflection profiles. In addition, a reevaluation of the United States Geological Survey (USGS) gravity data used in earlier structural interpretations seemed to be appropriate. Various borehole and other geologic data were obtained from Los Alamos National Laboratory (LANL) and published sources to aid this research.

Yucca Flat, Nevada, is a graben-like structure of Cenozoic age. The underlying strata are mainly sediments of Paleozoic (Pz) age. Major volcanic centers to the west have introduced a thick sequence of tuff units which are generally less than 20 million years old (Tv). Within Yucca Flat and adjacent valleys alluvium of Quaternary age (Qal) covers the volcanics to a thickness of over 300 m. Major normal fault sets strike east-west, northwest-southeast and north-south. The last

group are apparently the youngest and have a substantial strike slip component of motion. This brief geologic description will be expanded after introduction of the geophysical model.

The interpretative procedure used from the outset of this study required the examination of as many different types of data as possible in order that the resulting model be a complete explanation of the basin phenomena, consistent with all observations. In particular, gravity observations, borehole data and seismic reflection profiles were simultaneously used in the interpretative process. It was also found that the structure must be modeled in three dimensions to achieve reliable results.

This report presents the resulting three dimensional geophysical model for Yucca Flat. Results of numerical wave propagation experiments will be presented in a later report directed toward the seismological aspects of this study.

## GEOLOGIC INFORMATION

Geologic maps produced by the USGS and compiled at a 1:24000 (7.5 minute quandrangle) scale were available for the entire study area. These are map sheets GQ 213, 214, 215, 363, 384, 577, 582, 746, and 1327. The geologic base map upon which the geophysical data are compiled is derived from these maps. Additional geologic maps and data have become available from LANL and USGS sources concerned with the Nevada Test Site (NTS). The Geological Society of America Memoir 110, Nevada Test Site, edited by Eckel (1968) contains a great deal of pertinent information.

Borehole stratagraphic and geophysical data have been of particular importance. Most of the borehole data were obtained from LANL; consequently, only limited data from areas managed by Lawrence Livermore Laboratory (LLL) or from areas that are of little interest to either group. The borehole geophysical data consist of summaries compiled by LANL of average properties for various stratagraphic units. In some cases the original logs were available. There are 36 such boreholes summarized, including 7 which penetrate to the Paleozoic, 17 which penetrate into the Tertiary, and 12 which bottom in the Quaternary alluvium. In addition we have examined borehole gravity data for 41 holes in Yucca Flat. Control on the Paleozoic surface is provided by the 90 holes shown in figure 1. The alluvium-volcanic contact is controlled by a total of 166 holes. These holes

are not the complete sample of borehole data at Yucca Flat. The numbering of these boreholes corresponds to various numbered areas defined on Yucca Flat for administrative purposes. Figure 1 provides a rough outline of these areas through the grouping of the holes themselves. At several places in this report it will be convenient to refer to the groupings by area number.

Fig. 1. Location map of boreholes contacting the Paleozoic Basement used in this study. The numerical portion of the borehole designation corresponds to area designations used in some sections of this dissertation. The geologic base map will be used in all subsequent maps. The dark shade represents Tertiary volcanic rocks, the light shade represents Quaternary alluvium and the white areas are Paleozoic outcrop. The Climax stock in the northern part of the map is stippled. Nevada Central Zone coordinates in units of feet are provided.

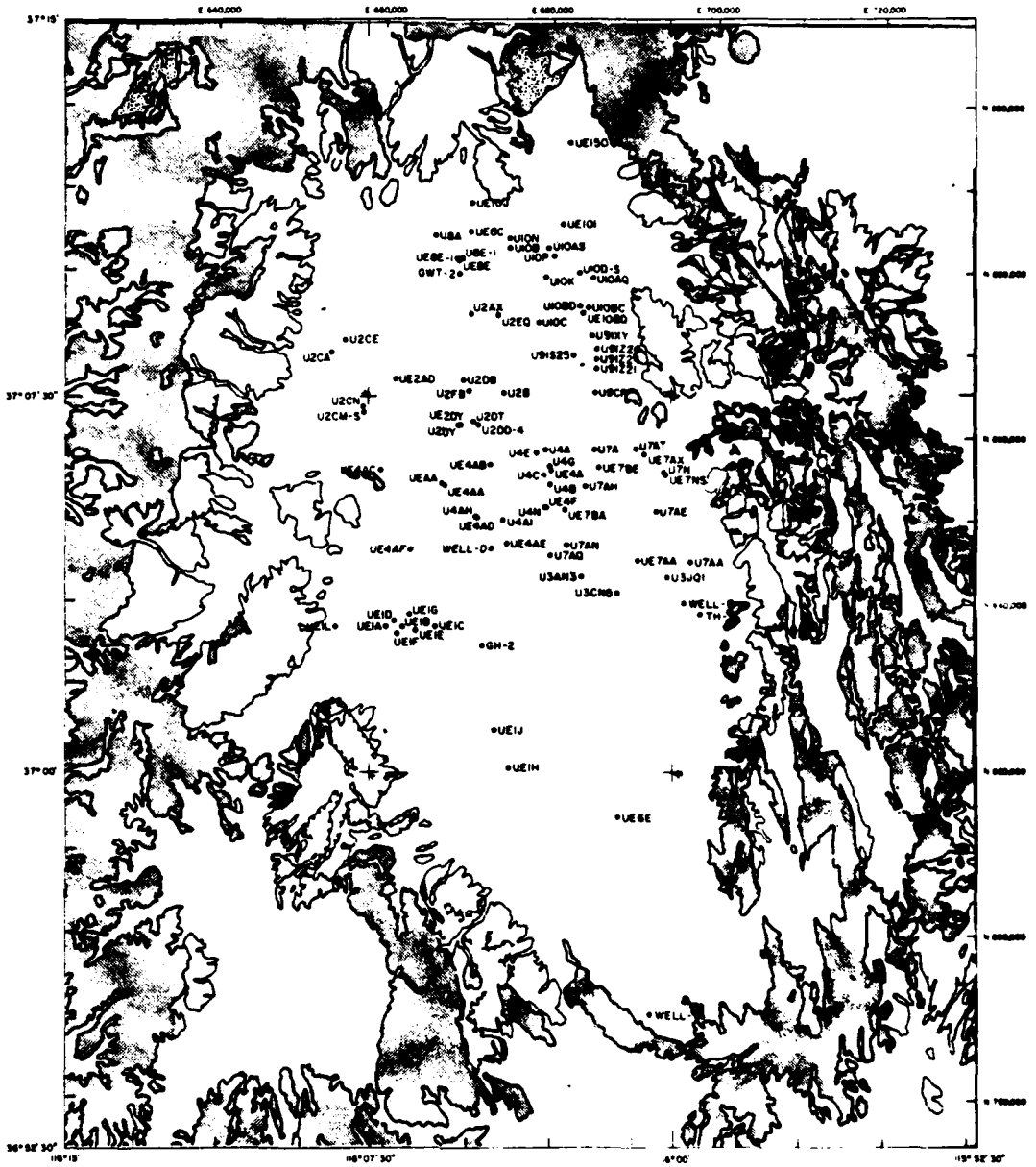
E 640,000
E 660,000
E 680,000
E 700,000
E 720,000
37°15'
37°07'30"
37°00'
36°52'30"
116°15'
116°07'30"
116°00'
115°52'30"
UE15O
UE10I
UE8C
U8A
UE8E-1
UE8E
GWT-2
U2AX
U2EQ
U10C
U2CE
U2CA
U2CN
U2CM-S
UE2AD
U2DB
U2FB
U2B
UE2DY
U2DT
U2DD-6
U4E
U4G
U4A
U7A
U7BT
UE7AX
U7N
UE7NS
UE7BE
UE44B
UE4A
U4C
U4B
U7AH
UE4AA
UE44A
U4AH
UE4AD
U4AJ
UE4F
UE7BA
U7AE
UE4AF
WELL-D
UE44E
U7AR
U7AG
UE7AA
U7AA
U3JQ1
U34N3
U3CN8
WELL-
TH-
UE1D
UE1G
UE1A
UE1B
UE1C
UE1F
UE1E
GH-2
UE1J
UE1H
UE6E
WELL-
YUCCA FLAT
NEVADA
KILOMETERS
MILES

## GRAVITY DATA

Some 8459 gravity stations are located within an area 22.5 minute on a side around Yucca Flat. The data are from USGS open files and were collected over a twenty year period by various people using different instruments. Most of these data, 6383 stations, are within Yucca Flat. Of the remainder, 351 are sited on Paleozoic outcrops and 1725 are in neighboring basins and on the volcanic outcrops which border the basins. The magnetic tape file containing this compilation specified location to 0.01 minute, elevation to 0.1 foot and terrain corrected Bouguer anomaly to 0.01 milligal. The precision and quality of these data are variable. An accuracy of estimate of $\pm$0.5 milligal is assumed for the overall data set, although the newer data is probably good to $\pm$0.15 milligal (Felch, 1979). Figure 2 is a contour map of this Bouguer gravity data.

Fig. 2. Complete Bouguer anomaly map of the Yucca Flat, Nevada area. The contour interval is 1 milligal.

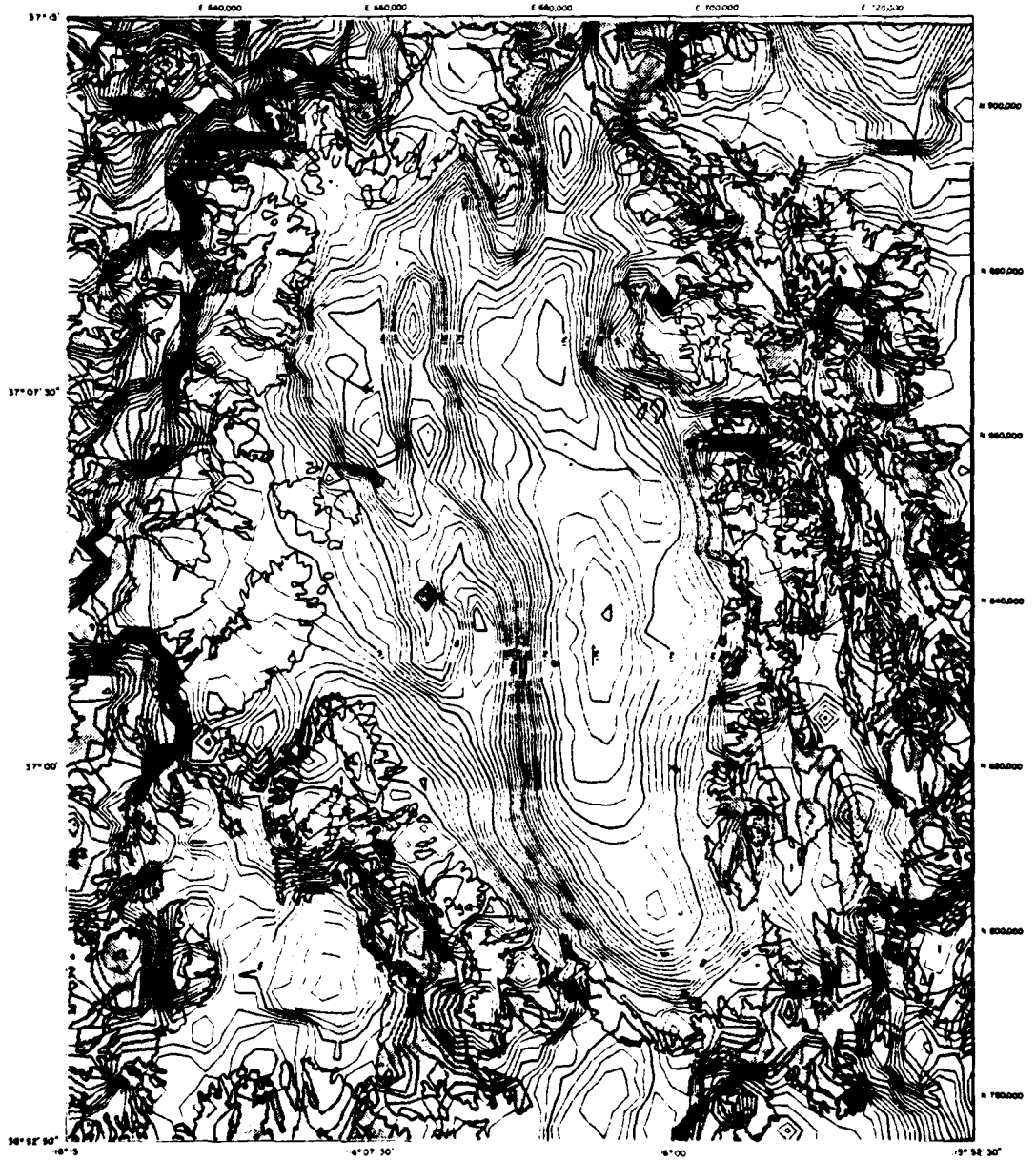


YUCCA FLAT

NEVADA

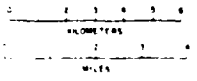

# ANALYSIS OF THE GRAVITY DATA

The abundant gravity observations (over 8000 stations) in a properly devised gravity inversion, constrained by the more sparse geologic and geophysical data, should produce a relatively detailed geophysical model. The model geometry most appropriate in this case is that of a basin of low density fill overlying a higher density half space. The shape of the model's lower perimeter will be sought as a function of position using the observed gravitational acceleration. The upper boundary is the earth's surface, which is known in advance. If the density distribution is also known, the interface shape is uniquely determined (Smith, 1961), for an infinite number of accurate observations. A finite and inaccurate data set will in general not permit a unique solution, but some average model can always be found. The inverse gravity problem for model shape is nonlinear and can be performed iteratively by techniques such as Gauss-Newton or successive approximations.

There exist many published inversion methods which have differing strengths and weaknesses in a given context. There is no perfect inversion theory of universal applicability. The following criteria were considered in the choice of an inversion routine:

1) Ability to recover a best fitting solution (according to some norm).
2) Ability to assess the accuracy of the solution.
3) Ability to include a priori geologic and statistical information.
4) Speed and computer memory requirements necessary to invert thousands of observations.
5) Provision for a three dimensional model and variable density contrast, if necessary.

Trial and error methods were rejected as too crude. Initially some thought was given to vertical prism parameterization and linearized inversion similar to the technique of Burkhard and Jackson (1976). Preliminary experiments indicated that although this technique satisfied most of the criteria, the speed and memory economy were insufficient to be practical for the large data set. In addition, discrete parameterizations tend to produce models which are rather dependent on the parameterization (i.e., block size and location). An example of a block parameterized model based on these same data is contained in Felch (1979) who applied the Cordell and Henderson (1968) method to the Yucca Flat data.

An integral equation formulation of the problem could be specified which would overcome at least some of these problems. The interface would be represented by a continuous function of the spatial coordinates. A prototype program of this sort was written for two dimensional basin models which worked quite well. Results of that program were presented by Goforth, et al. (1979). However, this experience indicated that computational limitations would rule out a three-dimensional implementation of that technique. The method finally selected is similar in some respects to the integral equation formulation. It is the Parker-Oldenburg-Huestis method (Parker, 1972, Oldenberg, 1974, Parker and Huestis, 1974), which uses Fourier expansions to achieve computational speed through application of the fast Fourier transform. The details will be discussed in a later section.

In a local study the regional gravity anomaly is really part of the model specification. It is that part of the field which is not accounted for by the model in question and usually is arbitrarily parameterized. We choose to specify the regional gravity by a low-order Fourier trend surface, which is fit to those gravity stations occuring on the Paleozoic outcrop (i.e., the half space of the model). Additionally, the estimation of this anomaly is made a part of the inversion process by removal of the modeled basin gravity effect at the borehole Pz control points within the basin and the use of the resulting anomalies in the least squares surface fitting. This concept was applied to Yucca Flat by Felch (1979). The notion has been extended in this application to a procedure which iteratively improves the regional gravity estimate. Starting with a surface with no borehole control, the residual anomaly is inverted. The depth residuals at the boreholes are used to correct the stripping of the basin anomaly, a new regional anomaly surface is better defined. It is possible that long wavelength variations in density contrast, if improperly specified, will be confounded with the regional anomaly produced by this process. A simplified flow chart of the entire procedure is presented in figure 3. Each box is a separate computer program which operates on various intermediate data files. The process may be cycled as many times as necessary to achieve stable error statistics.

Fig. 3. Flow chart depicting the major elements of the gravity interpretation procedure. The rectangular boxes represent processes performed by computer programs and the elliptical boxes represent data files both generated and operated on by the programs.

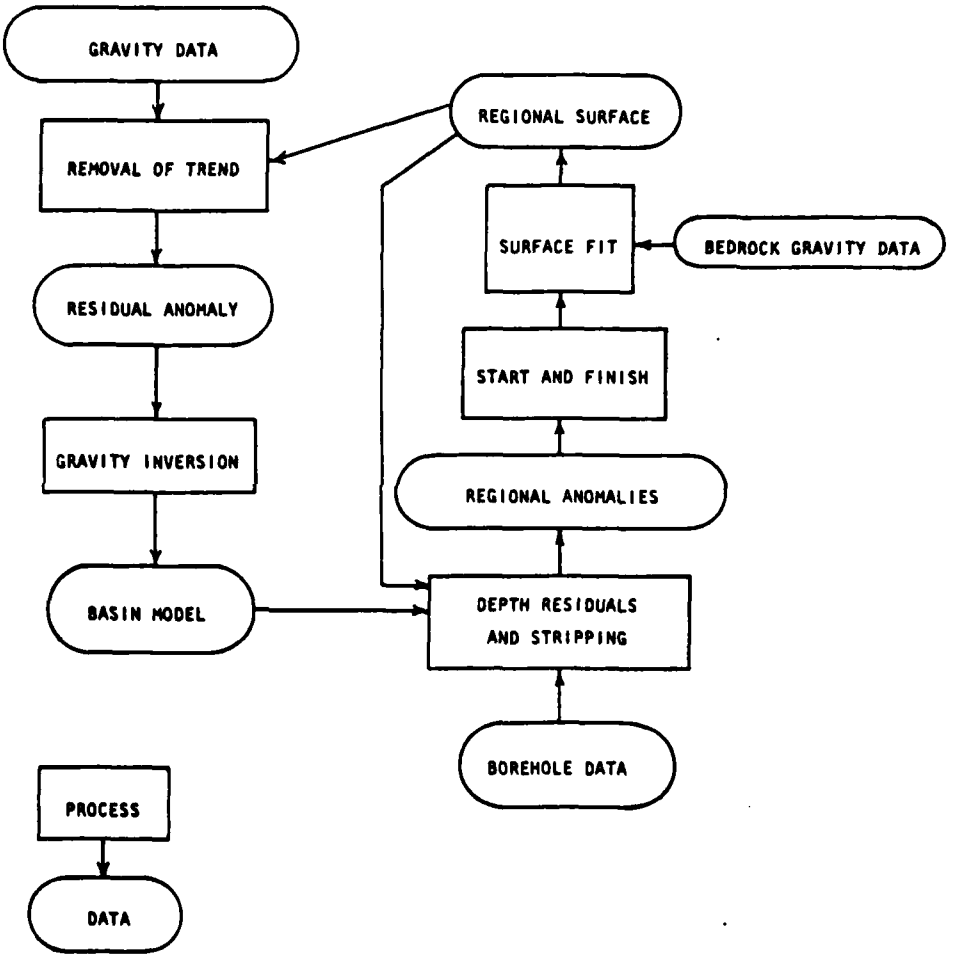
GRAVITY DATA
REMOVAL OF TREND
RESIDUAL ANOMALY
GRAVITY INVERSION
BASIN MODEL
REGIONAL SURFACE
SURFACE FIT
BEDROCK GRAVITY DATA
START AND FINISH
REGIONAL ANOMALIES
DEPTH RESIDUALS AND STRIPPING
BOREHOLE DATA
PROCESS
DATA

## THE PARKER-OLDENBURG-HUESTIS POTENTIAL INVERSION

Parker (1972) devised an expansion of the integral equation for the gravitational (or magnetic) potential in the form of a series of Fourier transforms. In the following we define the z-axis to be positive downward. The anomalous potential is assumed to be due to a layer of contrasting density and variable thickness, which vanishes outside of some finite area, D, and is specified by

$$1) \quad U(\vec{r}_o) = G \iint_D \int_{h(\vec{r})}^{g(\vec{r})} \frac{\rho(\vec{r})}{|\vec{r}_o - \vec{r}|} \, dz \, dS ,$$

where $g(\vec{r})$ and $h(\vec{r})$ are the lower and upper surfaces of the layer. The potential is observed on a plane, $z_o$, above the layer at all points and in finite domain, X. We may Fourier transform equation 1,

$$2) \quad \begin{aligned} \mathcal{F}[U(\vec{r}_o)] &= \int_x U(\vec{r}_o) \exp(i\underline{k}\vec{r}_o) \, dS_o \\ &= G \iiint_{x D} \int_{h(\vec{r})}^{g(\vec{r})} \frac{\rho(\vec{r}) \exp(i\underline{k}\vec{r}_o)}{|\vec{r}_o - \vec{r}|} \, dz \, dS \, dS_o . \end{aligned}$$

The integrals over X and z can be performed analytically to produce

$$3) \quad \mathcal{F}[U(\vec{r}_o)] = 2\pi G \int_D \rho(\underline{r}) \exp(i\underline{k}\underline{r} + |\underline{k}| z_o) \cdot [\exp(|\underline{k}|(h(\underline{r}) - g(\underline{r}))) / |\underline{k}|^2] \, dS .$$

The vector $\underline{r}$ is the projection of $\vec{r}$ onto the plane $z_o$. Parker then expands the second exponential in a Taylor series and exhanges the order of summation and integration resulting in the rather novel representation of the potential spectrum as an infinite series of Fourier transforms,

$$4) \quad \mathcal{F}[U(\underline{r}_o)] = -2\pi G \exp(|\underline{k}|z_o) \sum_{n=1}^{\infty} \frac{|\underline{k}|^{n-2}}{n!} \mathcal{F}[\rho(\underline{r})(h^n(\underline{r}) - g^n(\underline{r}))]$$

The potential may be differentiated with respect to z to obtain the gravitational acceleration. Equation 4 can be rearranged slightly into a remarkable triplet of formulas:

$$5a) \quad \mathcal{F}[\Delta g(\underline{r}_o)] = -2\pi G \exp(|\underline{k}|z_o) \sum_{n=1}^{\infty} \frac{|\underline{k}|^{n-1}}{n!} \cdot \mathcal{F}[\rho(\underline{r})(h^n(\underline{r}) - g^n(\underline{r}))],$$

$$5b) \quad \mathcal{F}[\rho(\underline{r})] = \frac{-\mathcal{F}[\Delta g(\underline{r}_o)] \exp(-|\underline{k}|z_o)}{2\pi G \mathcal{F}[h(\underline{r}) - g(\underline{r})]} - \sum_{n=2}^{\infty} \frac{|\underline{k}|^{n-1}}{n!}$$

$$\cdot \mathcal{F}[\rho(\underline{r})(h^n(\underline{r}) - g^n(\underline{r}))],$$

$$5c) \quad \mathcal{F}[g(\underline{r})] = \frac{-\mathcal{F}[\Delta g(\underline{r}_o)] \exp(-|\underline{k}|z_o)}{2\pi G \mathcal{F}[\rho(\underline{r})]} - \sum_{n=2}^{\infty} \frac{|\underline{k}|^{n-1}}{n!}$$

$$\cdot \mathcal{F}[\rho(\underline{r})(h^n(\underline{r}) - g^n(\underline{r}))].$$

Now 5a states the forward problem of finding the gravitational field given the density and layer shape. Equation 5b states the linear

inverse problem of the determination of density given gravity observations and layer geometry, and 5c states the nonlinear inverse problem for layer shape given the gravity data, density, and upper surface. The geophysical model of a basin would have fixed upper and variable lower surfaces. Variation of the upper surface, with a fixed lower surface, could model an intrusion. The inverse problems may be solved by successive approximations given some initial guess for $g(\underline{r})$ or $\rho(\underline{r})$. In this approach the correction to the function guess is a nonlinear step at each iteration and hence has some desirable properties relative to the linearized inversion schemes currently popular. In addition, for N observations the Fourier integrals may be computed in N log(N) operations for gridded data, whereas the integral equation methods require order $N^3$ operations for the decomposition of a system of linear equations.

Notice that the leading, linear term of the expansion in equation 5 is merely the continuation operator in the wavenumber domain. To first order the method is equivalent to Peters' method (Peters, 1949 and Gunn, 1975) for the interpretation of gravity and magnetic data, which has been in use for nearly fifty years. This now classic technique applied a downward continuation operator in the space domain to obtain a surface density distribution at depth called an equivalent stratum. For a constant density contrast the density variations on the equivalent stratum translate into topography on a surface about the depth of continuation. The linearized method requires that the topography be very small relative to the depth. Parker's technique adds in the higher order terms as necessary to provide convergence for arbitrary topography.

Some important results on series convergence and other properties are given by Parker (1972), Parker and Huestis (1974), and Oldenburg (1974). A discussion of this theory from the standpoint of integral equations may be found in Dorman and Lewis (1974) and in a similar derivation from the Russian literature in Tsirul'skiy (1968) and Tsirul'skiy and Ospischeva (1968).

A rather serious problem in the two inversion formulas arises from the downward continuation operation. Downward continuation is an ill-posed problem; that is, any small perturbation of the gravity field, such as that due to noise in the data, may result in an unbounded perturbation in the continued field. Some form of regularization or smoothing is essential to bound for the solution of such problems. This is particularly important in nonlinear problems when the inverse mapping is approximate. Parker, Oldenburg and Huestis have used a rather arbitrary low-pass filter to eliminate short wavelengths from the solution, but our experience shows that this is not a satisfactory approach. A better filter derives from the work of Tikonov (1963). A regularization is defined as

$$6) \qquad \min \left[M_\alpha (m)\right] = \min \left[\int (u(r) - A(r,m))^2 \, dr + \alpha \, \|m(r)\|\right].$$

The operator, A, defines the forward problem, where U(r) is the observed data, and m(r) is the approximate function sought. The first term is the data misfit and the second is some measure of model smoothness. The parameter, $\alpha$, will be called the regularization

parameter; it controls the smoothing in the inversion for the approximate model. The first error term will never be zero but can be made quite small with a proper choice of a regularized inverse operator.

In Tikhonov et al. (1968) several approximate inverses for the downward continuation problem are given. The function,

$$7) \quad A(\underline{k}) = \mathcal{F}[\Delta g(\vec{r}_o)] \exp(-|\underline{k}|z_o) / (1+\alpha|\underline{k}|^2 \exp(-|\underline{k}|z_o)),$$

was selected as most suitable for this purpose. It has the form of a smooth low pass filter which cuts off a faster rate than the downward continuation operator grows. The regularization parameter, $\alpha$, is choosen by forming a family of approximate inverses by varying $\alpha$ in a systematic way, testing each one by forward calculation and computing the rms error between the theoretical and the observed accelerations. The simplex procedure of Nelder and Mead (1965), as presented by O'Neil (1971), provides a convenient method for this minimization. In one dimension (the $\alpha$ dimension) the simplex is a line segment which attempts to bracket the minimum. This line segment will flip back and forth and expand or contract as necessary to obtain the minimum. Convergence is reached when the segment shrinks below a certain length.

Unlike the methods based on linearized solutions to the integral equations, the Fourier transform method does not produce the Frechet derivatives as a by-product. This complicates the calculation of Backus-Gilbert linear resolving kernels. Parker and Huestis (1974) offered an approximate resolving measure for the linear inverse problem (5b), but it performed poorly. The resolving widths were larger than the model even for the highest variance solutions. The space domain

width of the regularizing filter provides some information on resolution, but it lacks the space variable quality of the Backus-Gilbert resolution measures. Because of the lack of a linear mapping it is also difficult to compute model variance. It is conjectured that the magnitude of the variance could be inferred by consideration of the terms which are suppressed by regularization. Acknowledging these difficulties the error analysis utilized here will be based on the errors between the model and known (borehole) depths.

## THE DENSITY MODEL

The geophysical model proposed here consists of a Paleozoic half space with a lower density basin with Cenozoic age fill on top. The density contrast could have any manner of spatial variability. The simplest density distribution one can assume in order to model the basin would be a single constant density contrast across the interface between the Cenozoic and Paleozoic strata. However, in the Great Basin it is common to encounter density functions which increase more or less exponentially with depth. Cordell (1979) has proposed that lateral variations, with density decreasing toward the basin center may be important. Some basis for the choice of a density model must be found in the observed density data.

For many years a constant density contrast, between the Cenozoic and Paleozoic rocks, of -0.7 gm/cc has been the standard model for Yucca Flat (Hazelwood, et.al., 1963, Healey, 1966 and 1968). It has also been recognized that there are departures from this average, but the importance of the departures has not previously been determined. Density log information from 34 boreholes was used in a simple statistical analysis of this question. This information is from a zone extending from roughly the center of the valley to the eastern margin and covering about the middle fourth. It is questionable how representative of the remainder of the valley these densities may be. Table I

TABLE I

BOREHOLE DENSITY STATISTICS FOR YUCCA FLAT, NEVADA

| GEOLOGIC UNIT | NUMBER OF SAMPLES | MEAN | STANDARD DEVIATION | MEDIAN | INTERQUARTILE DEVIATION | MIDRANGE | RANGE |
|---|---|---|---|---|---|---|---|
| QAL | 34 | 1.77 | 0.16 | 1.77 | 0.10 | 1.84 | 0.72 |
| TV | 123 | 1.79 | 0.19 | 1.81 | 0.12 | 1.90 | 1.06 |
| PZ | 3 | 2.47 | 0.32 | 2.45 | 0.64 | 2.48 | 0.64 |

UNITS ARE GM/CC

summarizes the statistics on the geologic units Qal, Tv, and Pz. A t test for the equality of the means of the Qal and Tv population was performed with the conclusion that the means were equal at the 90% confidence level. The mean and standard deviation of the combined population are 1.79 gm/cc and 0.18 gm/cc. Figure 4 is a plot of the histograms of the Qal and Tv samples with the normal distribution parameters (mean and standard deviation) for the combined population superimposed. The frequency distributions are not normal and are skewed towards the low density end. A major deficiency in this analysis is the lack of volumetric weighting of the density values. Samples from thin layers are given equal weight with samples from thick layers. The conclusion is that the Qal is indistinguishable from the Tv in density, and hence only one layer of fill with no vertical density variation need be considered for the valley model. The quality of the summary data from density logs probably does not warrant a more detailed analysis.

Better data for the purpose of density modelling can be obtained from the borehole gravity logs. Borehole gravity provides a better average density for the area around the hole than density logs which may be complicated by local borehole effects; however, lateral variations in structure may bias the gravity results. The borehole gravity logs which start at depths of less than 200 meters and extend to depths greater than 500 meters were selected from the 41 logs available. The derived density and the average density were plotted as a function of depth. The latter function is more useful because it rectifies the data and suppresses the effect of thin, anomalously

Fig. 4. Histograms of the occurance frequency of density values for all stratigraphic units in the Quaternary (a) and Tertiary (b) rocks of Yucca Flat. The data were compiled from interval density estimates from the central latitude portion of the valley. The bar scale at the top of each graph shows the mean and one standard deviation fiducials for the combined distribution.

## DENSITY STATISTICS YUCCA FLAT, NEVADA

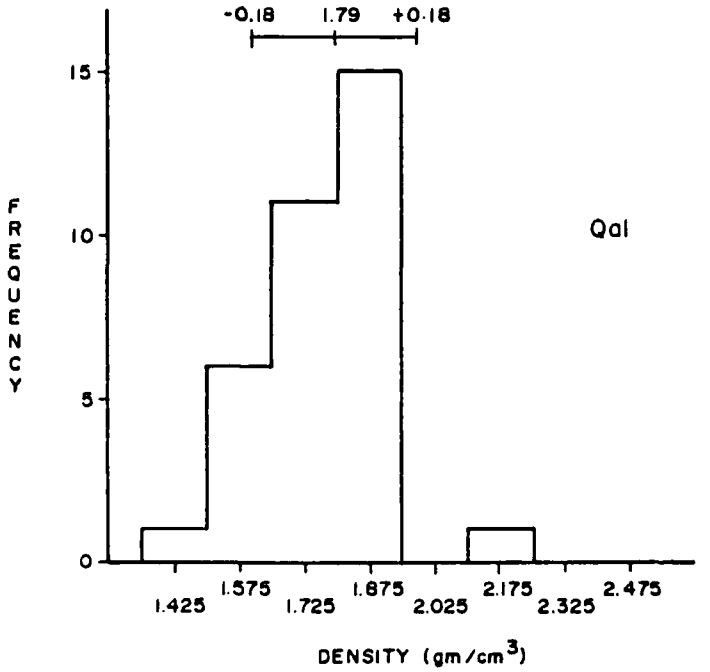


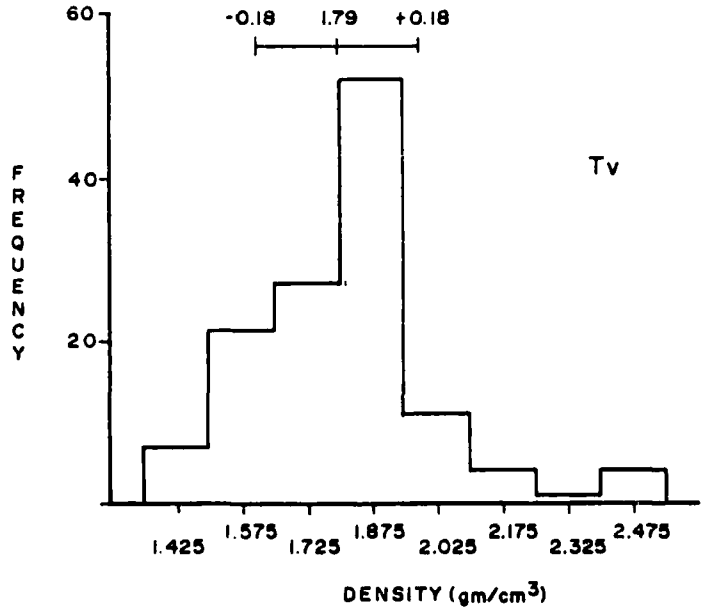

dense, layers. When the average density curve changes slope, it indicates a profound density change. A comparison of the Yucca Flat average density profile and those of several other western localities in the United States are shown in figure 5. The comparison illustrates the unusual nature of the Yucca Flat distribution. The Yucca Flat curves are rather constant with depth and show little evidence of a significant exponential increase in density with depth; many curves even show a decrease in density with depth. The limits drawn on the graph are the mean and standard deviation from the geophysical log distribution. Although lateral variation is present it is generally less than $\pm$ 0.1 gm/cc and no systematic variation is apparent.

The density of the Paleozoic basement is less well determined. Some samples have been tested in the laboratory and some geophysical data exist. The choice of 2.5 gm/cc seems to be justified by these data. Lateral variations are known to exist, but we have insufficient information to characterize them. These observations support a constant density contrast model of -0.7 gm/cc. With more data, variations of $\pm$ 0.1 gm/cc could be included in the model, but this is probably unnecessary for this study.

Fig. 5. (a) is a plot of average density as a function of depth for Yucca Flat, Nevada and (b) shows the same data for several other representative localities in the Basin and Range province. All density estimates are from borehole gravity measurements except those in Hachita and Sulphur Springs valleys. The fiducials lines drawn vertically on the left graph are the mean and one standard deviation, derived from the Quaternary and Tertiary density data used in Table I.

AVERAGE DENSITY VS DEPTH FUNCTIONS

YUCCA FLAT, NEVADA

- ◆ U2EI
- \+ U4E-1
- × U7AP
- ⊙ U7AU

OTHER BASIN AND RANGE AREAS

- ◆ FRENCHMAN FLAT, NEVADA
- ✱ HACHITA VALLEY, CHIHUAHUA
- ▸ HOT CREEK VALLEY, NEVADA
- ▫ SULPHUR SPRINGS VALLEY, ARIZONA

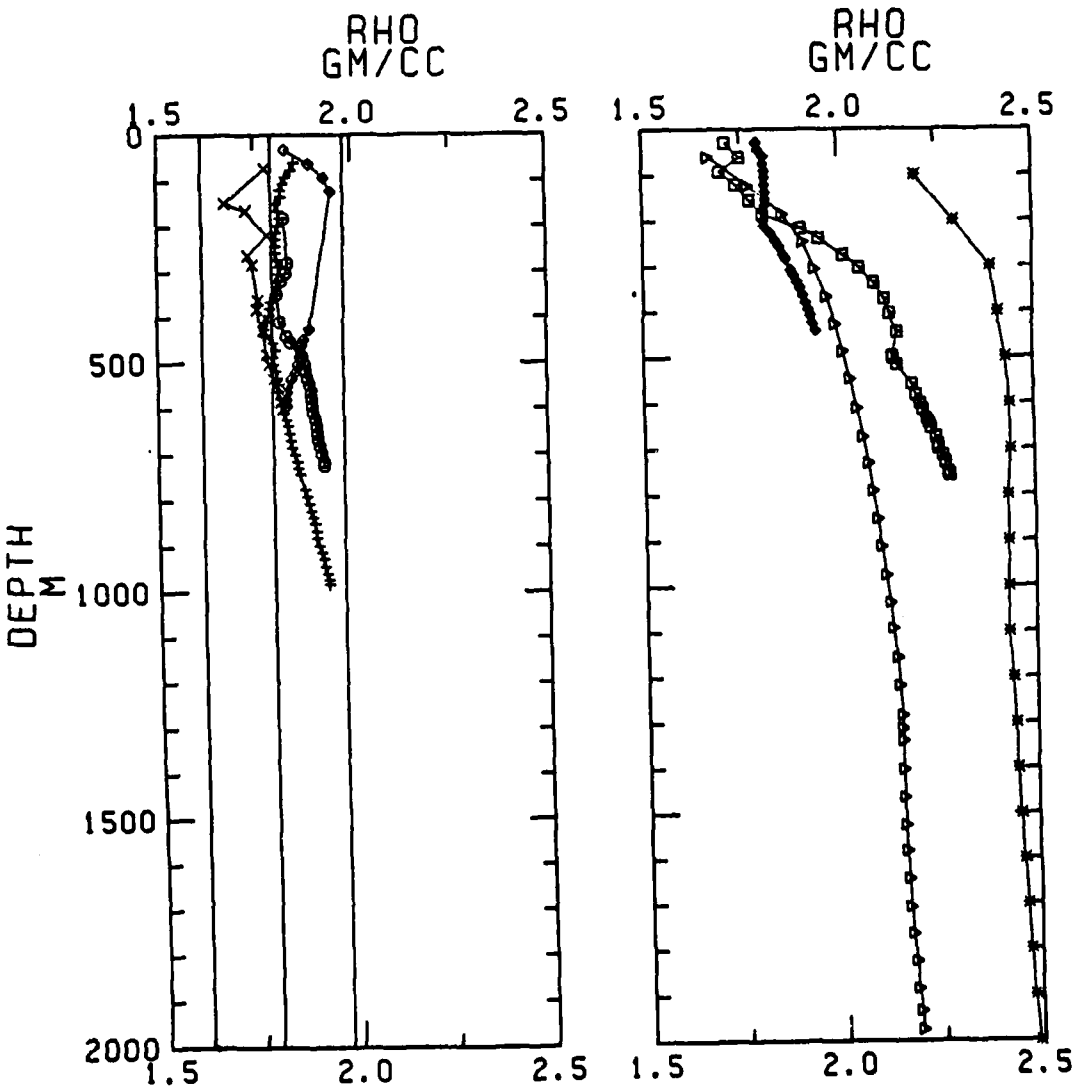

## THE GRAVITY MODEL

As outlined previously a gravity interpretation scheme employing the Parker-Oldenburg technique formed the heart of the structural interpretation. A basin model was estimated in conjunction with the regional anomaly. The density function was specified *a priori*. Ninety boreholes were used as intrabasin control points. The gravity field and the interface were specified on a rectangular grid with the y-axis north and the x-axis east. The grid is specified by 76 x nodes, 65 y nodes, 1600 feet x spacing, 2000 feet y spacing and origin 620000 E and 780000 N in the Nevada central zone coordinate system (units are feet). The gridding is required for efficient computation of the Fourier integrals in the inversion process using the fast Fourier transform. Since the density was assumed to be homogeneous in the basin it was not specified on a grid as it otherwise would have been. The gridding was accomplished by use of Shepard's bivariate interpolation function (Shepard, 1968) combined with a rapid search technique adapted for the high data density (6383 stations) encountered at Yucca Flat. Some smoothing is inherent in the gridding, which helps to suppress aliasing and high frequency noise in the grid.

Proper determination of the regional gravity anomaly is of particular importance at Yucca Flat. Inspection of small scale Bouguer anomaly maps of the western United States, such as Eaton, *et al.*,

(1978), reveal that the valley sits astride a high ridge extending north from the California border. Just to the northwest, a large volcanic caldera complex produces a large, circular low which truncates this trend. The locally-defined regional anomaly should account for this gravity ridge.

The regional anomaly was defined by a low order Fourier surface of two harmonics (25 terms). The fundamental wavelengths of 100000 feet east to west and 220000 feet north to south are roughly twice the basin dimensions. This surface was computed by least squares fit to 350 gravity stations, which occur in areas of Paleozoic outcrop, and gravity anomalies corrected for the basin effect at the 90 borehole locations in Yucca Flat. The data from stations and holes were weighted so that both groups of data would provide approximately equal effects on the resultant surface. The regional anomaly is displayed in figure 6. This map shows the ridge and part of the expected circular depression. The anomaly is gently convex upward. If it were not, and linear gradients were employed as is common practice, the depth would be substantially underestimated.

The residual anomaly at each iteration was multiplied by an areal rectangular truncation window of highly irregular shape, which was somewhat larger than the basin itself but smaller than the total grid. To the extent that the regional separation removed the effect of the half space of the model, a satisfactory taper was achieved. In the southeast corner of the basin the Paleozoic rocks do not outcrop and hence a fundamental assumption of the model is violated. The residual

Fig. 6. The regional gravity anomaly used in the calculation of the final depth model. A low order Fourier trend surface was fit to gravity stations on the Paleozoic outcrop and estimated anomalies at the borehole control points shown in figure 1. The contour interval is 1 milligal.

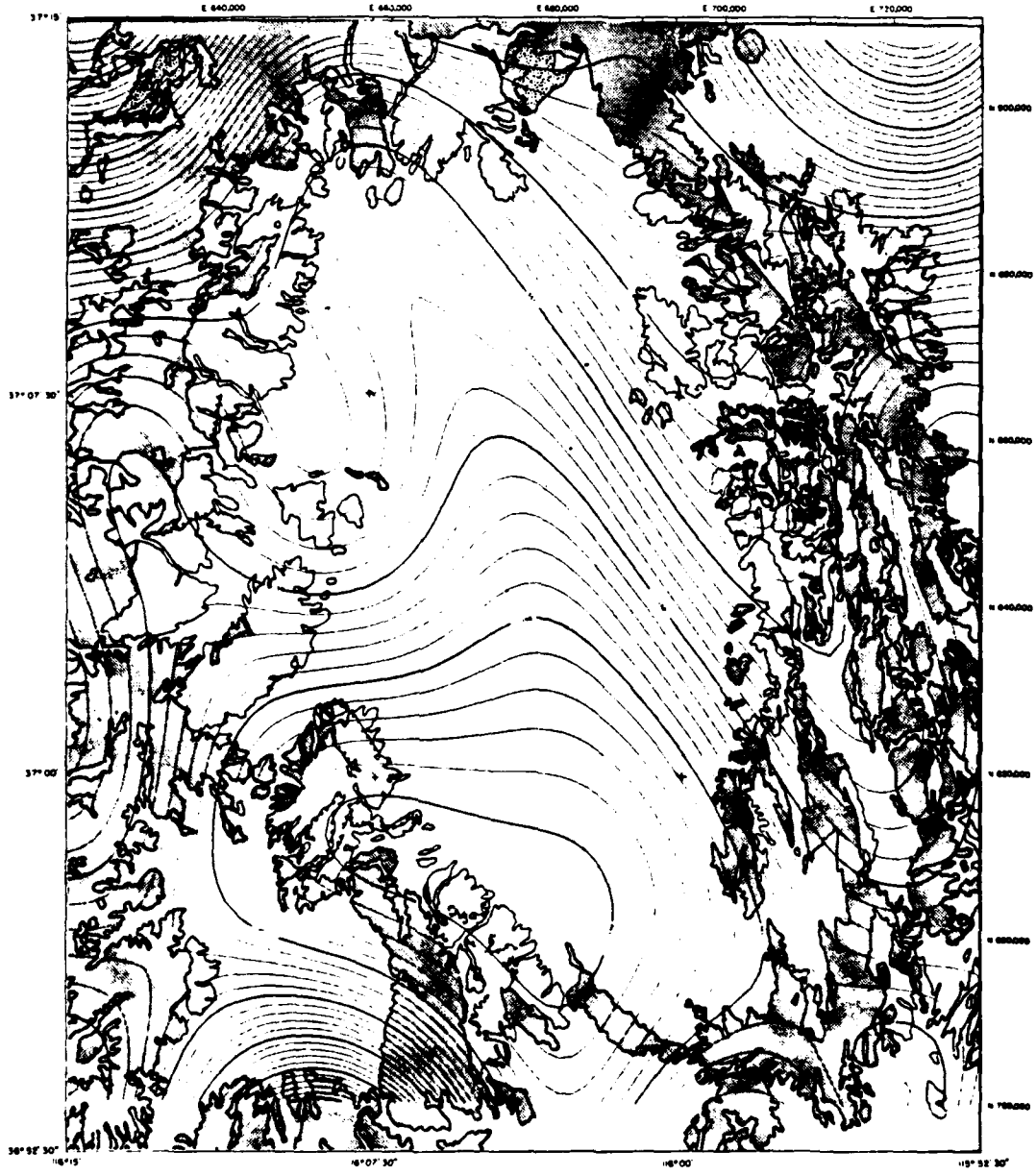


YUCCA FLAT

NEVADA

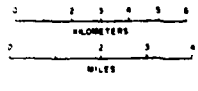

does not taper and is abruptly truncated by the window. The resulting Gibb's oscillations do not seem to be significant within the basin. In future calculations a better window will be developed. The residual which was invented for the final model is mapped in figure 7.

In each iteration of the interpretation process (see figure 3) the error statistics at the boreholes were monitored. After six iterations no real improvement in the fit was obtained and the procedure was terminated. The final model is referred to as F1B and is shown in figure 8. The gravity misfit, as shown in figure 9, is acceptably low over the deeper parts of the basin and increases slightly in the shallow areas. The error statistics are summarized in Table II; histograms of the gravity data misfit and borehole misfit are provided in figure 10. The distributions are not Gaussian and have some very significant outliers. The rank order statistics, the median and inter-quartile deviation, are much more reliable estimates of location and scale in this case. The model thus satisfies the data within $\pm$ 0.5 mgal with some negative bias. The borehole depth mismatch is biased slightly positive which would agree with the data error. The borehole data have several known mislocations and some ambiguity in the definition of the Paleozoic contact is introduced by a thick colluvium on the Paleozoic rocks. The stated borehole depths do not always agree with the modeled depths due to this ambiguity. It should also be remembered that the model depths are really spatial averages and not point measurements like the boreholes. The basement depth deviation would be robustly estimated to be $\pm$ 80 m, which represents about a 15% error on the average. These statistics are in good agreement with Felch (1979).

Fig. 7. The residual gravity anomaly, which results from the subtraction of the regional anomaly in figure 6 from the Bouguer anomaly in figure 2. The contour interval is 1 milligal.

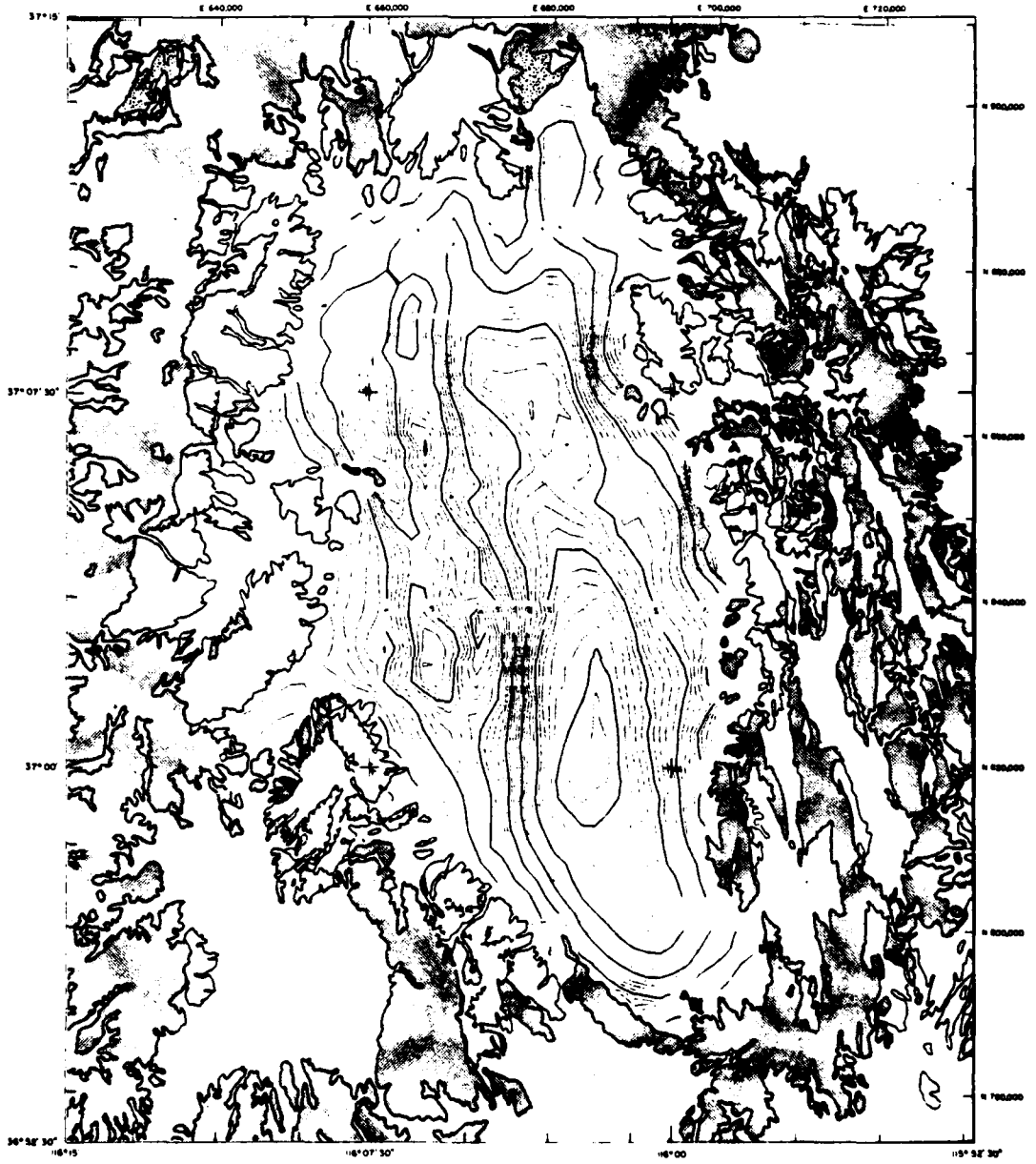


YUCCA FLAT
NEVADA

Fig. 8. The Tertiary-Paleozoic contact depth model for Yucca Flat, Nevada, designated F1B. Note the deep low areas on the east and the shallow lows on the west separated by a horst. The contour interval is 100 meters.

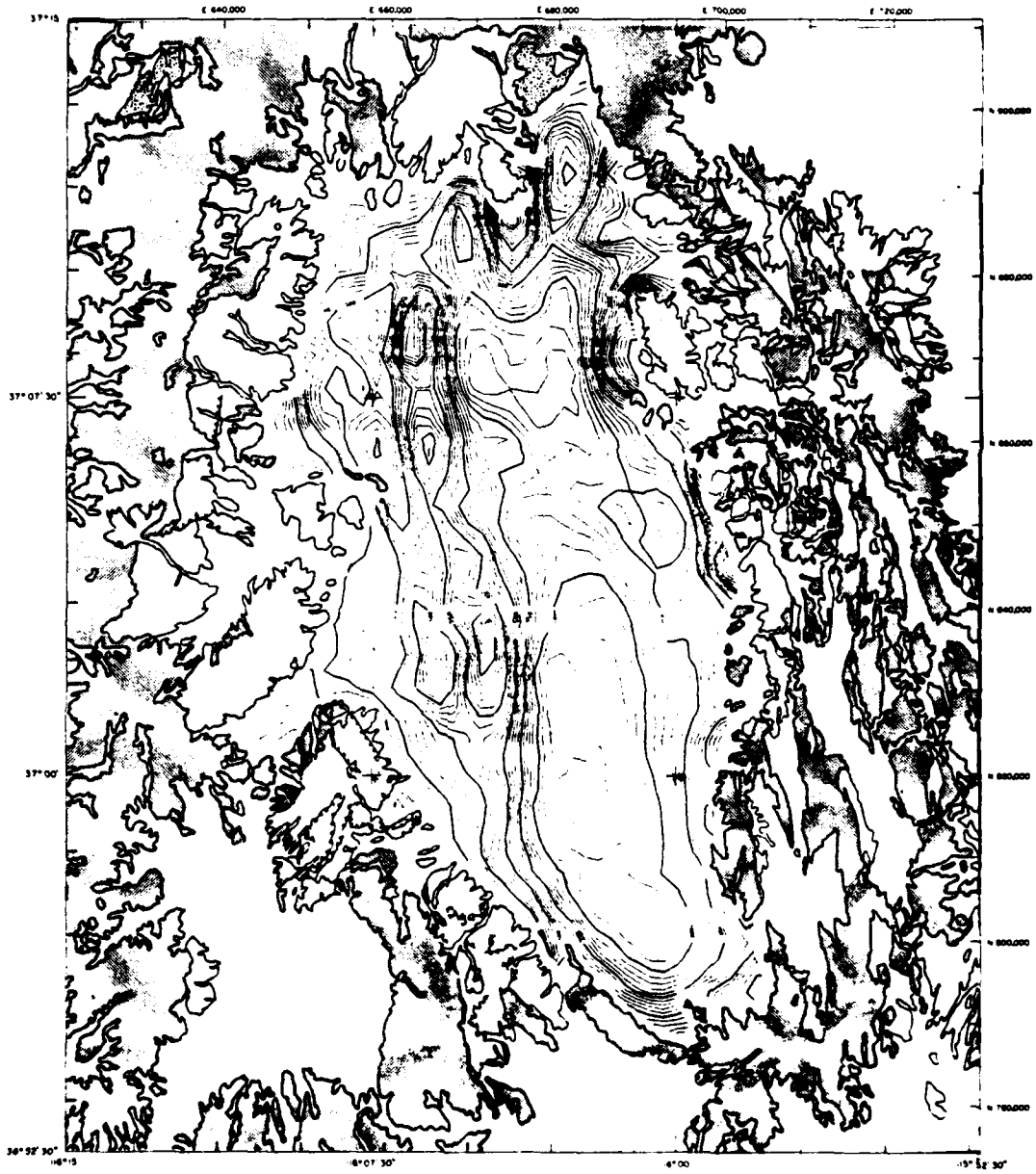


YUCCA FLAT
NEVADA

Fig. 9. The error between the residual Bouguer anomaly of figure 7 and the theoretical anomaly computed from the model in figure 8. The contours are in units of 0.5 milligal. The error is less than 1 milligal except in shallow areas near the basin margins and over the horst.

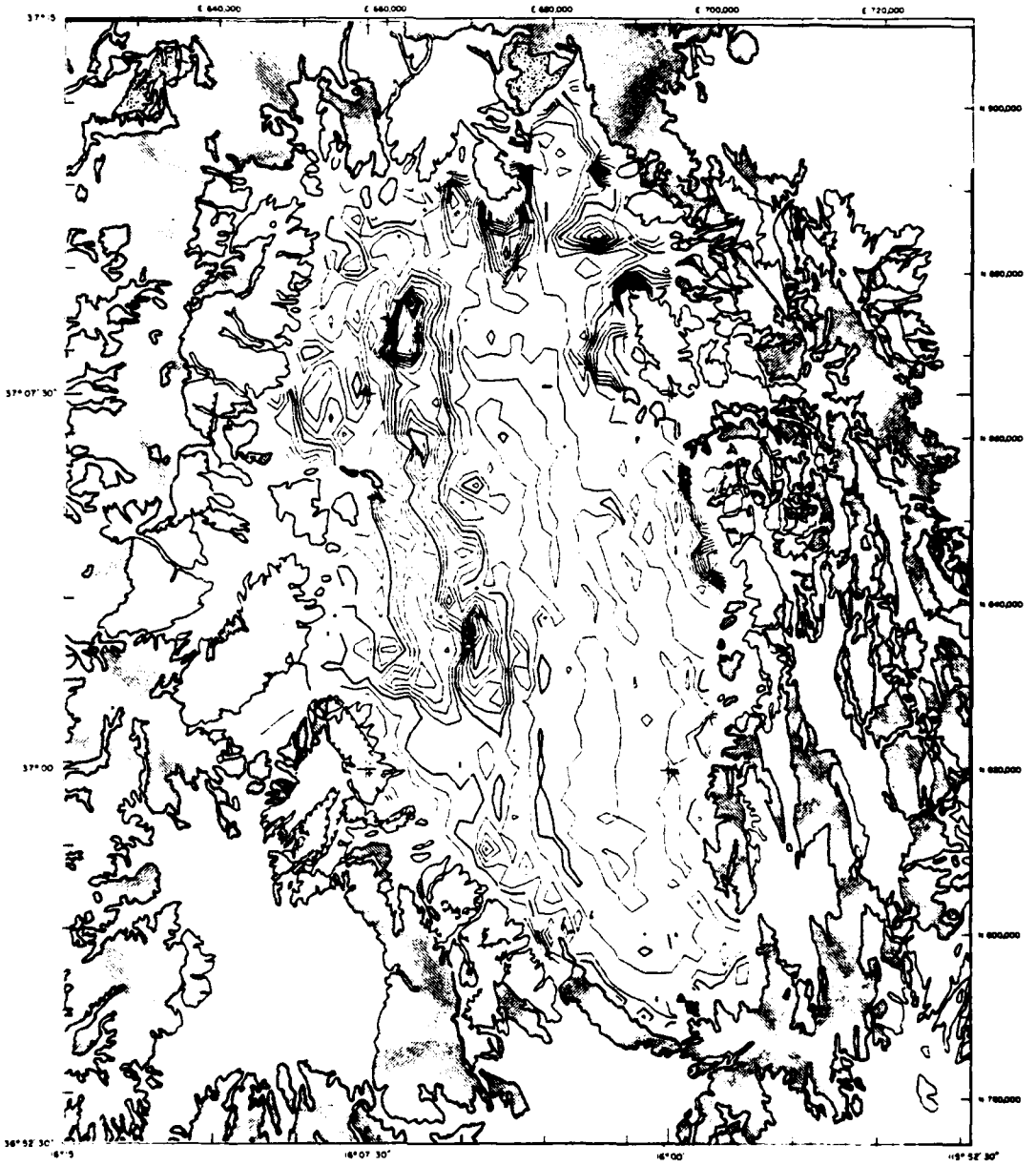


YUCCA FLAT
NEVADA

0 1 2 3 4 5 6
KILOMETERS
0 2 4 6
MILES

TABLE II

ERROR STATISTICS FOR MODEL F1B YUCCA FLAT, NEVADA

DEPTH MISFIT AT 90 BOREHOLES IN KM

MEAN = 0.031
STANDARD DEVIATION = 0.121
ROOT MEAN SQUARE = 0.125
MEDIAN = 0.026
INTERQUARTILE DEVIATION = 0.083
QUARTILE COEFFICIENT OF SKEWNESS = -0.03

GRAVITY MISFIT AT 1336 GRID NODES IN MGAL

MEAN = -0.18
STANDARD DEVIATION = 1.10
ROOT MEAN SQUARE = 1.12
MEDIAN = -0.39
INTERQUARTILE DEVIATION = 0.49
QUARTILE COEFFICIENT OF SKEWNESS = -0.69

Fig. 10. (a) shows the frequency of depth error values in meters at the borehole locations on figure 1 for the model shown in figure 8. (b) is a histogram of gravity misfit errors at the grid nodes within Yucca Flat which are contoured in figure 9. The fiducial limits of one standard deviation about the mean are placed above both histograms.

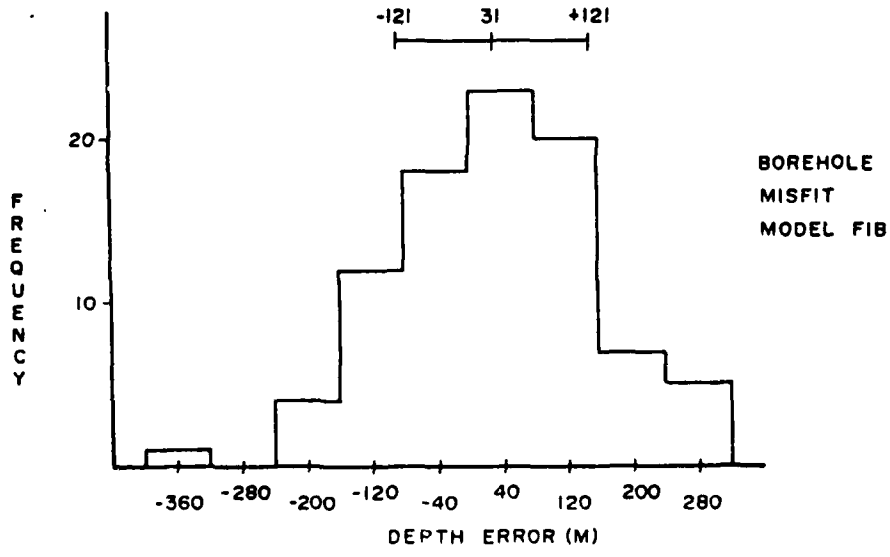
-121
31
+121
20
10
FREQUENCY
-360
-280
-200
-120
-40
40
120
200
280
DEPTH ERROR (M)
BOREHOLE
MISFIT
MODEL FIB

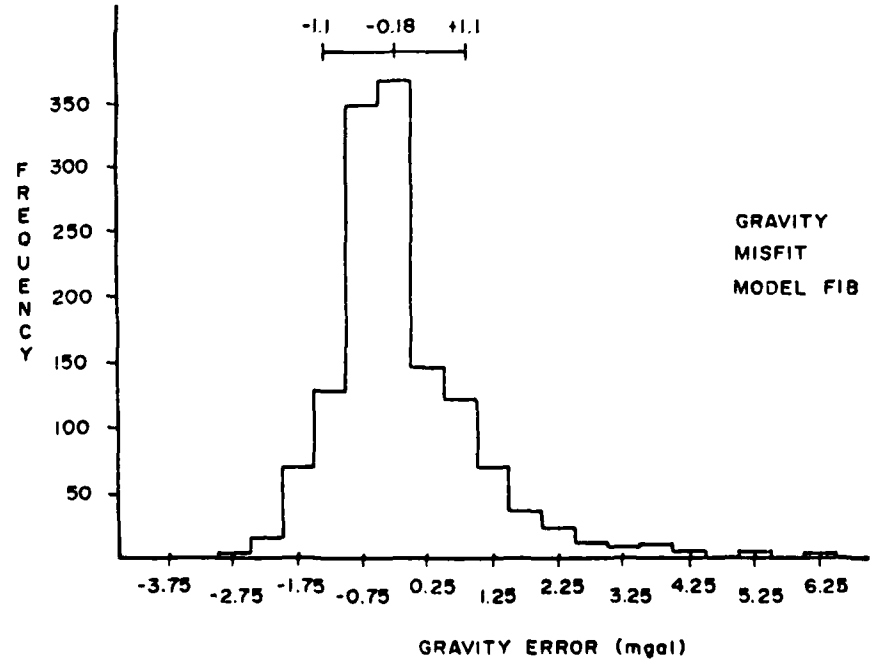
-1.1
-0.18
+1.1
350
300
250
200
150
100
50
FREQUENCY
-3.75
-2.75
-1.75
-0.75
0.25
1.25
2.25
3.25
4.25
5.25
6.25
GRAVITY ERROR (mgal)
GRAVITY
MISFIT
MODEL FIB

This model is only a first effort and has limitations on it which are rather artificial at this time. In the Yucca Flat area over 6000 gravity stations are available and only 1300 grid nodes occur in the same area. Thus, the data grid could be considerably refined. About 100 borehole gravity soundings are available in addition to a selection of density logs. These data could be used to construct a laterally and vertically variable density function which would undoubtedly improve the fit in some areas. In addition some technical improvements to the algorithm especially in the areas of windowing, regional surface fitting and model regularization criteria are possible. These limitations in the data processing result in a decreased resolution and increased smoothness compared to what is actually possible using the available gravity data.

## SEISMIC REFLECTION PROFILES

Three seismic reflection lines, one oriented north to south designated N-3, and two east to west, labeled E-1 and E-3, were recorded in January 1978. The locations of the lines are shown in figure 11. Four Y-900 vibrators provided sweeps of 8 to 32 Hz for 18 sec on N-3. Sweeps of 6 to 32 Hz for 12 sec were used on lines E-1 and E-3. Low frequency (4.5 Hz) geophones were used with 330 foot group intervals on N-3 and 220 foot group intervals on the east to west lines. All lines had 24-fold coverage. The north to south line, which was oriented parallel to the strike in an area with generally thin alluvial cover, was intended to recover deep crustal reflections, if possible. A more detailed description of the seismic reflection profiles is contained in Goforth, et al. (1979). The data processing will be discussed at some length in the next section.

Fig. 11. The location of the seismic reflection profiles E-1, E-3 and N-3. The borehole control points are also plotted. The small numbers, by the profiles, refer to vibration point numbers.

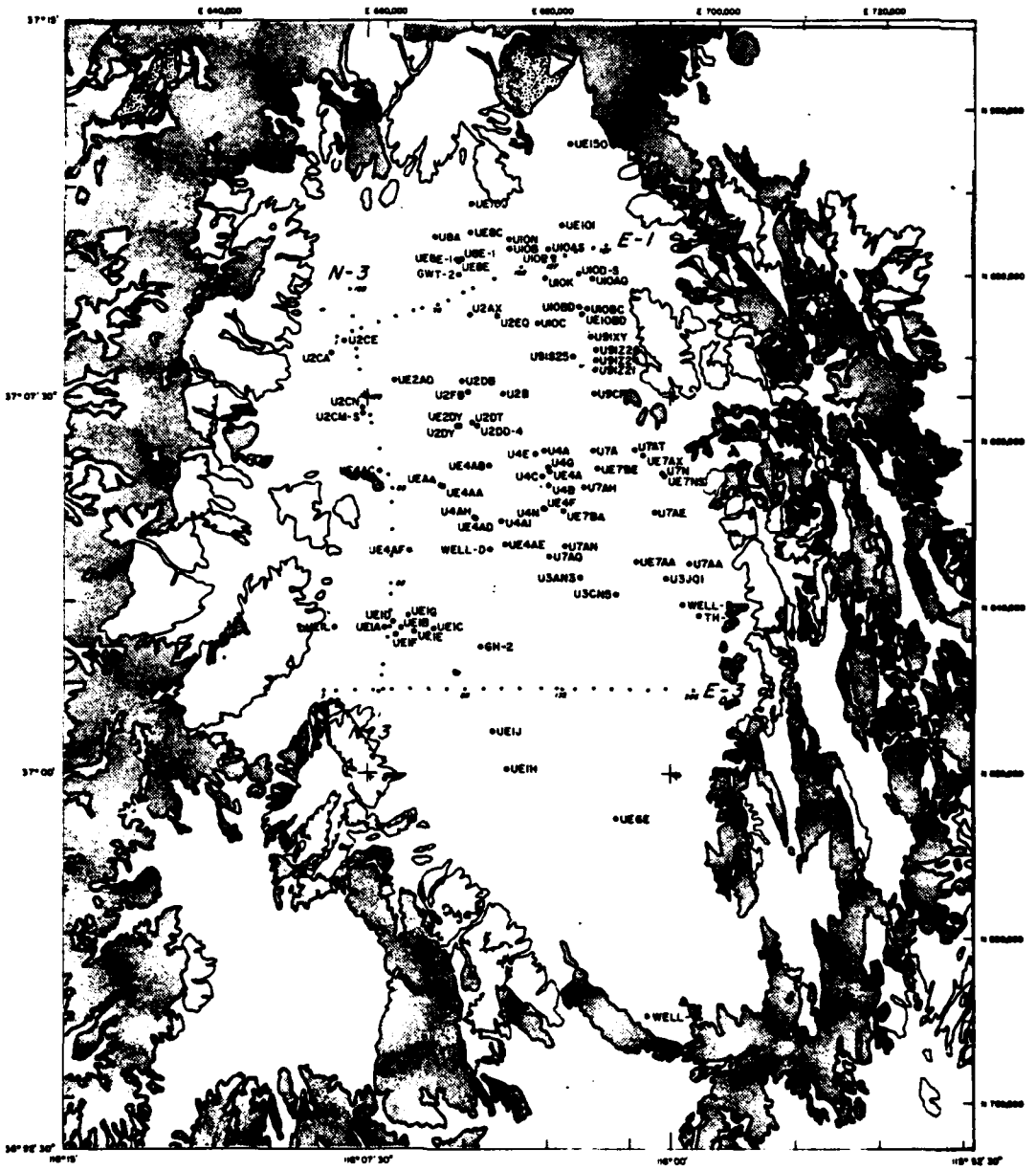


YUCCA FLAT

NEVADA

## PROCESSING OF THE SEISMIC REFLECTION PROFILES AND VELOCITY ANALYSIS

The three seismic reflection profiles available for analysis were VIBROSEIS® data and were initially cross correlated with the source waveform to recover zero phase wavelet seismograms. The records were static corrected for elevation to a datum of 4300 ft. and first arrivals were muted. VELAN® velocity scans were performed at numerous intervals on all three lines. VELAN® analysis is a standard velocity scan program which computes trial normal moveout corrections and tests for coherence within certain time windows. High coherence indicates that the rms velocity (approximated by the stacking velocity) has been correctly determined and thus the velocity as a function of depth is determined. There are the critical assumptions of horizontal layering and lateral homogeneity inherent in this procedure. Departures from these assumptions result in over-estimates of the rms velocity. For homogeneous layers, dip alone will produce an over-estimate proportional to the cosine of the dip angle. Lateral heterogeneity within the limits of the geophone spread along with diffraction phenomena result in even greater errors. This is complicated by the fact that reliable velocity estimates require a large geophone spread in order to sample the large moveout on the tail of the travel time curve. Within Yucca Flat strong lateral variation due to faulting resulted in very

poor velocity estimates at depth; the shallow velocity structure, down to approximately 500 m was adequately determined. Many of the VELAN(R) profiles were unusable, and those that were used produced structural relief estimates which were inconsistant with the gravity and borehole analysis. The seismic sections were migrated by a finite difference scheme after stacking and are displayed in figures 12, 13, 14.

The lateral velocity variations result in a degraded common mid-point stack (CMP) and subsequent migration of the stack is also in error. The solution to this difficulty lies in migration of the original, unstacked data and possibly the use of migration velocity determination analogous to the normal moveout velocity (the normal moveout correction and stack is the correct migration of data observed over horizontal stratification). Several approaches to this problem have been outlined. Satlegger (1975) and Dohr and Stiller (1975) proposed migration velocity determination and Doherty and Claerbout (1976) offer a procedure for approximate migration before stack. These processes are complicated by the fact that migration calculations are relatively more costly to perform than normal moveout corrections in that the better algorithms are based on wave theory rather than geometrical ray theory. Schultz and Claerbout (1978) point out that CMP gathers and stacks are generally not realizable wave fields especially where there are significant lateral velocity variations. They propose to migrate stacks of constant ray parameter (slant stacks). In this process a number of beams would be formed and each beam migrated separately, a very costly procedure. The E-3 section was processed in

Fig. 12. This section is a migrated, common midpoint stack of the east-west seismic line E-1. The vibration points are numbered across the top. The total two-way travel time is 4 seconds.

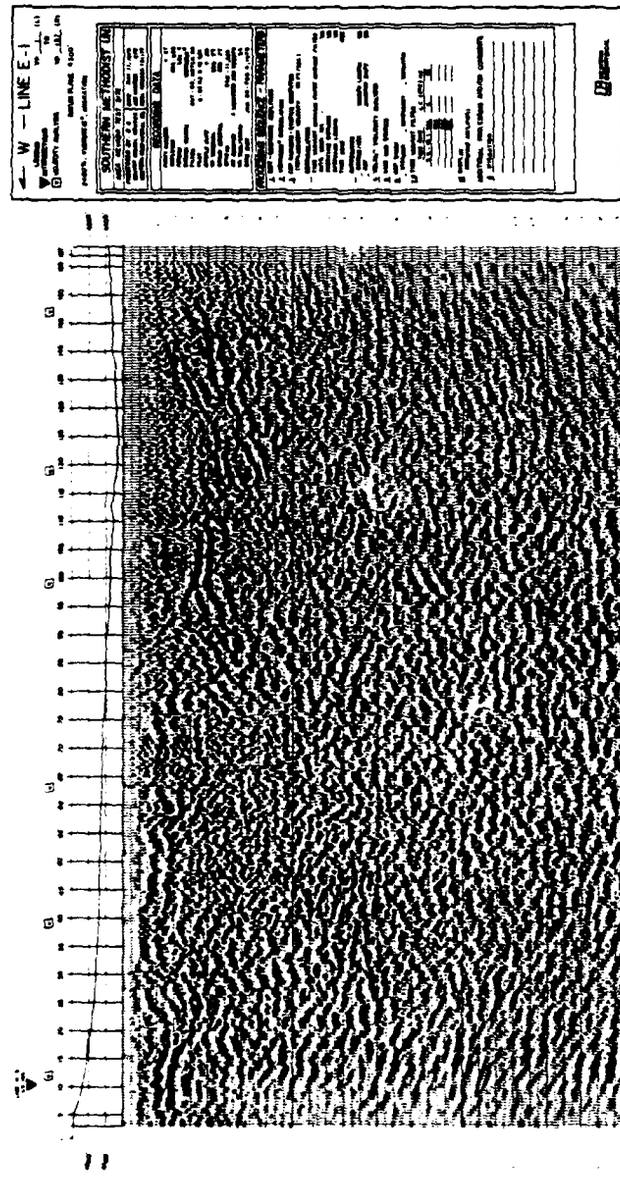

Fig. 13. This section is a migrated, common midpoint stack of the east-west seismic line E-3. The vibration points are numbered across the top. The total two-way travel time is 4 seconds.

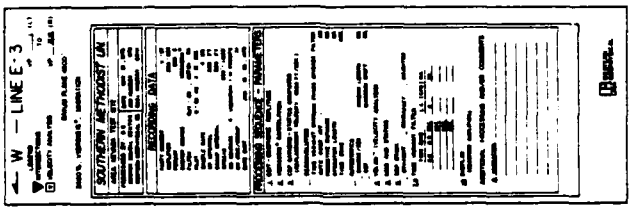
W — LINE E-3

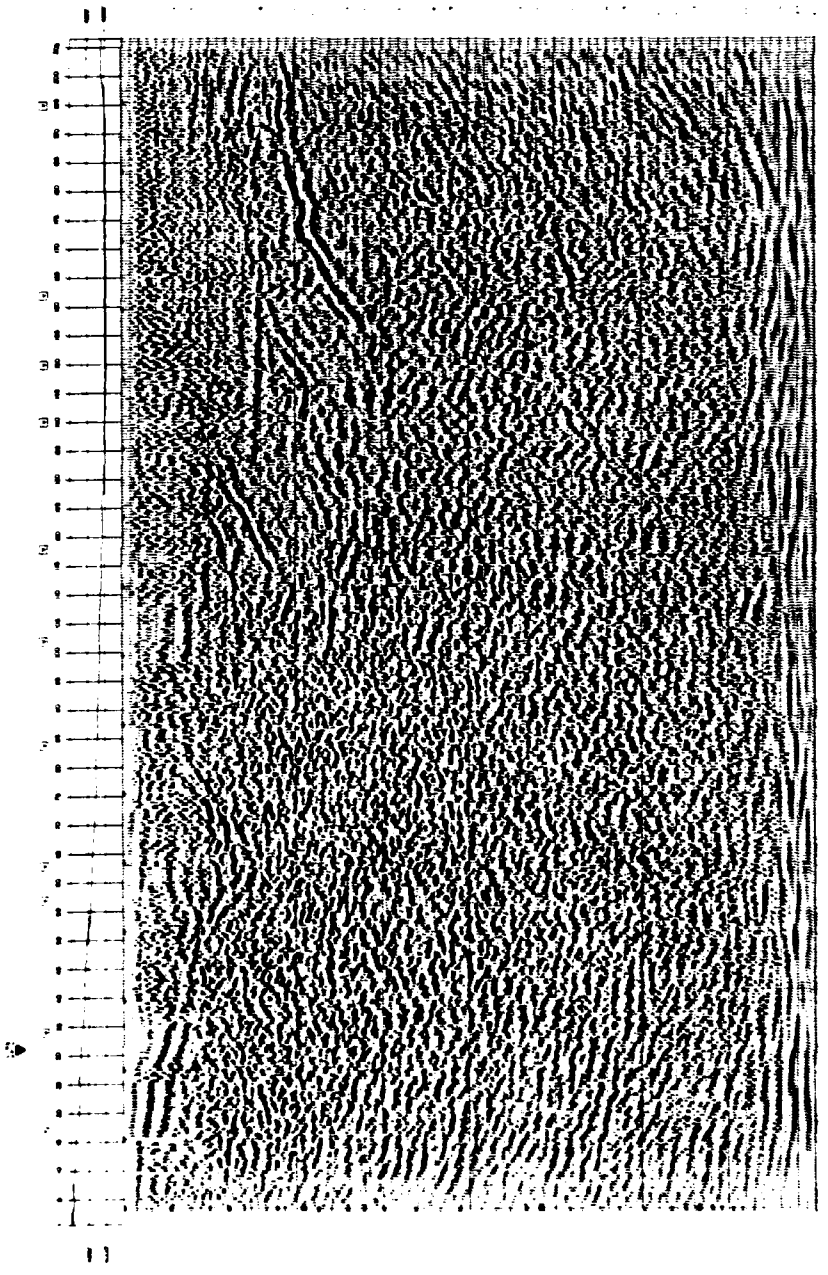

Fig. 14. This section is a migrated, common midpoint stack of the north-south seismic line N-3. The vibration points are numbered across the top. The total two-way travel time is 4 seconds.

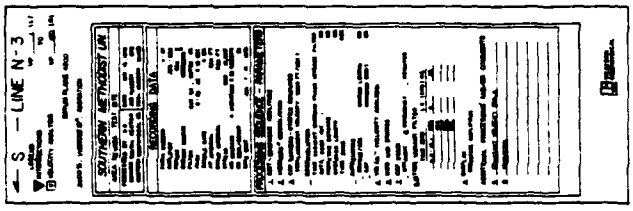
S — LINE N-3
SOUTHERN METHODIST UN

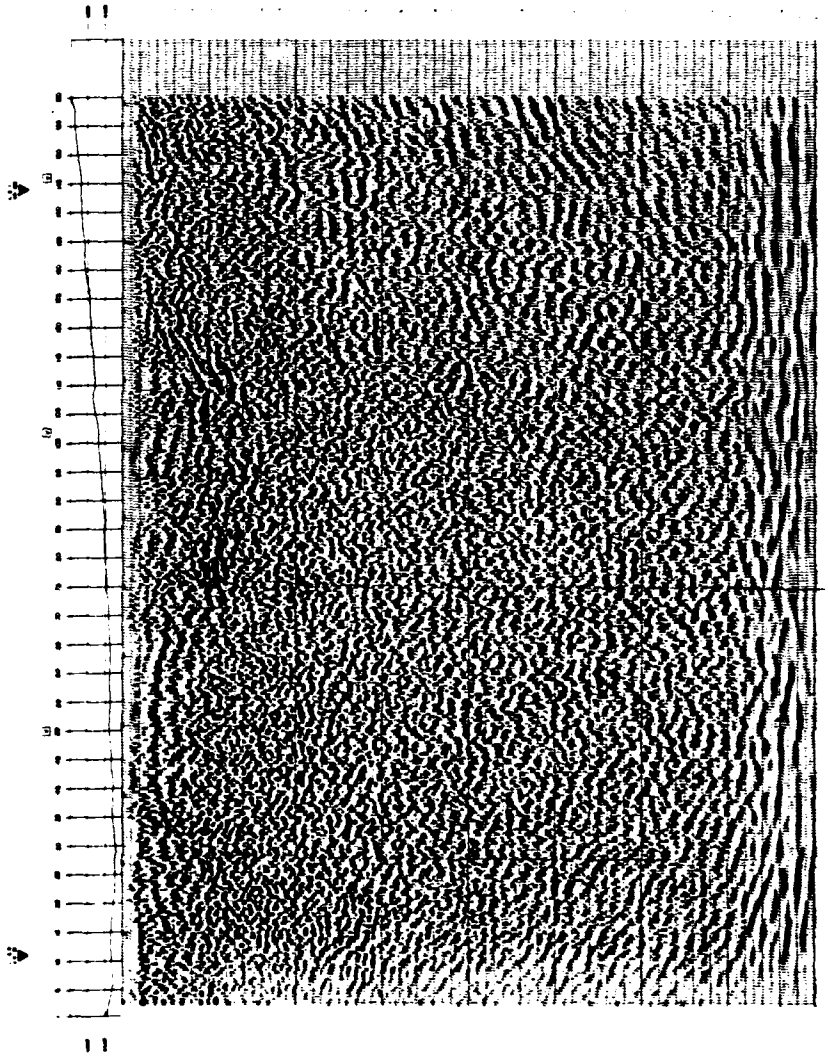

a manner similar to the method described by Doherty and Claerbout (1976). Each normal moveout corrected CMP gather was migrated independently with a rather arbitrary choice of velocity function, a new velocity analysis was performed, and the migrated gathers were stacked with the new velocity. This processing was more expensive (24 times) than conventional processing, but not as expensive as migration of common source gathers would have been. The "migration before stack" section is shown in figure 15. The new velocity analysis improved the deeper velocity estimates by over ten percent.

The choice of a velocity function suitable for use in depth estimation was complicated by the lack of good velocity scans and the sparsity of deep velocity logs. It was not possible to construct laterally variable velocity models; however, reasonable results were obtained with a single velocity function. A comparison of interval velocity data from areas 3,4,6, and 7 is made in figure 16. The velocity function defined by borehole UE6E is close to the median and is the deepest available hole. An uphole velocity survey conducted in UE10BD by LANL and LLL agrees quite well with that in UE6E. Some holes in Area 7 and Area 3 have much lower velocities down to a 600 m depth and some Area 7 holes show rather higher velocities at shallow depth. Figure 17 is a comparison of the UE6E velocity function with the orginal VELAN® and "migration before stack" velocity functions. The velocity analyses chosen are the best available. They agree quite well in the shallow regions, but diverge at depth. The conventional VELAN® would produce errors of 100 m in depth. The UE6E velocity function was chosen as the

Fig. 15. Seismic reflection profile E-3. This is the same data shown in figure 13 with different processing. In this case the common midpoint gathers were migrated prior to stacking and a new stacking velocity was derived which was less effected by lateral velocity variation. The vibration points are numbered across the top. The total two-way travel time is 4 seconds.

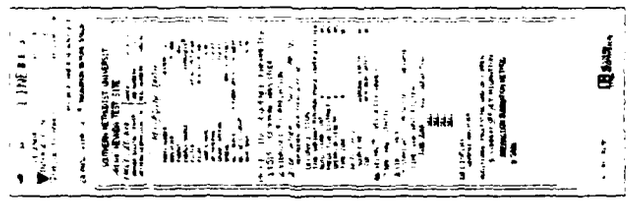

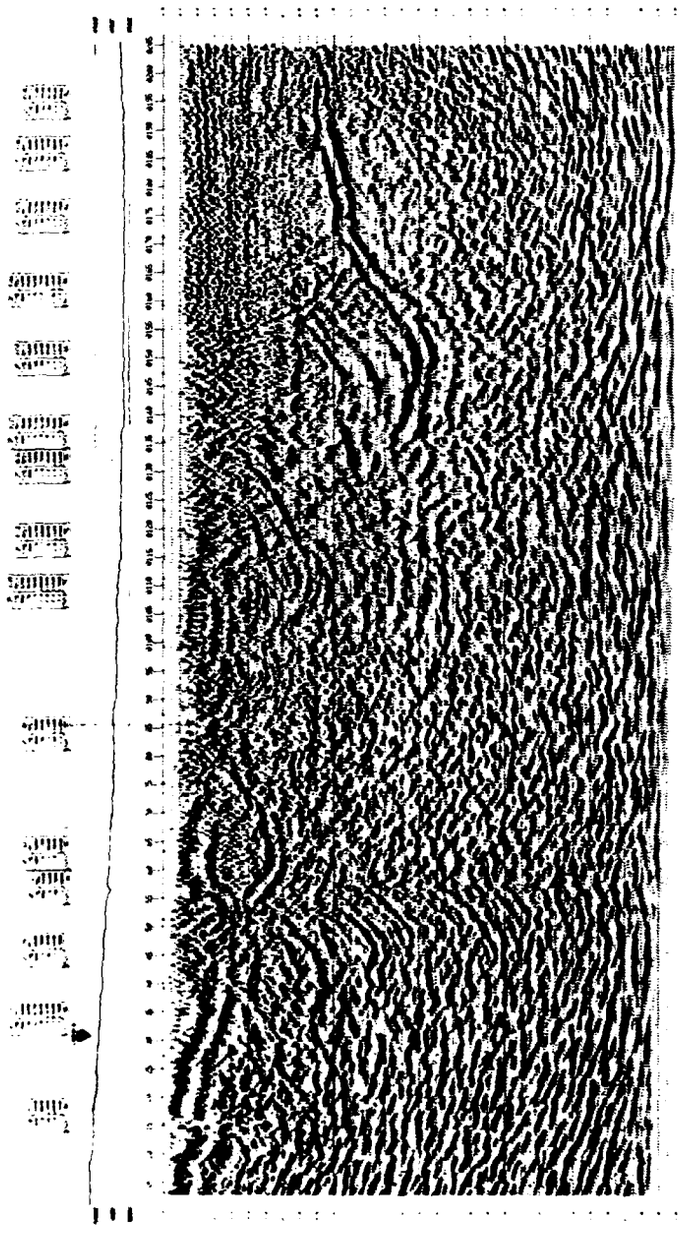

Fig. 16. Average velocity as a function of depth determined from interval velocities at Yucca Flat, Nevada. The curve labeled UE6E is from a deep borehole located in the southern portion of the basin (see figure 11). The UE6E curve represents the median choice for the velocity function.

AVERAGE VELOCITY VS DEPTH
YUCCA FLAT, NEVADA
INTERVAL VELOCITY SURVEYS FROM
AREAS 3, 4, 6, 7 AND 10

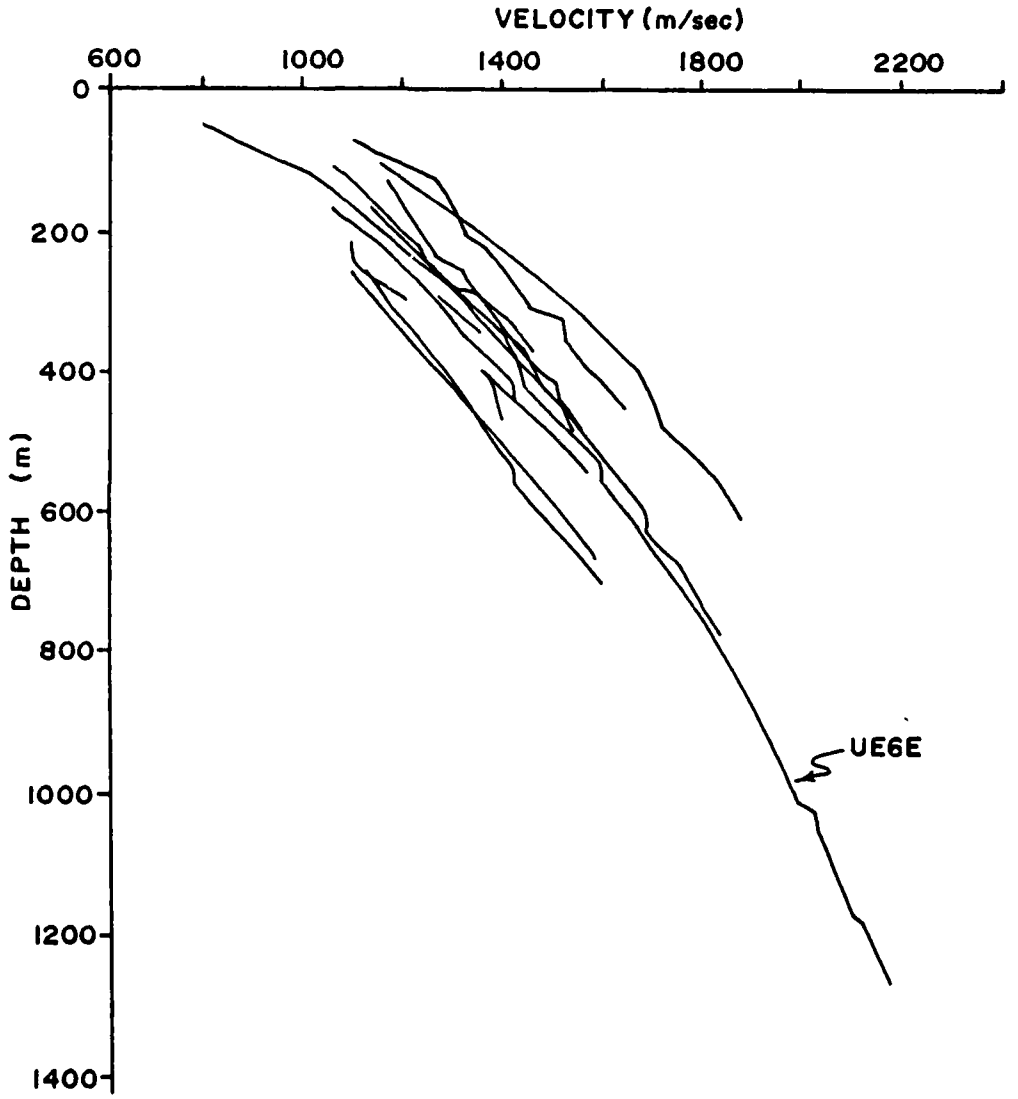

Fig. 17. The veolcity functions derived from stacking velocities and the UE6E interval velocities. SP150 on profile E-3 is located only 5 kilometers from UE6E in an area of rather uniform structure. Notice that the migration before stack function is in better agreement with the UE6E function at depth and that little difference is present among the three estimates above 700 m depth.

# COMPARISON OF VELOCITY FUNCTIONS
# YUCCA FLAT, NEVADA

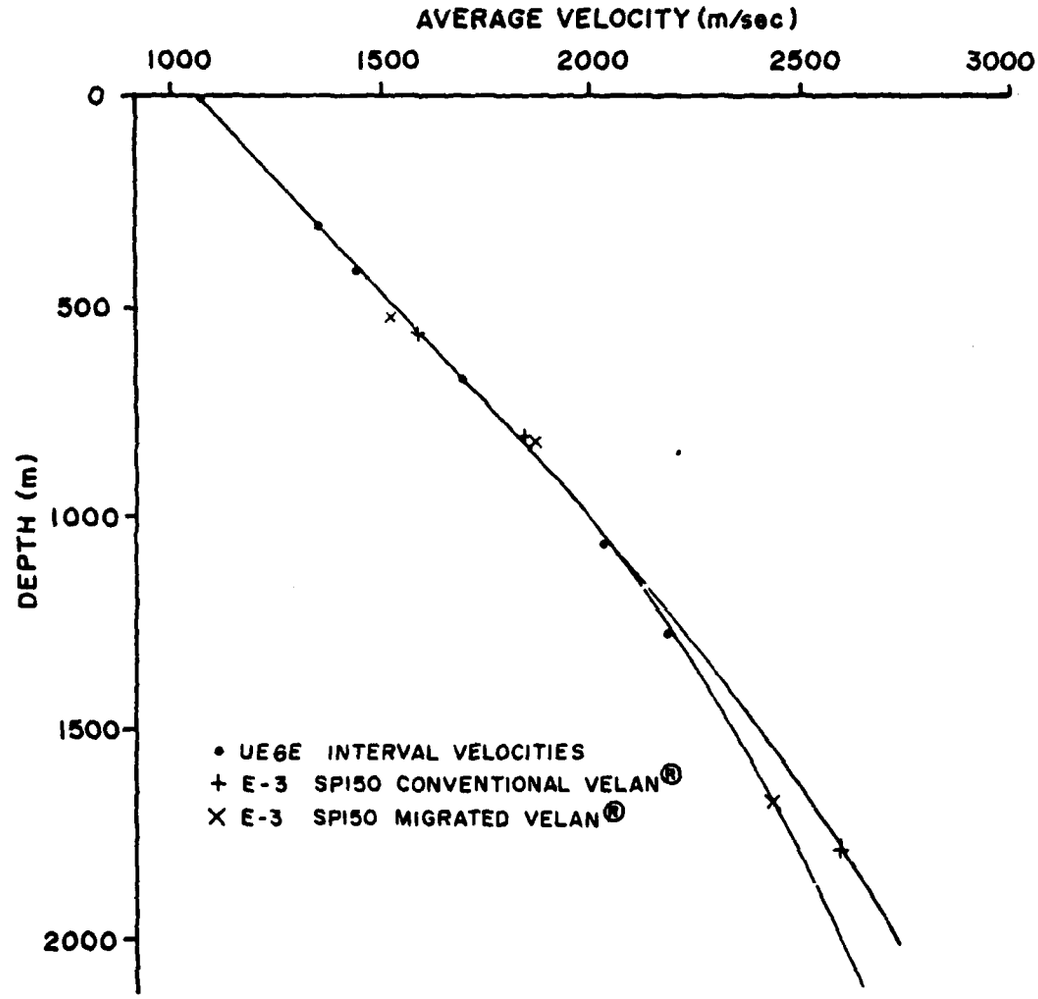

standard and has been used in all depth estimates from the reflection data. This function may need modification in Areas 3 and 7 (profile E-3 is in Area 3), but it serves quite well in most of the basin.

## ANALYSIS OF THE SEISMIC SECTIONS AND GRAVITY MODEL

The three seismic sections, E-1, E-3 and N-3, have been analyzed in an attempt to define the most prominent geologic features of the Yucca Flat Basin. The seismic sections have been compared to the gravity model and to the borehole data with the UE6E velocity model providing depth to time conversion.

The F1B gravity model and geologic map shown in figure 18 demonstrate several important features of the basin. The deepest part of the basin is in the southeast. A saddle separates the deeper basin from a bilobate northern basin. The saddle trends northwest along the strike of several faults seen on the eastern and western margins of the valley. The western boundaries of these deeper, eastern basins will be referred to as the Carpetbag Fault system as the fault segment so named is coincident with it. The better known Yucca Fault runs down the center of the eastern basins. Both the Yucca and Carpetbag faults have right lateral strike slip component of motion as well as dip slip. A narrow horst, which rises to within a hundred meters of the surface, isolates a string of shallower smaller basins on the west from the main eastern basins.

The N-3 line unfortunately runs parallel to the western basin and slightly to the west of its center. This causes the reflections recorded to migrate from out of the plane of the section, thus pro-

Fig. 18. The three seismic profiles superimposed on a map of the Tertiary-Paleozoic interface and normal faults from the geologic maps. Notice the Yucca Fault in the middle of the basin and also the northwest trending faults in the northwest and east central portions of the map, which align with the saddle in mid-basin. The contour interval is 100 m.

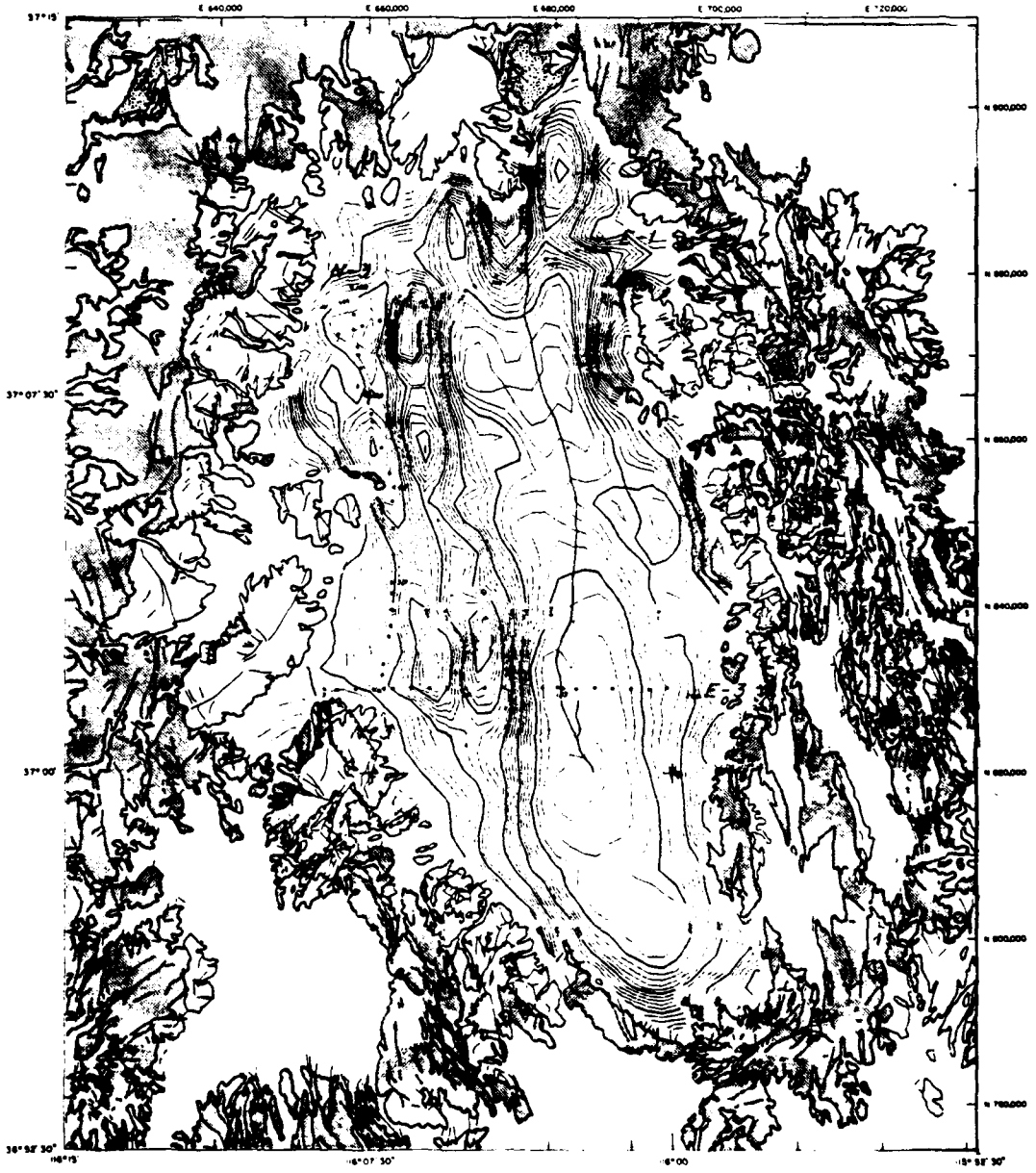


YUCCA FLAT
NEVADA

0 1 2 3 4 5 6
KILOMETERS

0 1 2 3 4
MILES

viding more limited resolution of vertical depth. The N-3 section was successful in recovering structural information from below the basin and possibly a mantle reflection at 10.7 seconds two-way travel time near vibration point 140.

The two east to west trending seismic lines provide very good structural information. In order to facilitate the interpretation of these sections the F1B model was converted into time sections along the three reflection lines and then overlain on the migrated common depth point sections, as shown in figures 12, 13, and 14. Prominent reflecting events and faults delineated by diffractions were traced onto the overlays, as seen in figures 19, 20, and 21. In many areas the correlation between the gravity anomaly and the seismic reflections is quite good, but in other areas the Paleozoic contact does not appear to be a conspicuous reflector. In these cases the deeper reflections may be masked by thin, high velocity welded tuff units at shallower depths. The horst, bounded on the east by the Carpetbag Fault system, is evident, as is the Yucca Fault. Dip slip motion on these faults, especially the Carpetbag, accounts for the asymmetric basin that has recently developed at Yucca Flat. The dips of these faults seem to be somewhat low for normal faults, between 45° and 60°. Note that the curved lines drawn on the time sections (which map nonlinearly into depth) would appear as planes in a depth section. West dipping faults on the eastern end of the lines have steeper dips on the order of 70° and are conjugate to the basin forming faults. In section E-3 the water table accounts for the horizontal reflector at 0.7 seconds travel

Fig. 19. An interpretation of the first second of two-way travel time for the E-1 profile shown in figure 12. The depth scale is derived from the UE6E velocity function. The continuous, light line is from the gravity model shown in figure 8. The short, heavy lines mark the presence of coherent reflectors. Notice the agreement of the gravity model with coherent reflections between vibration points 20 to 60 and 70 to 150.

AD-A129 604 DEVELOPMENT OF AUTOMATED DETECTION AND DISCRIMINATION TECHNIQUES FOR USE A..(U) INSTITUTE FOR THE STUDY OF EARTH AND MAN DALLAS TX GEOPHYSICA.. E HERRIN ET AL. 2/2

UNCLASSIFIED 14 OCT 82 AFOSR-TR-83-0528 F49620-81-C-0010 F/G 8/11 NL

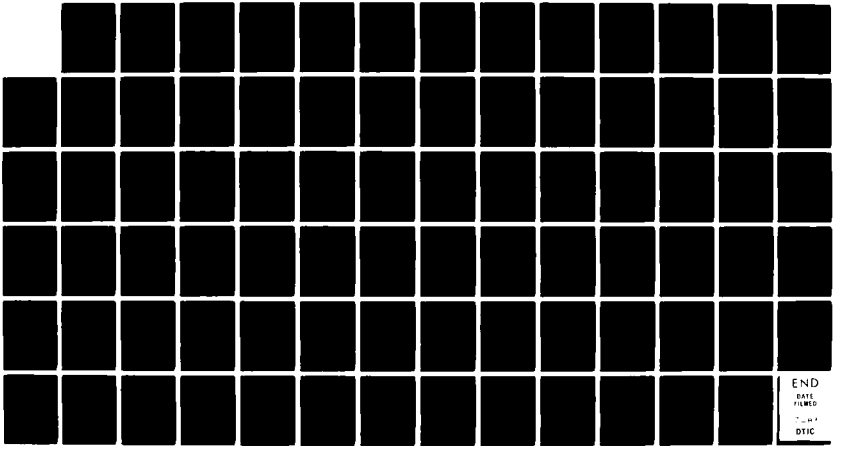

END

DATE FILMED

DTIC

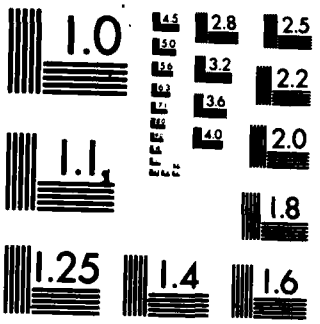

INTERPRETATION OF
LINE E-1 MIGRATED SECTION
*AND GRAVITY MODEL FIB*
YUCCA FLAT, NEVADA

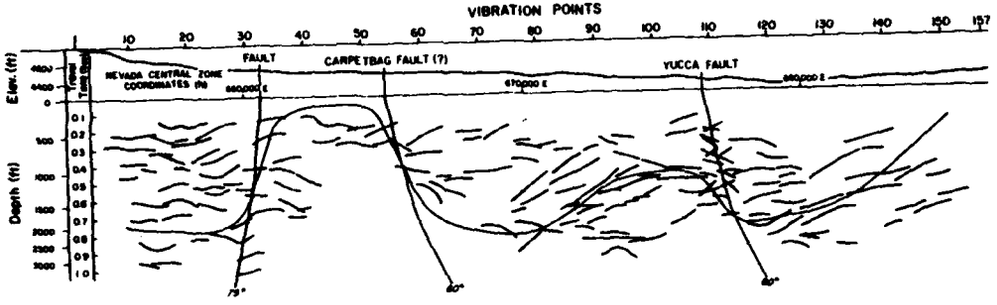

Fig. 20. An interpretation of the first 1.5 seconds of two-way travel time for the E-3 profile shown in figure 13. The depth scale is derived from the UE6E velocity function. The continuous, light line is from the gravity model shown in figure 8. The short, heavy lines mark the presence of coherent reflectors. In the interval between vibration points 130 and 160 the agreement of the gravity model with the reflectors is not high. The resolution in this area is not as high in the three-dimensional gravity model as in the two-dimensional model presented in Goforth, et. al. (1979).

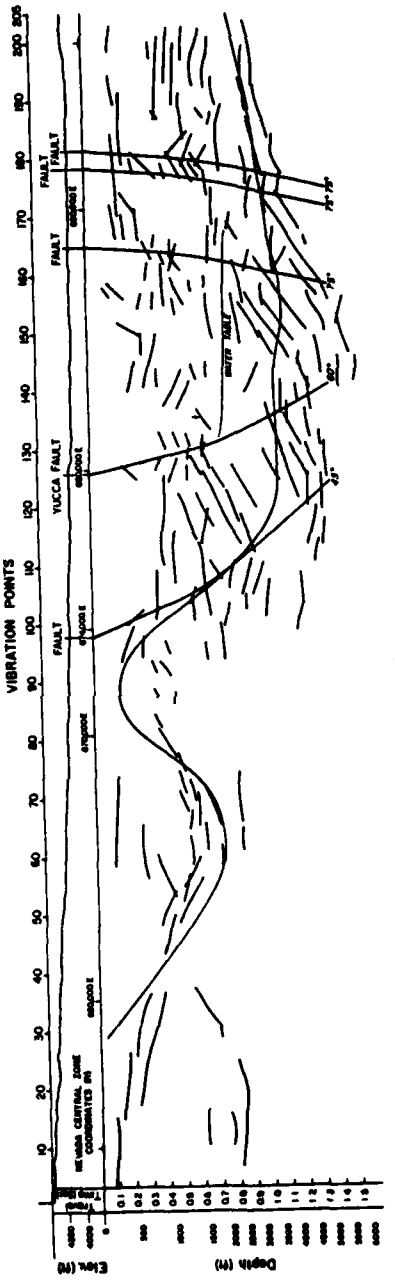


INTERPRETATION OF
LINE E-3 MIGRATED SECTION
AND GRAVITY MODEL F1B
YUCCA FLAT, NEVADA

Fig. 21. An interpretation of the first 1.2 seconds of two-way travel time for the N-3 profile shown in figure 14. The depth scale is dervied from the UE6E velocity function. The continuous, light line is from the gravity model shown in figure 8. The short, heavy lines mark the presence of coherent reflectors. In figure 18 it is evident that line N-3 runs parallel to and on the margin of a synform. This geometry causes the reflectors to migrate out of the plane of the profile, a difficulty which is impossible to overcome quantitatively. In spite of this problem the section shows more detail below the basin than either of the east to west profiles

INTERPRETATION OF
LINE N-3 MIGRATED SECTION
AND GRAVITY MODEL FIB
YUCCA FLAT, NEVADA

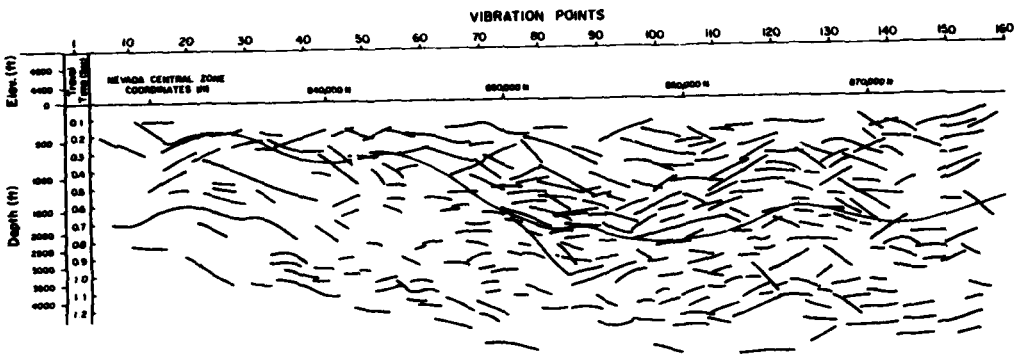

time. The volcanic units dip to the west at approximatly 45°. This is due to tectonic rotation by the Carpetbag and Yucca Fault systems.

Dip slip motion on the Carpetbag Fault probably postdates the deposition of the volcanics and hence is less than about 11 million years old. The early opening of the basin at Yucca Flat is probably part of the general east-west extension of the Great Basin associated with the progressive development of the San Andreas Fault (Atwater, 1970). The strike slip motion results from a progressive reorientation of the stress field due to major plate interactions. The Yucca fault represents an eastward migration of the locus of faulting as strike slip motion and constraints, such as the Climax Stock, have become more important (Oldow, personal communication, 1981). The Yucca fault generally has less than 200 meters of displacement on it. The saddle region, which was not traversed by seismic lines in the eastern basin, is likely to be a remnant of a previous topographic high related to northwest to southeast trending faults which predate the volcanics. In the saddle the Yucca-Carpetbag Fault system breaks up into a very diffuse zone of en echelon faults known as the Topgallant system. The geometrical features observed in the Yucca Flat geophysical model now have a structural interpretation consistent with the regional tectonic trends.

# CONCLUSIONS

The application of a systematic gravity inversion procedure, which utilizes known structural and density information, has resulted in a model of the Tertiary-Paleozoic interface at Yucca Flat, Nevada. This model is accurate to better than 100 m in most areas and is capable of predicting basin depths to a similar accuracy. This is achieved without recourse to complex density variations, but with only a single density contrast. The estimation of the regional anomaly is crucial to the interpretation, and an effective procedure for this purpose has been demonstrated.

The seismic reflection method is useful for mapping the Tertiary-Paleozoic interface in areas where reflections are not obscured by high velocity layers, such as welded tuffs, and where three-dimensional structural effects are not too serious. The high attenuation resulting from Quarternary sediments in this locality means that low frequency sources and seismometers should be employed. VIBROSEIS® techniques using low frequency sweeps were particularly suitable, however, resolution was correspondingly low. In addition, automatic velocity determinations are suspect, at least in the deeper areas, because of structural complications. Processing with migration before stacking and the use of interval velocity determinations in wells helped alleviate this difficulty. Faulting is usually well defined on the seismic reflection profiles.

The combined interpretation of geologic, gravity and seismic data depicts the general structural configuration of the basin very well. Major normal faults on the west rotate the basin down about a broad hinge zone at the eastern margin. This structural development occurred after depostion of the volcanics. A pre-existing northwest structural lineation forms a saddle which divides the basin into north and south parts. This saddle affects later structural elements such as the Carpetbag and Yucca Fault systems in the central saddle region. A tectonic pattern of increasing strike slip motion on the western bounding faults in recent time can explain the shift of activity from the Carpetbag to the Yucca Fault systems.

Body wave magnitude variations, when properly normalized to constant explosion yield, show a variation which correlates with the model presented here. In particular, location of the explosions relative to the Carpetbag fault and to the saddle is highly significant. The theoretical response of this structure will be calculated to further verify this hypothesis and provide a predictive capability.

# PART II

## INTRODUCTION

Body wave magnitude estimates for a number of nuclear explosions at Yucca Flat, Nevada have been analyzed for spatial variation (Alewine, personal communication). Each explosion was corrected to a common datum by the use of well established scaling laws for yield and depth of burial (Mueller and Murphy, 1971). These data, when plotted on the map of Yucca Flat in figure 22, show a progressive decline of about 0.5 magnitude units from the middle of the valley toward the east over a distance of four kilometers. This variation complicates the analysis and calibration of seismic yield estimation and source discrimination techniques.

The magnitude variation is correlative with the structure contours of the top of the Paleozoic units as presented in the F1B model of Yucca Flat. The systematic nature of the variation suggests a deterministic explanation of the phenomena in terms of scattering of the outgoing body waves by the local structure.

This problem is not soluble in any simple form for realistic geophysical models of Yucca Flat. A numerical solution might be computed by any of several techniques such as finite difference, finite element or some form of ray tracing. After a review of the literature on numerical wave propagation techniques, the above alternatives were rejected in favor of the Aki and Larner (1970)

Fig. 22. Contours of body wave magnitude variation ($m_b$) superimposed on a contour map of the Tertiary-Paleozoic interface for Yucca Flat, Nevada. The $m_b$ contours were modified from Alewine (personal communication).

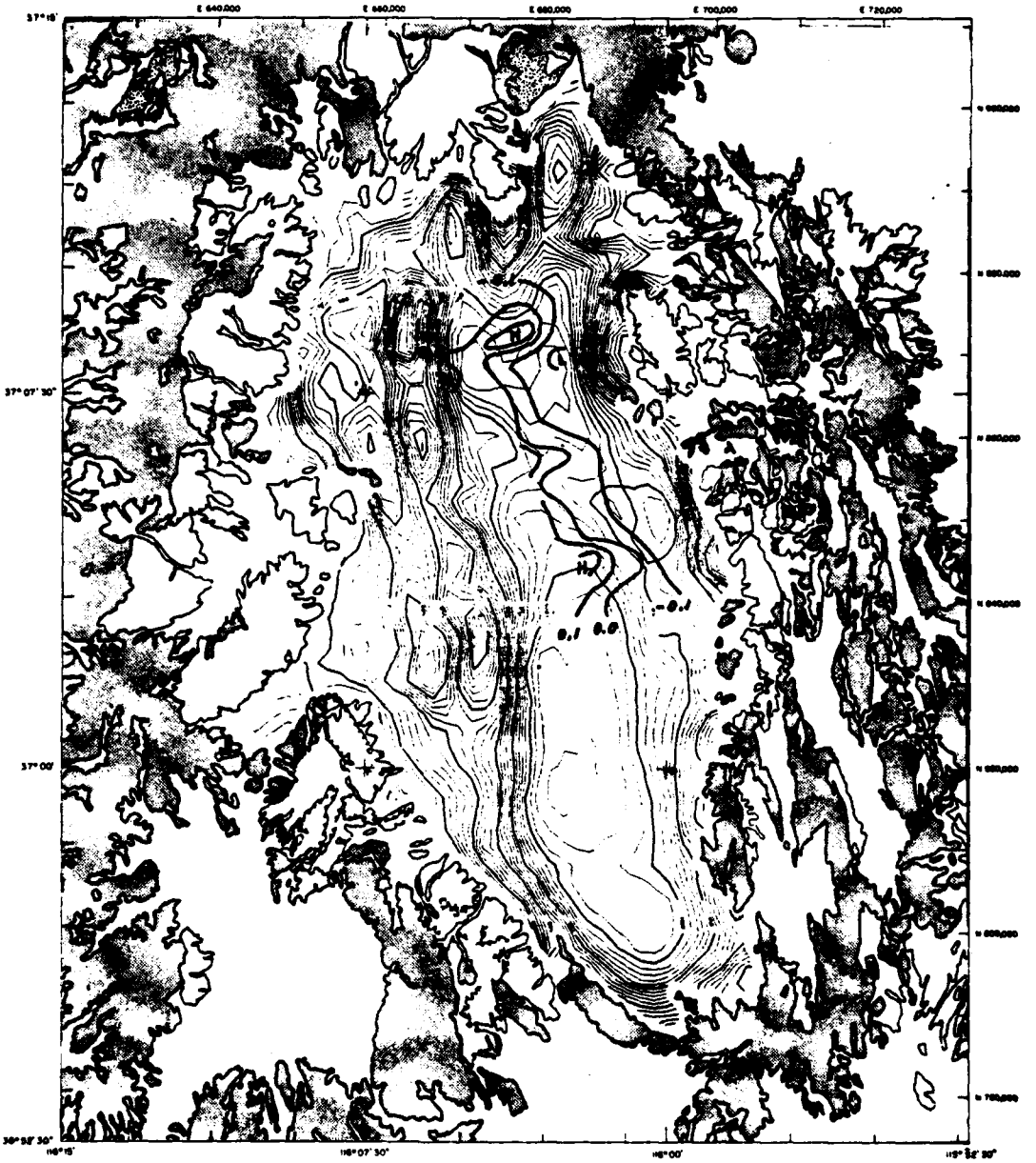


YUCCA FLAT
NEVADA

0 1 2 3 4 5 6
KILOMETERS
0 1 2 3 4
MILES

collocation method. This technique promised to have high accuracy and reasonable computation speed. It is not limited to plain strain theory like the finite difference calculation or high frequency like the asymtotic ray theory, also the solution is not restricted to a limited set of rays or modes.

## DERIVATION OF THE METHOD

In this section a technique introduced into seismology by Aki and Larner (1970), Larner (1970), Bouchon (1973) and Bouchon and Aki (1977), will be developed in a general form. The method assumes a solution in each homogeneous layer or region in terms of a series of plane waves. The boundary conditions between the regions are matched at a finite number of points on the boundaries. In numerical analysis this type of calculation is called an orthogonal basis boundary value collocation scheme. The solution is expanded in an orthogonal basis of known solutions to the partial differential equation and forced to satisfy the boundary conditions at a finite number of points. The interpolatory characteristics of the solution are used to provide an approximate satisfaction of the boundary conditions at unsampled boundary points. Due to certain requirements of the reciprocal method that will be used to apply the explosion source, it is more convenient to develop the method in terms of potentials. From Lame's theorem (Aki and Richards, 1980, p 68), the equations of motion for a homogeneous elastic medium will yield solutions in terms of a scalar and a vector potential.

$$\text{1a)} \qquad \underline{u} = \nabla\phi + \nabla \times \underline{\Psi},$$

$$\text{1b)} \qquad \nabla \cdot \underline{\Psi} = 0,$$

$$1c) \quad \ddot{\phi} = \alpha^2 \nabla^2 \phi ,$$

$$1d) \quad \ddot{\underline{\Psi}} = \beta^2 \nabla^2 \underline{\Psi} .$$

These equations include separate wave equations for compressional, 1c, and shear, 1d, waves. In general the potentials are ambiguously determined and hence are useful only when certain symmetries are present in the formulation.

Plane wave solutions with harmonic time dependence,

$$2) \quad \phi = A \exp\left(-i(\omega t + kx + \eta y \pm \nu z)\right),$$

will be assumed. In the case of a wave incident on a horizontal interface all scattered wave vectors will be contained in the same vertical plane as the incident wave. An alternative statement is that k and $\eta$ are constant for all waves satisfying the boundary conditions. Thus the coordinates may be rotated to eliminate one wavenumber component and the potentials reduced to three scalar potentials, with horizontally polarized shear (SH) motion uncoupled from compressional (P) and vertically polarized shear (SV) motion (Aki and Richards, 1980, p 215). In the case of an interface with topography variable in the x-direction only and incident waves making the angle $\Omega$ with that direction, the y wavenumber component, $\eta$ , will remain constant, but the x wavenumber component, k , will couple over the entire wavenumber spectral range. The constancy of $\eta$ permits the specification of a vertical plane for each value of k which will contain the scattered waves. The P-SV and SH motions will uncouple for

each $k$ and only three scalar potentials are required (Larner, 1970, p 25-44). The new propagation coordinates are:

$$3a) \quad K = (k^2 + \eta^2)^{1/2},$$

$$3b) \quad |Kx'| = |kx + \eta y|,$$

$$3c) \quad K = K \cos(\Omega),$$

$$3d) \quad \underline{r'} = \underline{\underline{R}}\,\underline{r} = \begin{pmatrix} x' \\ y' \\ z \end{pmatrix} = \begin{pmatrix} \cos(\Omega) & \sin(\Omega) & 0 \\ -\sin(\Omega) & \cos(\Omega) & 0 \\ 0 & 0 & 1 \end{pmatrix} \begin{pmatrix} x \\ y \\ z \end{pmatrix}.$$

The displacements are written in terms of the required potentials as:

$$4a) \quad U_1(x', y', z) = \frac{\partial \phi}{\partial x'} - \frac{\partial \Psi}{\partial z},$$

$$4b) \quad U_2(x', y', z) = \frac{\partial \chi}{\partial z},$$

$$4c) \quad U_3(x', y', z) = \frac{\partial \phi}{\partial z} + \frac{\partial \Psi}{\partial x'}.$$

In each homogeneous region the general solution will be expanded in an infinite number of plane wave contributions:

$$5a)\quad \phi(x,y,z,k) = \left[A_1(k)\exp(-i\nu z) + A_2(k)\exp(i\nu z)\right]\exp(-i(kx+\eta y)),$$

$$5b)\quad \psi(x,y,z,k) = \left[A_3(k)\exp(-i\gamma z) + A_4(k)\exp(i\gamma z)\right]\exp(-i(kx+\eta y)),$$

$$5c)\quad \chi(x,y,z,k) = \left[A_5(k)\exp(-i\gamma z) + A_6(k)\exp(i\gamma z)\right]\exp(-i(kx+\eta y)).$$

the term, $\exp(-i\omega t)$, is suppressed in all the following equations.

The boundary conditions to be satisfied are continuity of displacement and traction normal to the boundary at each internal interface. The normal traction is set to zero on the free surface. The general solutions for the displacement and stress components are:

$$6a)\quad u_i(x,y,z) = \int R_{ki}\, e_{k\ell}\, A_\ell \exp(-ikx)\, dk,$$

$$6b)\quad \sigma_{ij}(x,y,z) = \int R_{ki}\, R_{jm}\, f_{km\ell}\, A_\ell \exp(-ikx)\, dk,$$

$$i,j,k,m = 1,2,3, \quad \ell = 1,2,\ldots,6.$$

The normal tractions at an interface are obtained from the inner product of the unit normal vector and the stress tensor or the operator,

$$7)\quad F_{i\ell} = f_{ij\ell}\,\hat{n}_j(\xi), \quad i,j = 1,2,3, \quad \ell = 1,2,\ldots,6.$$

The unit normal is a function of the interface topography, $\xi(x)$. The operators $\underline{e}$, $\underline{f}$ and $\underline{F}$ are exponential functions of y, z, k and $\eta$, as well as the elastic constants and density. They are wavenumber domain spacial derivative operators as required by 4. The internal

boundary conditions require that these quantities be evaluated on each side of the interface. In matrix form this is expressed;

$$8)\quad \begin{bmatrix} \underline{u} \\ \underline{\underline{\sigma}}\cdot\hat{\underline{n}} \end{bmatrix} = \int \begin{bmatrix} \underline{\underline{R}}^T \underline{\underline{e}} \\ \underline{\underline{R}}^T \underline{\underline{F}} \end{bmatrix} \begin{bmatrix} \underline{A} \end{bmatrix} \exp(-ikx)\, dk \ .$$

The integration over k must be performed numerically, so the Fourier transform is replaced by a Fourier series of finite length (rectangle rule integration or discrete Fourier transform). This results in a periodic repetition of the interface topography with fundamental wavelength, L. The collocation technique evaluates the displacements and tractions at a finite number of points in the interval [0,L]. The space and spectral discretizations are:

$$9a)\quad x_n = \Delta x\, n, \quad n = 0, 1, \ldots, N-1,$$

$$9b)\quad k_m = \frac{2\pi}{L} m, \quad m = 0, \pm 1, \ldots, \pm \frac{(M-1)}{2}$$

At this point the notation required becomes rather complex. In addition to the tensor indices we now have indices associated with the series summation and collocation points. The differing layers of the model must also be distinguished. Figure 23 is introduced to clarify some of the additional notation. The superscripts, i, will serve to identify interfaces starting with the free surface, i=1. The superscripts, l, refer to the layers, where layer l is just below

Fig. 23. An introduction to the indicial notation used to identify the homogeneous regions and interfaces used in the Aki-Larner technique derivation.

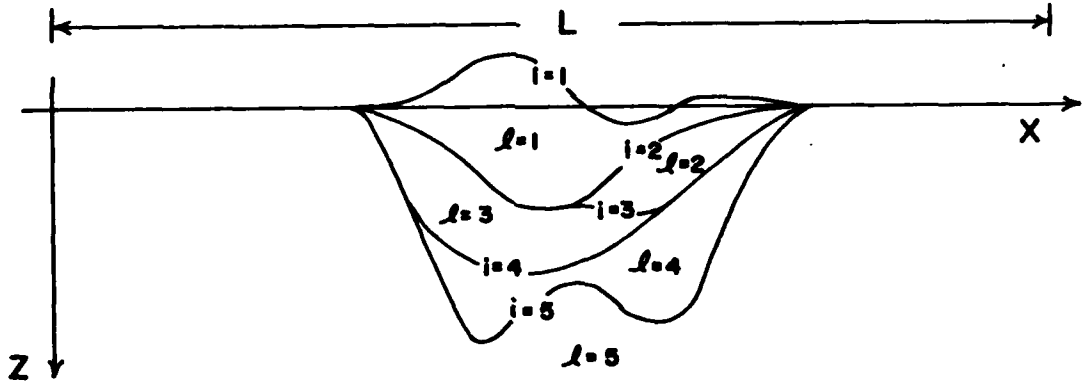


| | |
|---|---|
| $i = 1, 2, 3, 4, 5$ | INTERFACE INDICES |
| $\ell = 1, 2, 3, 4, 5$ | LAYER INDICES |
| $\zeta_{i(x)}$ | INTERFACE TOPOGRAPHY |
| $v_P^\ell,\ v_S^\ell,\ \rho^\ell$ | P AND S WAVE VELOCITIES AND DENSITIES FOR EACH LAYER |
| $L$ | MODEL REPETITION DISTANCE |

INTERFACE TOPOGRAPHY IS INVARIANT IN THE Y-DIRECTION (OUT OF THE PAGE)

## MODEL STRUCTURE AND NOTATION

the 1th interface. There are P layers and interfaces. For the discrete space specified by 9, equation 8 may be written,

$$10) \quad \underline{U}^i = \underline{\underline{G}}^i \underline{A}^i .$$

In 10, $\underline{U}^i$ is the $6 \cdot N$ vector of displacements and tractions evaluated at the discrete interface points, $\underline{\underline{G}}^i$ is the $6 \cdot M \times 6 \cdot N$ matrix which transforms the discrete k, $6 \cdot M$ vector of potential coefficients, $\underline{A}^i$, in layer i. In the simplest application we will set M=N for a square linear system of equations. A similar equation exists in layer i + 1 at the same interface, which would be the (i + 1)th interface. If the $\underline{U}^i$ and $\underline{U}^{i+1}$ vectors evaluated at $\xi^{i+1}(x)$ are set equal the result may be solved for $\underline{A}^i$ in terms of $\underline{A}^{i+1}$,

$$11) \quad \underline{A}^i = \left[ \underline{\underline{G}}^i \right]^{-1} \underline{\underline{G}}^{i+1} \underline{A}^{i+1} .$$

The product matrix is the propagator matrix for this problem. The product of each such propagator at all interfaces,

$$12) \quad \underline{\underline{J}} = \underline{\underline{G}}^1 (\xi^1) \prod_{j=2}^{P} \left[ \underline{\underline{G}}^{j-1} (\xi^j) \right]^{-1} \underline{\underline{G}}^j (\xi^j) ,$$

results in a relationship between the displacement and stress at the free surface and the wave field in the half-space, layer P, given by

$$13) \quad \underline{U}^1 = \underline{\underline{J}} \underline{A}^P$$

An incident body wave is specified in the half space, then the free surface boundary conditions of vanishing stress are used to solve for the reflected waves in the halfspace thus completely specifying $\underline{A}^P$.

The $\underline{A}^i$ vectors in each other layer are found by application of the propagator matrices in equation 11.

Larner (1970) introduced a variation of the collocation method which is of considerable importance. The partitions of $\underline{U}$ and the columns of the partitions of $\underline{\underline{G}}$ are Fourier transformed over N space samples. The boundary conditions are then specified in the wavenumber domain. The resulting Fourier series is then truncated to $M \leq N$ points and the equations solved as before, except for an inverse transform to convert the displacements and tractions back to the space domain. For M=N this procedure is identical to the space domain collocation, otherwise it is a least squares solution of the collocation equation.

The wavenumber spectrum for this problem possesses poles corresponding to surface wave modes. Integration along the real wavenumber axis will result in numerical instability. The inclusion of viscoelastic attenuation will remove the poles from the real k - axis and permit integration along contours parallel to that axis. The attenuation may be specified as an average temporal Q for the model with a complex frequency and wavenumber or as an average spatial Q with complex velocity and wavenumber. In order that the proper phase relationships exist across the incident wavefront the imaginary part of the horizontal wavenumber, in all layers, must equal the imaginary part of the horizontal wavenumber of the incident wave (Aki and Larner, 1970). The imaginary part of the frequency is

determined by,

$$14) \quad Im(\omega) = i 2\pi |f| / (2Q),$$

for a temporal Q.

The numerical accuracy of the solution technique is very high. If the interface topography is adequately sampled, so that no aliasing occurs (i.e., the Fourier expansions are convergent), then the solutions are computed with accuracy equivalent to the rounding error of the computer. The simultaneous equations in 11 and 13 are usually well conditioned, so that little loss of significance occurs in their solution. A different form of error results from the so called Rayleigh ansatz (Aki and Larner, 1970). For interface slopes greater than about $60^{o}$, the solution should contain multiply reflected waves which are not provided for in the specification. In practice this error has not been very important.

## SOURCE-RECEIVER RECIPROCITY

The Aki-Larner formulation may be used to calculate the response of an irregularly layered model to an incident plane body wave. The theory must be extended to include point explosive sources. Bouchon and Aki (1977) demonstrate how a discrete wave-number representation can be used to calculate the near field response of complex sources in irregularly layered structures. Because of our interest in teleseismic measurements and the far field response, a more efficient procedure results from the use of the seismic reciprocity theorem (Bouchon, 1976) and the plane wave response. The reciprocity theorem, after White (1965), states:

> If, in a bounded, inhomogeneous, anisotropic elastic medium, a transient force f(t) applied in some particular direction at some point P creates at a second point Q a transient displacement whose component in some direction is u(t), then the application of the same force f(t) at point Q in direction will cause a displacement at point P whose component in the direction is u(t).

The response of a point dilatational source, located at P in layer j, at a point Q, in the half space layer n, can be derived from the consideration of a force F at Q. The force, F, is directed along the ray connecting P and Q and results in a vector displacement $\underline{U}(P)$ at P. By the reciprocity theorem the same force at P, in the displacement direction, will produce a displacement $\underline{U}(Q)$ in the ray direction (P-wave motion). The dilatational source is modeled by three orthogonal force dipoles. To obtain the displacement at Q, in

ray direction, we compute the dilatation at P and modulate by M, the desired source moment spectrum (von Seggern and Blandford, 1972).

$$15) \quad \underline{u}(Q) = \frac{M}{F}\left(\frac{\partial u_1(P)}{\partial x} + \frac{\partial u_2(P)}{\partial y} + \frac{\partial u_3(P)}{\partial z}\right).$$

We substitute the potential at P due to a plane wave incident along the desired ray into 15 to obtain,

$$16) \quad \underline{u}(Q) = \frac{-\omega^2}{\alpha_j^2} \frac{M}{F}\left(A_1^j \exp(-i\nu^j z) + A_2^j \exp(i\nu^j z)\right) \exp(-i(kx+\eta y)).$$

Equation 16 provides the teleseismic P-wave motion due to the explosive source. The efficiency of this method derives from the ability to calculate the response from any source location for a given ray with only one model plane wave response calculation. In contrast, the discrete wavenumber source representation would require a re-evaluation of the propagator matrices for each source location.

## A THEORETICAL RESPONSE PROFILE

The procedure outlined in the previous sections has been coded in FORTRAN IV. The program has been tested on a number of simple problems including flat layered and gently perturbed structures. Working versions exist for both the Control Data Corporation 6600 and the Digital Equipment Corporation VAX 11-780.

The scattering hypothesis can be tested on a profile taken from the Yucca Flat model. The first calculation has been done on an east-west profile at a latitude of $37^{o}$ 02' N. The basin has very little variation parallel to strike and good structural control is provided by geophysical surveys in that area. In figure 24, the observed $m_b$ variation south of $37^{o}$ 05' is plotted along with a profile taken from Goforth, et. al. (1979). The calculated, one Hertz P-wave amplitude variation for sources distributed along the profile in figure 24 should agree with this profile if the hypothesis is correct.

The geologic structure of the profile can be approximated by four layers. The Paleozoic limestone can be modeled as a half space which is faulted at a low angle ($\sim 50^{o}$) on the west by the Carpetbag fault system so that an asymmetrical basin is formed. The basin is filled with Tertiary volcanics and Quaternary alluvium. The water table at a depth of about 500 meters divides the volcanics into saturated and dry units. The alluvium is entirely free of water.

Fig. 24. A profile across Yucca Flat, Nevada at a latitude of 37° 02' N showing the observed $m_b$ variation. The geological structure was taken from Goforth, et. al (1979).

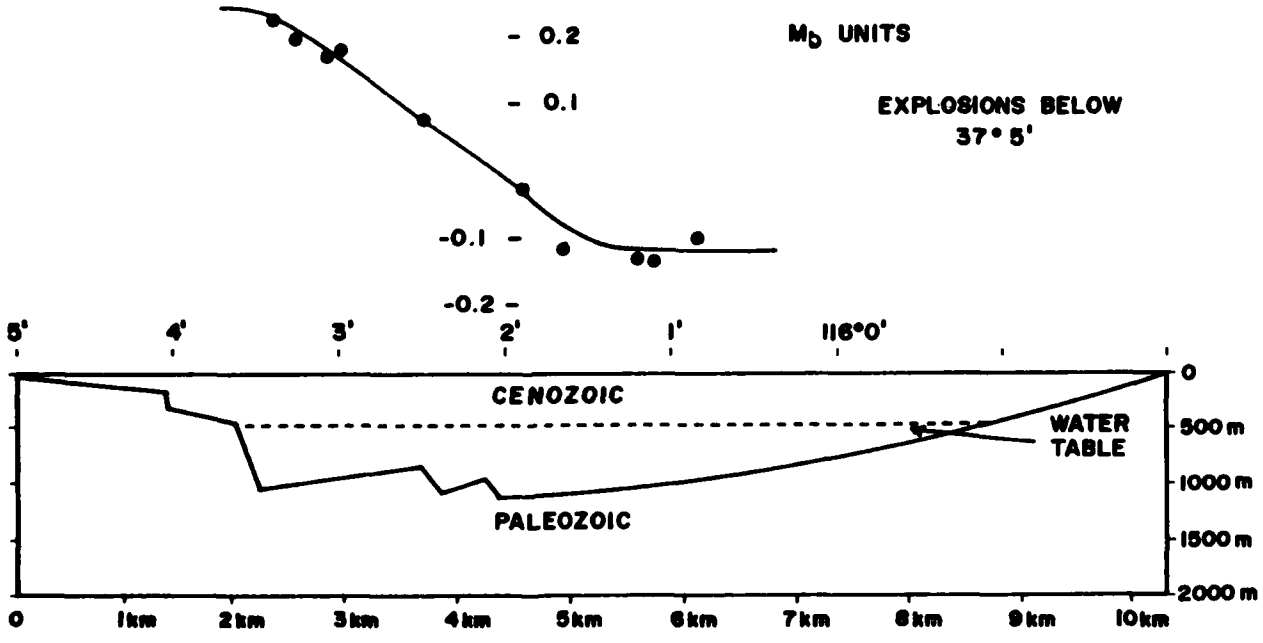
- 0.2
- 0.1
-0.1
-0.2
$M_b$ UNITS
EXPLOSIONS BELOW
37° 5'
5'
4'
3'
2'
1'
116°0'
CENOZOIC
WATER
TABLE
PALEOZOIC
0
500 m
1000 m
1500 m
2000 m
0
1km
2km
3km
4km
5km
6km
7km
8km
9km
10km

Average velocities and densities for these units were derived from well logs as contained in Table III. The profile is shown at the bottom of figure 25.

The response due to sources at the four locations shown in figure 25, for P-wave angles of emergence between -40 and 40 degrees (west and east) and propagation vectors within the model plane, were computed. An average Q of 50 was assumed at a frequency of one Hertz and a source depth of 0.8 kilometer was utilized. This calculation resulted in a polar radiation pattern of amplitude vs. emergence angle for each shot point as shown at the top of figure 25.

In order to model the averaging process inherent in the magnitude calculation the median amplitude of each shot will be compared. The median is plotted as a semi-circular arc on each radiation pattern. The ratio of median amplitudes between shots on the west (near the Carpetbag fault) and those on the east is 2.4. This corresponds to an $m_b$ variation of 0.4 magnitude units, in good agreement with the profile in figure 24.

The results of figure 25 are limited in several important ways. No out of plane rays are considered and only a single narrow frequency band was studied. Future calculations will include the out of plane rays and a time domain synthesis over a broader (one or two octave) frequency band. The radiation patterns display a rather complicated variation which may be observable in teleseismic observations. This phenomena can only be studied by examination of a number of specific shots and receivers, with spectral and time domain modeling of the observed P-waves.

TABLE III

VELOCITY STRUCTURE OF YUCCA FLAT, NEVADA

| Stratagraphic Unit | P-Wave Velocity | S-Wave Velocity | Poisson's Ratio | Density |
|---|---|---|---|---|
| QAL | 1.34 | 0.64 | 0.35 | 1.80 |
| TV (Dry) | 2.14 | 1.14 | 0.30 | 1.80 |
| TV (Wet) | 3.00 | 1.60 | 0.30 | 1.80 |
| PZ | 4.57 | 2.64 | 0.25 | 2.50 |

Units are km/sec and gm/cc.

Fig. 25. Polar radiation diagrams of teleseismic P-wave amplitude as a function of emergence angle for shots distributed across Yucca Flat, Nevada.

# P-WAVE AMPLITUDE VARIATION

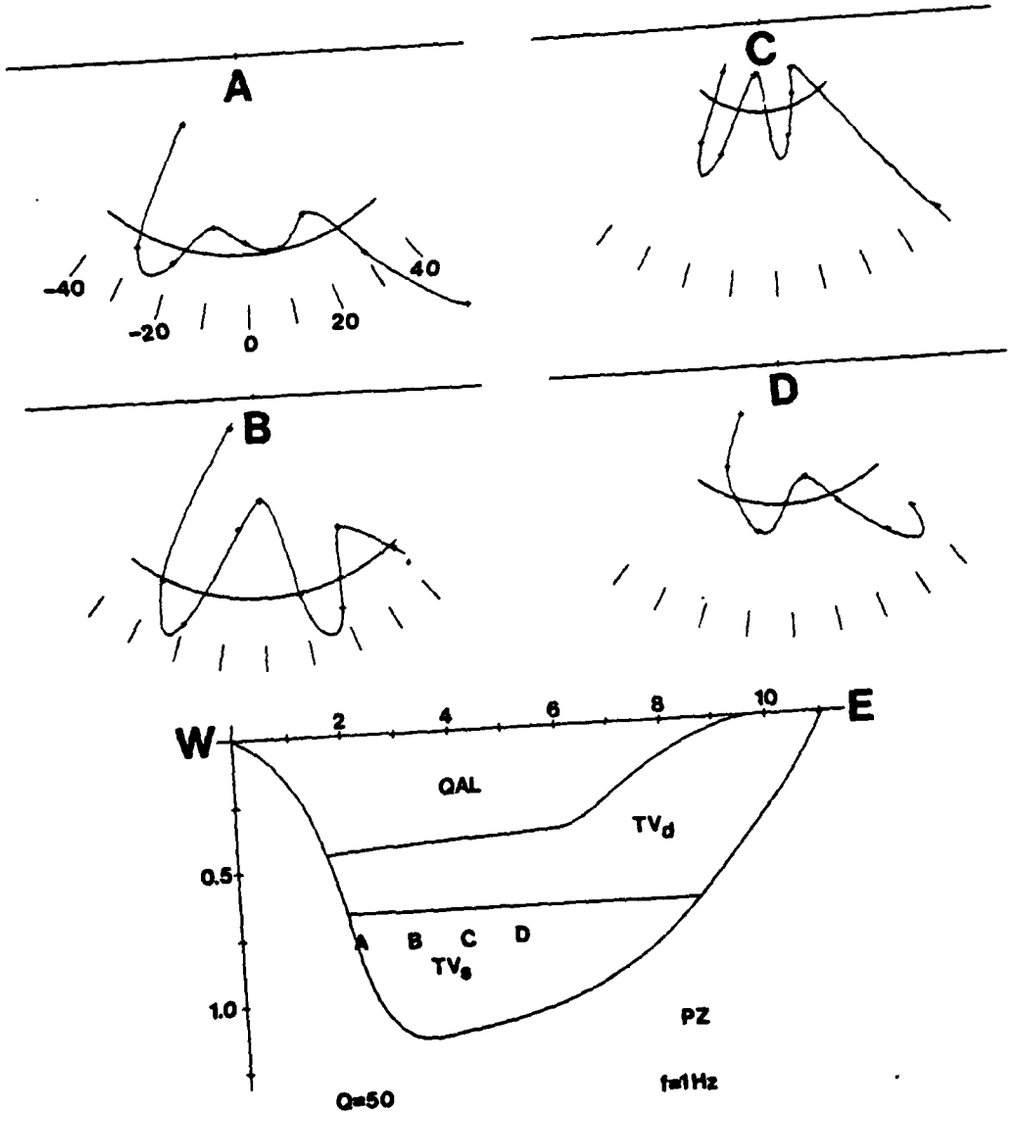

# CONCLUSIONS

The results of this investigation indicate that it is possible to model the effects of near-source scattering on teleseismic signals from Yucca Flat, Nevada. This is made possible by the existence of a reasonably accurate geophysical model of the geologic structure developed from gravity, borehole and seismic exploration. The Aki-Larner technique is a computationally effective means of performing response calculations for quite complicated models, such as the one exhibited here. Future efforts will concentrate on time domain waveform synthesis and detailed source receiver pair models. It is also possible to model other profiles across the valley. Similar studies on other test sites can guide the improvement of earthquake-explosion discrimination and yield estimation.

## REFERENCES

Aki, K. and K. Larner, Surface motion of a layered medium having an irregular interface due to incident plane SH waves, J. Geophys. Res., 75, pp. 933-954, 1970.

Aki, K. and P. G. Richards, Quantitative Seismology: Theory and Methods Vols. I and II, Freeman, San Francisco, 1980.

Atwater, T., Implications of plate tectonics for the Cenozoic tectonic evolution of western North American, Geol. Soc. Am. Bull., 81, pp. 3513-3535, 1970.

Bouchon, M., Effect of topography on surface motion, Bull. Seis. Soc. Am., 63, pp. 615-632, 1973.

Bouchon, M., Discrete Wavenumber Representation of Seismic Wave Fields with Application to Various Scattering Problems, Ph.D. Thesis, Massachusetts Institute of Technology, 1976.

Bouchon M., Teleseismic body wave radiation from a seismic source in a layered medium, Geophys. J. Roy. Astr. Soc., 47, pp. 515-530, 1976.

Bouchon, M. and K. Aki, Near-field of a seismic source in a layered medium with irregular interfaces, Geophys. J. Roy. Astr. Soc., 50, pp. 669-684, 1977.

Burkhard, N. and D. D. Jackson, Application of stabilized linear inverse theory to gravity data, J. Geophys. Res., 81, pp. 1513-1518, 1976.

Cordell, L., Sedimentary facies and gravity anomaly across master faults of the Rio Grande rift in New Mexico, Geology, 7, pp. 201-205, 1979.

Cordell, L. and R. B. Henderson, Iterative three-dimensional solution of gravity anomaly data using a digital computer, Geophys., 33, pp. 596-601, 1968.

Doherty, S. M. and J. F. Claerbout, Structure independent velocity estimation, Geophys., 41, pp. 850-881, 1976.

Dohr, G. P. and P. K. Stiller, Migration velocity determination: Part II. Applications, Geophys., 40, pp. 6-16, 1975.

Dorman, L. M. and B. T. R. Lewis, The use of nonlinear functional expansions in calculation of the terrain effect in airborne and marine gravimetry and gradiometry, Geophys., 39, pp. 33-38, 1974.

Eaton, G. P., R. R. Wahl, H. J. Prostka, D. R. Mabey and M. D. Kleinkopf, Regional gravity and tectonic patterns: Their relation to late Cenozoic epeirogeny and lateral spreading in the western Cordillera, in Smith, R. B. and G. P. Eaton, eds., Cenozoic Tectonics and Regional Geophysics of the Western Cordillera, Geol. Soc. Am. Mem. 152, pp. 51-91, 1978.

Eckel, E. B., ed., Nevada Test Site, Geol. Soc. Am. Mem. 110, 1968.

Felch, R. N., A Three-Dimensional Gravity Model of Basin Structure, Yucca Flat, Nevada, M.S. Thesis, Texas Christian University, 1979.

Goforth, T., J. Ferguson and E. Herrin, Crustal Studies of the Nevada Test Site: Interpretation of S.M.U. line E-3, Final Technical Report to the Air Force Office of Scientific Research, Contract Number: F49620-77-C-0216, Southern Methodist University, 1979.

Gunn, P. J., Linear transformations of gravity and magnetic fields, Geophys, Prosp., 23, pp. 300-312, 1975.

Hazelwood, R. M., D. L. Healey and C. M. Miller, U.S. Geological Survey Investigations of Yucca Flat, Nevada Test Site Part B--Geophysical Investigations, Tech. Letter, NTS-45, 1963.

Healey, D. L., Gravity and seismic study of Yucca Flat, Nevada Test Site, Nye County, Nevada, in Mining Geophysics Vol. I, Society of Exploration Geophysics, 1966.

Healey, D. L., Application of gravity data to geologic problems at Nevada Test Site, in Eckel, E. B., ed., Nevada Test Site, Geol. Soc. Am. Mem. 110, 1968.

Larner, K., Near-receiver scattering of Teleseismic Body Waves in Layered Crust-Mantle Models Having Irregular Interfaces, Ph.D. Thesis, Massachusetts Institute of Technology, 1970.

Mueller, R. A. and J. R. Murphy, Seismic characteristics of underground nuclear detonations: Part I. Seismic spectrum scaling, Bull. Seis. Soc. Am., 61, pp. 1675-1692, 1971.

Nelder, J. A. and R. Mead, A simplex method for function minimization, Comp. J. 7, pp. 308-313, 1965.

Oldenburg, D. W., The inversion and interpretation of gravity anomalies, Geophys., 39, pp. 526-536, 1974.

O'Neil, R., Function minimization using a simplex procedure, Appl. Stat., 20, pp. 338-345, 1971.

Parker, R. L., The rapid calculation of potential anomalies, Geophys. J. Roy. Astr. Soc., 41, pp. 447-455, 1972.

Parker. R. L. and S. P. Huestis, The inversion of magnetic anomalies in the presence of topography, J. Geophys. Res., 79, pp. 1587-1593, 1974.

Peters, L. J., The direct approach to magnetic interpretation and its practical application, Geophys, 18, pp. 290-320, 1949.

Satlegger, J. W., Migration velocity determination: Part I. Philosophy, Geophys., 40, pp. 1-5, 1975.

Schultz, P. S. and J. F. Claerbout, Velocity estimation and downward continuation by wavefront synthesis, Geophys., 43, pp. 691-714, 1978.

Shepard, D., A two-dimensional interpolation function for computer mapping of irregularly spaced data, Geography and Properties of surfaces series, n 15, Harvard University, 1968.

Smith, R. A., A uniqueness theorem concerning gravity fields, Proc. Comb. Phil. Soc., 57, pp. 865-870, 1961.

Tikhonov, A. N., Solution of incorrectly formulated problems and the regularization method, *Soviet Math. Dok.*, 4, pp. 1035-1038, 1963.

Tikhonov, A. N., V. B. Glasko, O. K. Litvinenko and V. P. Melikhov, Analytic continuation of a potential in the direction of disturbing masses by the regularization method. Izv. Earth Phys., 12, pp. 30-48, 1968.

Tsirul'skiy, A. V., The reduction of observed potential fields to a single level, Izv. Earth Phys., 3, pp, 85-89, 1968.

Tsirul'skiy, A. V. and L. Ya. Ospishcheva, An algorithm for the reduction of observed potential field values to a common level, Izv. Earth Phys., 4, pp. 105-111, 1968.

Von Seggern, D. and R. Blandford, Source time functions and spectra for underground nuclear explosions, Geophys. J. Roy. Astr. Soc., 31, pp. 83-97, 1972.

White, J. E., Seismic Waves, McGraw-Hill, New York, 1965.

# LAJITAS SEISMIC STATION

EUGENE HERRIN
GEOPHYSICAL LABORATORY
SOUTHERN METHODIST UNIVERSITY

# LAJITAS SEISMIC STATION
## Site Report

### Introduction

A number of unpublished seismic noise studies during the last 20 Years, mostly by E. Herrin, W. Guyton, J. Waugh and B. Brooks, have shown that sites in the limestone desert region just west of Big Bend National Park, Brewster County, Texas, show very low short-period noise levels. Peak-to-peak displacements at the surface in the absence of wind or other obvious disturbances have amplitudes less than $10^{-9}$ meter at a frequency of 1 Hz. and less than $10^{-10}$ meter at 10 Hz.

The area studied is very sparsly settled and has only one paved highway which is lightly travelled. The nearest railroad is 40 miles to the west and has only a few trains per week. The nearest heavily travelled highway and railroad, and the nearest town of any size - Alpine, Texas - is about 75 miles to the north of the area. We have obtained a lease on private land in this area and have established the Lajitas Seismic Station which is described in this report.

## Location

The Lajitas Station is located about 10 miles by road northeast of Lajitas, Texas, a small village on the Rio Grande just west of Big Bend National Park. The site location is shown as a circled dot just north of Terlingua Sinkhole on Figure 1, and is on land owned by Mr. Glen Pepper. Pertinent information on the location is as follows:

Coordinates: 29 29' 02"
103 40' 01"

Elevation: 3325 feet above mean sea level

The paved road (Texas FM 170) and graded road to Pepper's hacienda about ¼ mile south-southeast of the site can be seen in Figure 1. These roads provide all-weather access to the site and to Lajitas, Texas, to the west and Study Butte, Texas, to the east. The remoteness of the site is important in that man-made noise is minimal but leads to certain logistical problems. For example, the nearest scheduled airline service is to be found at Midland, Texas, 250 miles to the northeast and El Paso, Texas, 300 miles to the northwest.

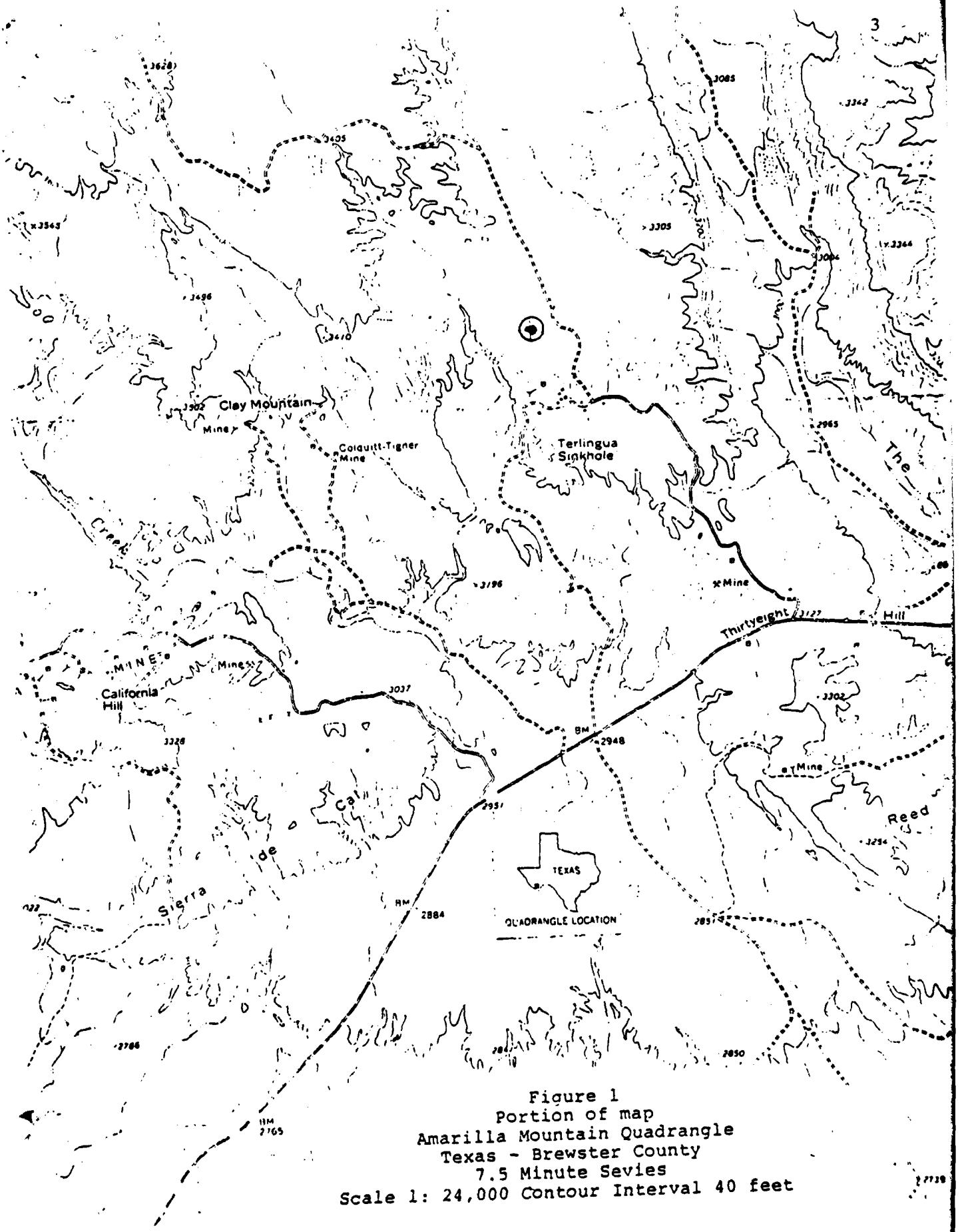


Figure 1
Portion of map
Amarilla Mountain Quadrangle
Texas - Brewster County
7.5 Minute Sevies
Scale 1: 24,000 Contour Interval 40 feet

## Geology

The Lajitas site lies on the top of the Santa Elena formation, a massive limestone unit of Cretaceous (Upper Albian) age. Cretaceous formations beneath the site are listed under the heading "Big Bend National Park Area" in the correlation table shown in Figure 2. Table 1 gives thicknesses and brief descriptions of the underlying Cretaceous formations as seen in exposures in Santa Elena Canyon (SEC) about 12 miles southeast and The Solitario (SOL) about 8 miles northwest of the site. The Santa Elena Canyon data are from Maxwell et. al., 1967, Univ. of Texas Publc. 6711, Buv. of Economic Geology, and The Solitario data are from Herrin, 1958, Geology of the Solitario area, Trans-Pecos Texas, Harvard University.

From Table 1 it can be seen that the site is underlain by more than 3600 feet of lower Cretaceous sediments consisting predominantly of massive limestones which should have P-wave velocities in excess of 5 km/sec.

The uppermost 800 ft consists of the massive, dense Santa Elena formation. Beneath the basal Cretaceous conglomerate (Shut Up formation) there are several thousand feet of folded Paleozoic sediments, mostly siliceous shales with some chert and limestone, underlain by a Cambrian and older basement complex.

The site is on a horst bounded on the east by a normal fault on the west side of the Long Draw graben and represented by the fault-line scarp seen on Figure 1 about ½ mile east of

Table 1

| Formation | Thickness (feet) SEC | SOL | Description |
|---|---|---|---|
| Santa Elena | 740 | 820 | Massive hard limestone with bedded chert |
| Sue Peaks | 265 | 187 | Marly limestone - Thin to medium bedded |
| Del Carmen | 465 | 685 | Massive, hard, cherty rudistid limestone |
| Telephone Canyon | 135 | 190 | Nodular limestone and marl- thin to medium bedded |
| Maxon | 0-10 | 0 | Calcareous sandstone |
| Glen Rose | ? | 1154 | Alternating units of massive limestone and highly fossiliferous marl |
| Yucca | ? | 482 | Sandy limestone and dolomite grading into massive limestone at top |
| Shut Up | ? | 100 | Chert boulder basal conglomerate |

| SYSTEM | EUROPEAN STAGES | | REFERENCE SEQUENCE FOR WESTERN INTERIOR | SERIES | GROUP | BIG BEND NATIONAL PARK AREA | RIO GRANDE EMBAYMENT OF SOUTHWEST TEXAS (Surface and Subsurface) | CENTRAL TEXAS | NORTHEAST TEXAS (Surface and Subsurface) |
|---|---|---|---|---|---|---|---|---|---|
| CRETACEOUS | MAESTRICHTIAN | | Fox Hills Sandstone | GULFIAN | TOMILLO | Javelina Formation Contains dinosaur bones, silicified wood, and coal beds | Escondido Formation | Kemp Clay | Kemp Clay |
| | | | | | | | Olmos Formation | Corsicana Marl | Corsicana Marl |
| | | | | | | | Upper San Miguel Formation | | Nacatoch Sandstone |
| | | | Pierre Shale | | | - - - ? - - - | | | |
| | CAMPANIAN | | | | | AGUJA FORMATION: Continental sandstone and shale with Upper Campanian age dinosaur bones | Lower San Miguel Formation | Bergstrom Formation | Neylandville Marl |
| | | | | | | | Anacacho Limestone | Pecan Gap Chalk and Clay | Pecan Gap Chalk |
| | | | | | | | | | Wolfe City Sandstone |
| | | | | | | AGUJA FORMATION: Marine sandstone and shale with *Exogyra ponderosa* and *Texanites* sp. | Upson Clay (with *Exogyra ponderosa* and *Texanites* sp.) | Sprinkle Formation | Lower Taylor Formation |
| | | | Eagle Sandstone | | | | | | Gober Chalk |
| | | | Telephone Creek Formation | | | Pen Formation (with *Exogyra ponderosa*) | Burditt Chalk | Burditt Chalk | |
| | | | | | | | Austin Chalk (with *Exogyra ponderosa*) | Dessau Chalk (with *Exogyra ponderosa*) | Brownstown Marl |
| | SANTONIAN | | Niobrara Formation | | TERLINGUA | BOQUILLAS FORMATION: San Vicente Member (without *Exogyra ponderosa*) | Austin Chalk (without *Exogyra ponderosa*) | Jonah Limestone | Blossom Sandstone |
| | | | | | | | | Vinson Chalk | Bonham Clay |
| | CONIACIAN | | | | | | | Atco Chalk | Dexter Chalk |
| | TURONIAN | | Carlisle Shale | | | BOQUILLAS FORMATION: Ernst Member | Eagle Ford Formation | Eagle Ford Formation | Eagle Ford Formation |
| | | | Greenhorn Limestone | | | | | | Lewisville Formation (volcanics) |
| | CENOMANIAN | | Belle Fourche Formation | | | | | Pepper Formation | Fuller Formation |
| | | | | | | | | | Dexter Formation |
| | | | | | | | | | South Tyler Formation |
| | | | Mowry Shale | | | Buda Limestone | Buda Limestone | Buda Limestone | Buda Limestone |
| | | | | | | Del Rio Clay | Del Rio Clay | Grayson Formation | Grayson Marl |
| | ALBIAN | Upper | Newcastle Sandstone | COMANCHEAN | | Santa Elena Limestone | Georgetown Limestone (undifferentiated) | Georgetown Limestone (undifferentiated) | Main Street Limestone |
| | | | | | | | | | Pawpaw Formation |
| | | | | | | | | | Weno Formation |
| | | | Skull Creek Shale | | | | | | Denton Formation |
| | | | | | | | | | Fort Worth Limestone |
| | | Middle | | | | | Duck Creek Formation (ammonites near base) | | Duck Creek Limestone |
| | | | | | | Sue Peaks Formation | Kiamichi Formation | Kiamichi Formation | Kiamichi Formation |
| | | | Falls River Sandstone | | | Del Carmen Limestone | Fredericksburg (undifferentiated) | Edwards Limestone | Goodland Limestone |
| | | | | | | | | Comanche Peak Limestone | |
| | | | | | | Telephone Canyon Formation | | Walnut Clay | |
| | | | | | | Maxon Sandstone | | Paluxy Sandstone | Paluxy Sandstone |
| | | Lower | Red shale | | | Glen Rose Limestone (undifferentiated) with basal sandstone and conglomerate | Glen Rose Formation (undifferentiated) | Glen Rose Formation (undifferentiated) | GLEN ROSE FORMATION: Mooringsport Formation |
| | | | | | | | | | GLEN ROSE FORMATION: Ferry Lake Anhydrite |
| | | | | | | | | | GLEN ROSE FORMATION: Rodessa Formation |



Figure 2
Correlation Table for Cretaceous Formations
(from Maxwell et al., 1967, Univ. of Texas
Public. 6711, Bur. of Economic Geology)

the circled dot. The horst is bounded on the west by a series of normal faults, mostly down-thrown to the west, culminating in the Well Creek graben which lies just north of California Hill. It is possible that this arrangement of normal faults serves to shield the site from short wave-length surface waves propagating from noise sources which do not lie on the horst.

## Drilling Operations

Dick Baker Drilling Company of Marfa, Texas, began operations at the site on 8 Sept. 1980. Operations, including drilling, setting casing and cementing three holes, were completed on 19 Sept. 1980. The three holes are located with ten-foot spacing on a north-northeast bearing line-of-centers. The north-most hole is labelled number 1; the south-most is number three. Specifications for the holes are given in Table 2.

Table 2

| Hole | (inches) Diameter | (feet) Total Depth | Maximum Inclination |
|---|---|---|---|
| 1 | 9 7/8 | 352 | 2° (at 350 ft) |
| 2 | 7 7/8 | 122 | 1° (at 120 ft) |
| 3 | 9 7/8 | 350 | 1½° (at 350 ft) |

Holes number 1 and 3 were cased and cemented to the bottom with API 7" OD 23# casing. Hole number 2 was cased and cemented to the bottom with API 5" OD N 80 casing.

The holes were air-drilled. No water was encountered in drilling, and no water is present within the casings. Nipples were installed so that 1½ to 2 feet of casing are exposed above the surface with male threads up and protected with suitable caps.

## Facilities

A rectangular concrete pad was poured around the three cased boreholes extending at least 5 feet horizontally from all holes. The site has been graded to provide a parking area for vehicles and trailers, and the road to the site from Pepper's main road has been graded and filled. The site is easily accessible by passenger car.

An adobe hut with approximately 15 ft. x 15 ft. of interior floor space has been constructed adjacent to the concrete pad. Electrical power (110 and 220 volt, single phase) was brought to the site. Three power drops were placed to serve the hut and at least two trailers. Telephone lines were strung (Big Bend Telephone Company) to provide a leased data line to Dallas (SMU campus) and a standard telephone.

A water line was laid from Pepper's main water supply to provide water for use in trailers and for fire protection. A drain system and septic tank was installed so that a camper-trailer could be placed on the site.

## INSTRUMENTATION

Initial tests were begun in December, 1981, using a Teledyne-Geotech 23900 vertical seismometer in the Number 2 Lajitas borehole with a Teledyne-Geotech 42.21 amplifier and resistive damping. This short-period system was designed to give approximately a flat-velocity response to ground motion between 1 Hz. and 10 Hz. A series of tests between January and June, 1981, showed that the resolution of this system was limited by system noise for seismically quiet periods at frequencies above about 5 Hz. On 24 June, 1981, a Geotech "brick" amplifier-prototype GS 43310- using feedback damping was installed at the Lajitas site, replacing the 42.21 amplifier. With this new configuration it was possible to resolve "quiet-period" ambient background noise to frequencies as high as 20 Hz. The response of the system was approximately flat to ground velocity from 2 Hz. to 17 Hz. with the response down 6 dB at 1 Hz. and 3 dB at 20 Hz.

The 23900- "brick" system remained in use at the Lajitas site until Fall, 1982. A typical "quiet-period" displacement background spectrum for Lajitas is shown in Figure 3 in terms of decibels-seismic vs. log frequency. It can be seen that the spectral level is limited by system noise rather than ground displacement for frequencies above about 20 Hz. and displacement power below about -225 dBs. This system noise level was predicted by O.D. Starkey (personal communication) of Teledyne-Geotech based on the design specifications of

Figure 3. Spectra of Lajitas background noise (dots) and Queen Creek noise (x's).

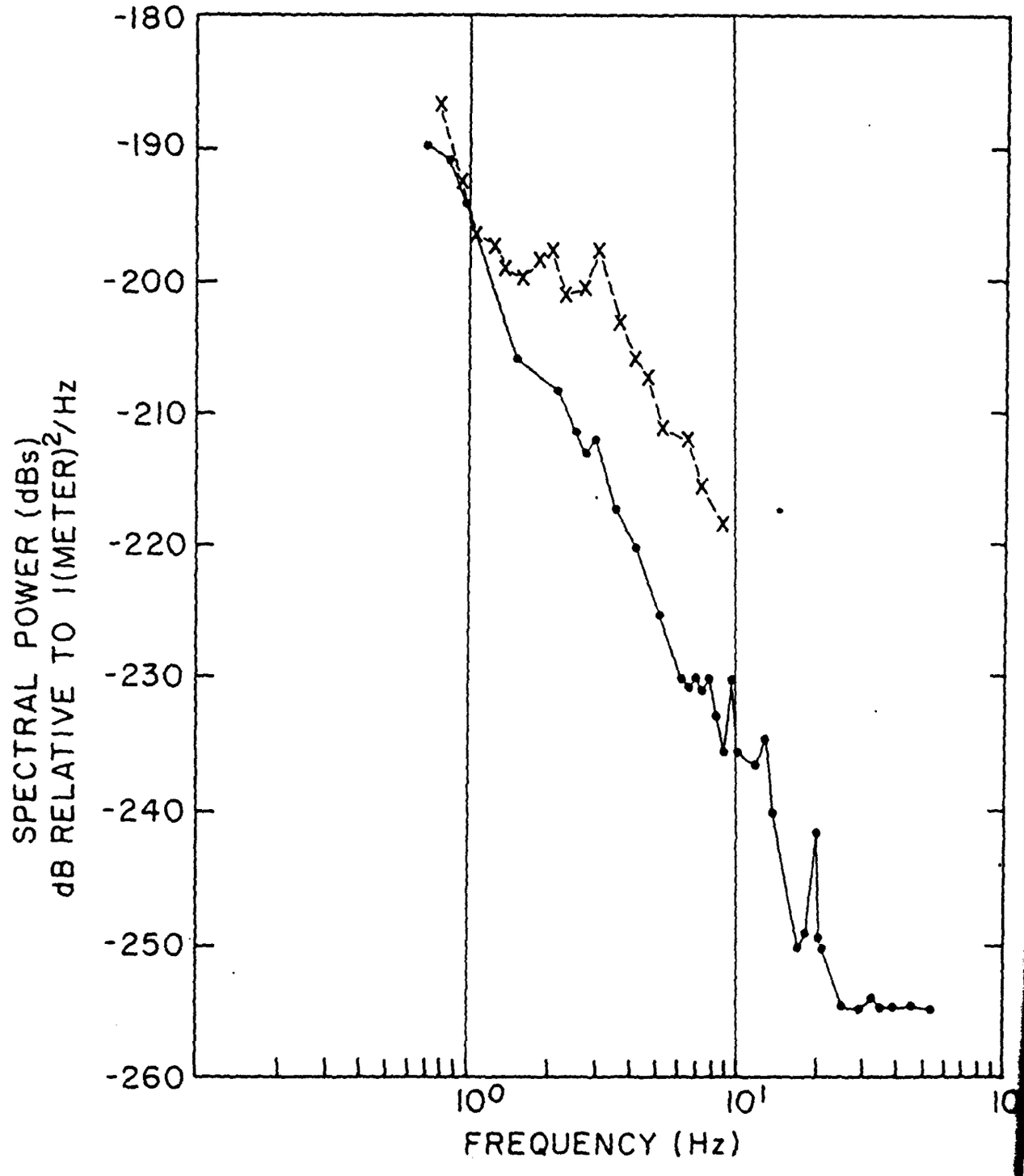

the seismometer and the amplifier.

In June of 1981 it became clear that a more remote site was needed near the Lajitas station. Activity going on around the Lajitas site was substantially increasing the ambient seismic background noise. Also it was planned that AFTAC would take over Lajitas holes numbers 1 and 2 for inclusion in their SOUS (Southern U.S.) tripartite network. On June 7, 1981, a remote site was established in an abandoned mine on Tres Cuevas mountain about 3.6 miles (5.8 km) WSW of the Lajitas site. At the Tres Cuevas site we used a Teledyne-Geotech 18300 short-period vertical seismometer with a "brick" amplifier. The frequency response and system noise levels were essentially the same as for the Lajitas bore-hole system. The Tres Cuevas site is remote from any travelled road; access is by jeep-road with locked gates. The station is powered by solar panels, and the data is transmitted by VHF telemetry to the Lajitas site. "Quiet-period" background noise spectra at the two sites are essentially the same; however, the mine site noise is not affected by activity at the Lajitas station.

In July of 1981 Teledyne-Geotech carried out some preliminary array studies at the Lajitas site and in July of 1982 Sandia National Laboratory began extensive high-frequency array experiments at the site. These experiments are still going on.

In the summer and fall of 1982 AFTAC completed work on their SOUS stations installing 23900 seismometers near

Marathon, Texas; Shafter, Texas; and in hole number 2 at the Lajitas site. A KS 36000 system was installed by AFTAC in Lajitas hole number 1. Under an agreement involving the U.S. Air Force (AFTAC), DARPA and SMU the data from the SOUS stations were made available to us at the Lajitas site. We are currently sending short-period seismic data by FM-telemetry from the Marathon, Shafter, Lajitas and Tres Cuevas (mine) sites back to our laboratory in Dallas. The locations of these stations in the Big Bend region of Texas are shown in Figure 4. The coordinates of the stations are given below:

| | |
|---|---|
| Lajitas | 29° 20' 02" N; 103° 40' 01" W |
| Tres Cuevas (mine) | 29° 18' 59" N; 103° 43' 05" W |
| Shafter | 29° 55' 27" N; 104° 22' 17" W |
| Marathon | 30° 18' 22" N; 103° 15' 17" W |

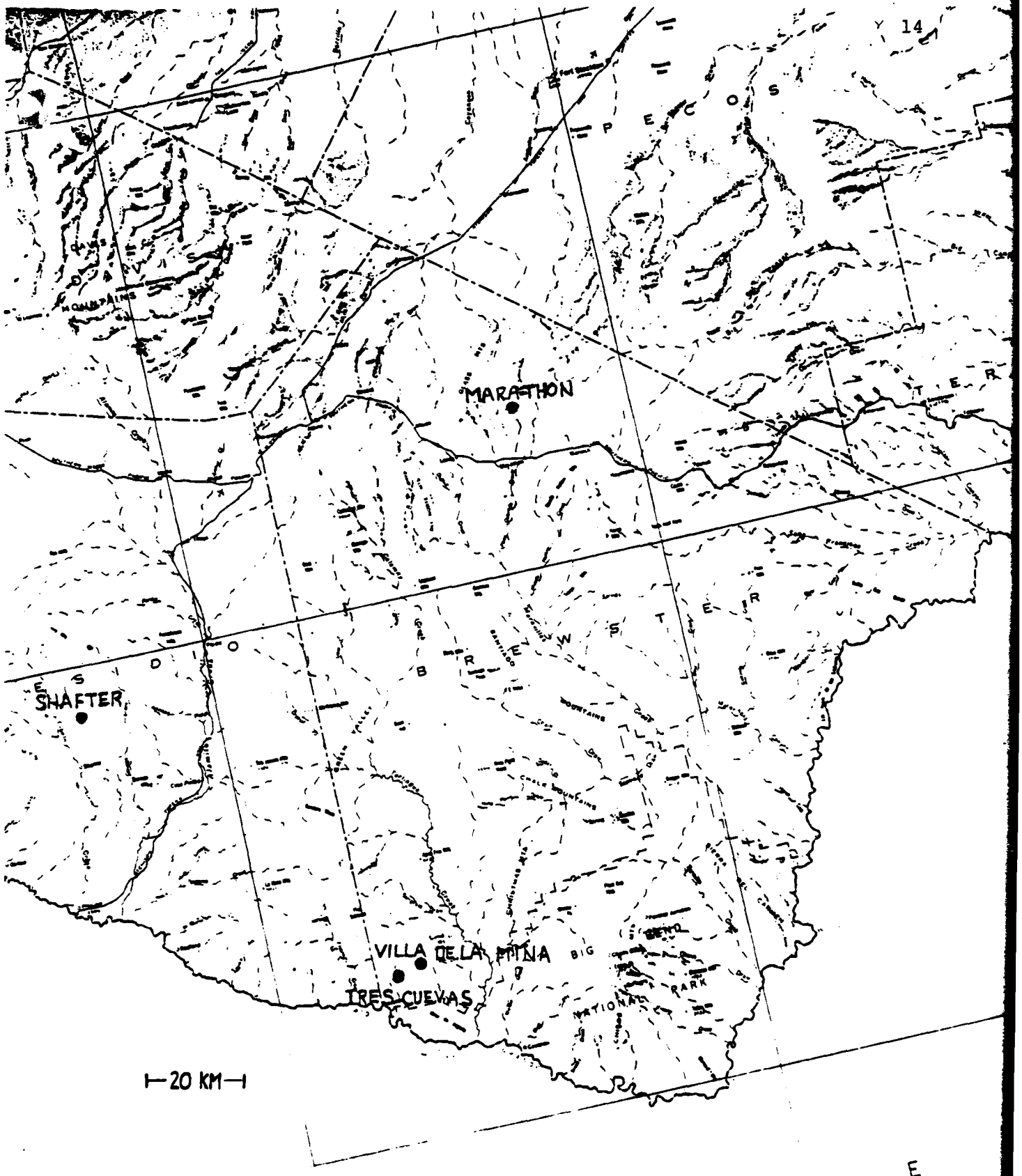


Figure 4. Map of Big Bend area of Texas showing Tres Cuevas, Villa de la Mina, Shafter and Marathon.

## DATA ANALYSIS

Using FM telemetry over leased telephone lines, data has been or is being transmitted from the SOUS sites (plus Tres Cuevas) - see Figure 4 - as well as from KS 36000 seismometers at Albuquerque (ANMO-SRO) and McKinney, Texas, to our laboratory at SMU - see Figure 5. Recently we have elected to substitute data from the KS 36000 located on campus for the McKinney data and so eliminate one of the FM telemetry links. At the price of increased ambient background noise we have, by this change, provided a source of high dynamic range data (not limited by the FM channel) which can give us unclipped digital data for large events which will cause all the other channels to be clipped.

Figure 6 shows the data flow from the field sites to Dallas with the exception of the SMU campus site being substituted for the McKinney, Texas, site.

Data from the FM lines are routed into analog-to-digital conversion system included in a DEC 11/23 dedicated computer as shown in Figure 7. Detection is performed using the Walsh detection algorithm (Goforth and Herrin, Bull. Seismol. Soc. Amer., vol. 71, no. 4, pp. 1351-1360, 1981). A detection bulletin is printed and the wave-forms containing the detected events, sampled at 40 sps, are transmitted to the VAX 11/750 computer for off-line analysis.

Since fall of 1982 we have been looking at events detected at the Lajitas site, particularly for near-regional

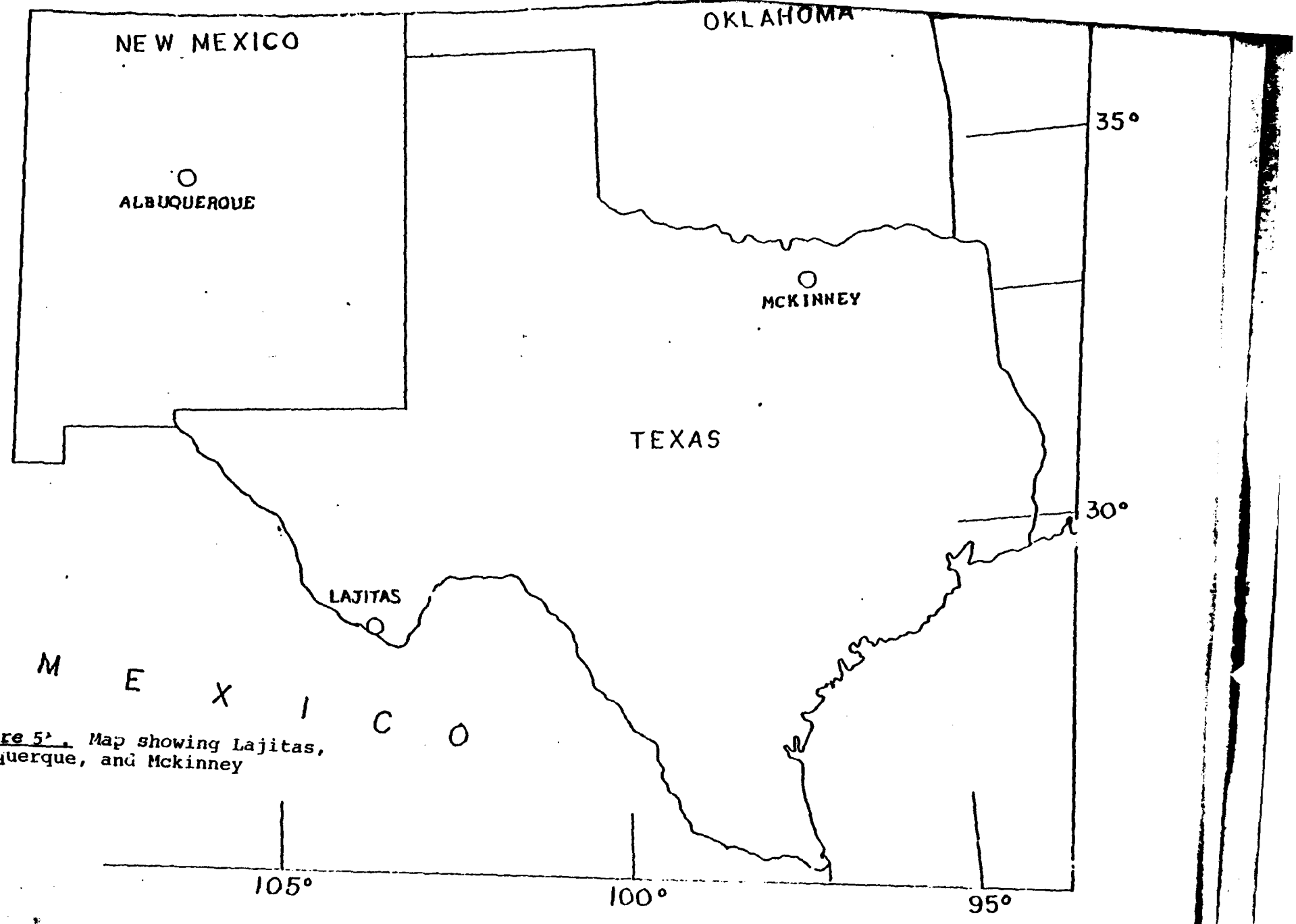


Figure 5. Map showing Lajitas, Albuquerque, and Mckinney

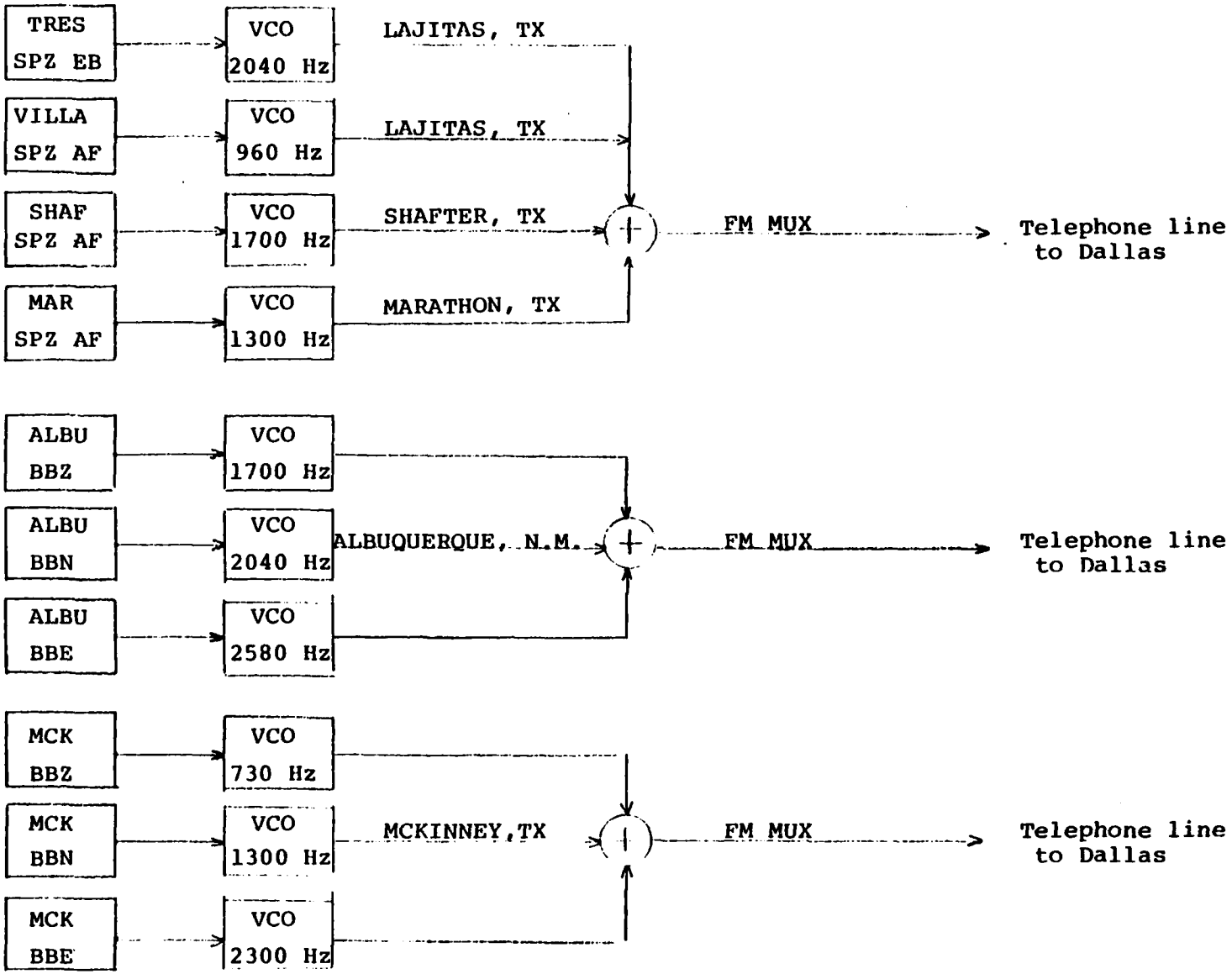


Figure 6 . Field data acquisition system

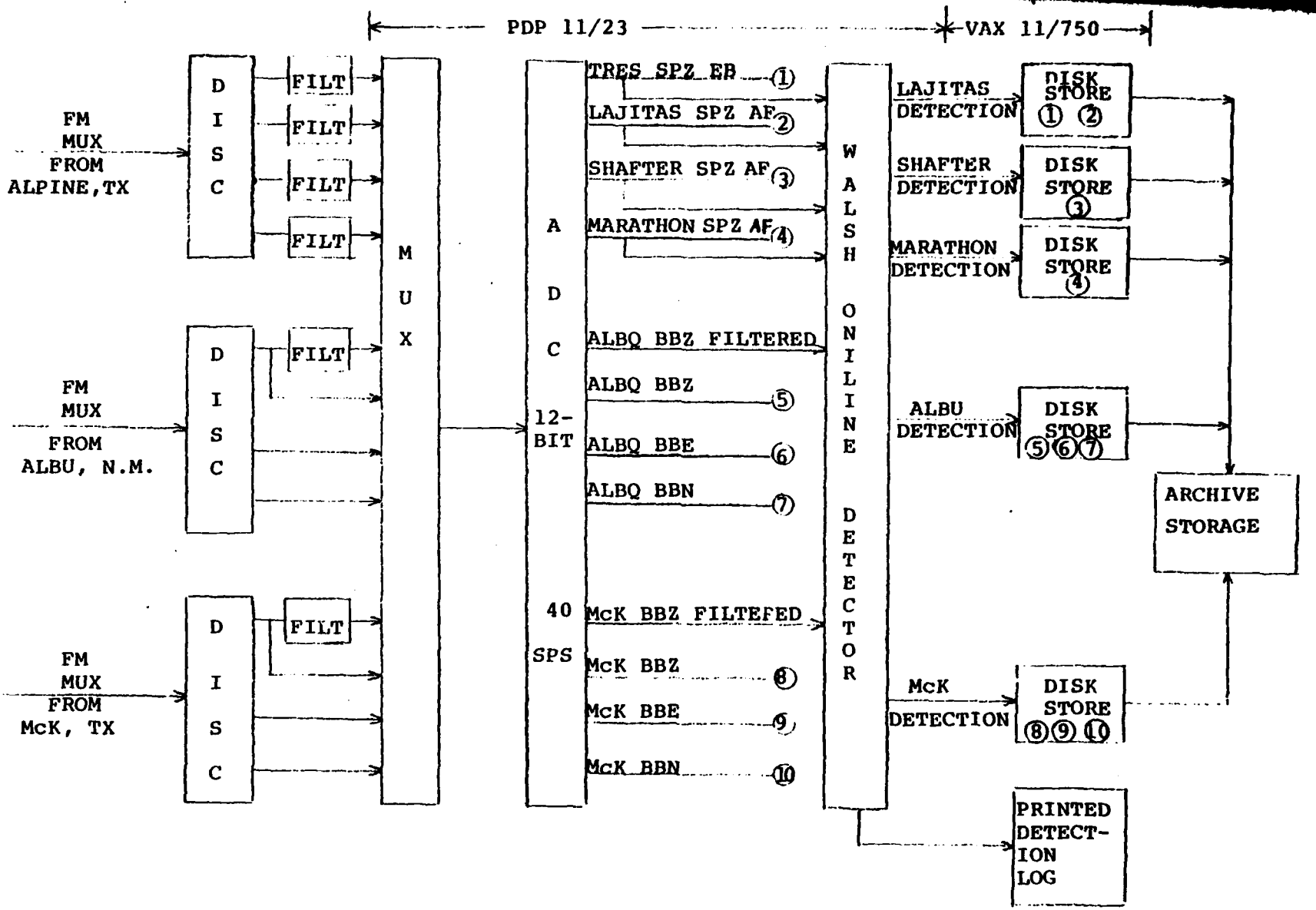


Figure 7 . Digital acquisition and detection system at SMU Geophysical Laboratory.

to regional distance. Analysis of teleseismic events will begin in the next contract period. Data for 20 regional events are shown in Table 2. Distances were estimated from single station data (Tres Cuevas site) based on Pn and Lg times (Pn velocity 8.0 km/sec, Lg velocity 3.5 km/sec., Pn intercept time 8 sec). The data was read from analog recordings, and corrections were made for instrument response based on visual estimation of the predominant period. Magnitudes were calculated using the following expressions:

For Pn: $Mb = -17.0 + \log \frac{A}{T} + 7 \log D$,

A in millimicrons (o-p) and distance (D) in km.

Based on Evernden's results (Bull. Seismol. Soc. Amer., vol. 57, n. 4, p. 611, Eqs. 7 and 8) for propagation of Pn from Nevada Test Site eastward through Texas.

For Lg: $Mb = -1.73 + 2.56 \log D + \log A$

with 200 km $\leq D \geq$ 800 km.

A is maximum sustained amplitude in microns (o-p).

Based on Mitchell and Nuttli's results for Lg in Northern Iran (Semi-Annual Tech. Report, 1 October 1977 - 31 March 1978, AFOSR - DARPA, St. Louis University).

As can be seen in Table 2, the estimated magnitudes based on Lg and Pn show surprising little scatter - the average value was taken as representative of the event. The signal to noise ratio was estimated for the Pn and Lg signals associated with each event. This ratio was normalized

LAJITAS - REGIONAL SIGNALS - TRES CUEVAS SITE

| (sec) T(Lg-P) | (km) Δ | (mm) P-P | Pn T | A (mμ) O-P | (mm) P-P | Lg T | A (mμ) O-P | Mpn | Mlg | $\bar{M}b$ | Pn S/N | Lg S/N |
|---|---|---|---|---|---|---|---|---|---|---|---|---|
| 46 | 336 | 5.0 | 0.5 | 1.5 | 6.0 | 0.5 | 1.8 | 2.3 | 2.0 | 2.2 | 7 | 8 |
| 44 | 323 | 3.5 | 0.25 | 0.5 | 6.0 | 0.3 | 1.2 | 2.0 | 1.8 | 1.9 | 10 | 15 |
| 90 | 610 | 2.0 | 0.5 | 0.6 | 5.0 | 0.7 | 2.2 | 2.8 | 2.7 | 2.8 | 3 | 8 |
| 36 | 211 | 6.0 | 0.3 | 1.2 | 7.0 | 0.5 | 2.1 | 1.7 | 1.5 | 1.6 | 15 | 10 |
| 87 | 591 | 1.0 | 0.6 | 0.4 | 4.0 | 0.8 | 3.6 | 2.4 | 2.9 | 2.6 | 2 | 10 |
| 85 | 578 | 4.0 | 0.4 | 1.0 | 6.0 | 0.6 | 2.4 | 3.1 | 2.7 | 2.9 | 8 | 10 |
| 44 | 323 | 2.5 | 0.3 | 0.5 | 7.0 | 0.5 | 2.1 | 2.0 | 2.0 | 2.0 | 6 | 10 |
| 85 | 578 | 5.0 | 0.5 | 1.5 | 11.0 | 0.6 | 4.4 | 3.2 | 3.0 | 3.1 | 7 | 18 |
| 85 | 578 | 2.0 | 0.4 | 0.5 | 5.0 | 0.5 | 1.5 | 2.7 | 2.5 | 2.6 | 4 | 7 |
| 94 | 634 | 1.0 | 0.6 | 0.4 | 7.0 | 0.5 | 1.4 | 2.5 | 2.6 | 2.6 | 2 | 6 |
| 28.5 | 227 | 5.0 | 0.3 | 1.0 | 12.0* | 0.4 | 3.0* | 1.8 | 1.8+ | 1.8 | 12 | 25 |
| 29 | 230 | 6.0 | 0.3 | 1.2 | 10.0 | 0.3 | 2.0 | 1.9 | 1.6 | 1.8 | 15 | 25 |
| 38 | 286 | 2.0 | 0.5 | 0.6 | 7.0 | 0.6 | 2.8 | 1.6 | 2.0 | 1.8 | 3 | 11 |
| 44 | 323 | 2.0 | 0.3 | 0.4 | 8.0 | 0.7 | 4.0 | 1.8 | 2.3 | 2.0 | 5 | 15 |
| 44 | 323 | 3.0 | 0.4 | 0.7 | 8.0 | 0.7 | 4.0 | 2.0 | 2.3 | 2.2 | 6 | 15 |
| 52 | 373 | 2.0 | 0.4 | 0.5 | 6.0 | 0.5 | 1.8 | 2.0 | 2.1 | 2.0 | 4 | 8 |
| 39 | 292 | 1.0 | 0.5 | 0.3 | 5.0 | 0.5 | 1.5 | 1.3 | 1.8 | 1.6 | 1.5 | 7 |
| 51 | 367 | 2.0 | 0.5 | 0.6 | 7.0 | 0.4 | 1.8 | 2.0 | 2.1 | 2.0 | 3 | 15 |
| 43 | 317 | 3.0 | 0.5 | 0.9 | 8.0 | 0.6 | 3.2 | 2.0 | 2.1 | 2.0 | 4 | 13 |
| 33 | 255 | 2.0 | 0.4 | 0.5 | 6.0 | 0.4 | 1.5 | 1.4 | 1.6 | 1.5 | 4 | 12 |

TABLE 2

*Slightly clipped

for an event of Mb 2.0. The S/N in dB were plotted against log distance to show two roughly linear trends, for Pn and Lg. These trends, all for Mb = 2, were as follows:

Lg: 35 dB at 200 km down to about 5 dB at 600 km

Pn: 28 dB at 200 km down to - 5 dB at 600 km

These results give a basis for determining the detection capability of a single seismometer at the Latjias site for Pn and Lg arrivals at regional distances. Inferences as to detection capabilities for magnitudes other than 2.0 can be made using simple scaling but only for the distance range 200 to 600 km.

Examples of two teleseismic events from the USSR are shown in Figures 8 and 9. It should be noted that the local (Lajitas) magnitude is about 0.3 units smaller than the NEIS mean magnitude. Whether this difference is real or a result of network bias in the NEIS data is not known at this time. Clearly one of the more important objectives of our on-going research program is to determine if an exceptionally quiet site like Lajitas also produces abnormally low teleseismic signal amplitudes. An answer to this question awaits the accumulation of data using the automated seismic analysis system now in development.

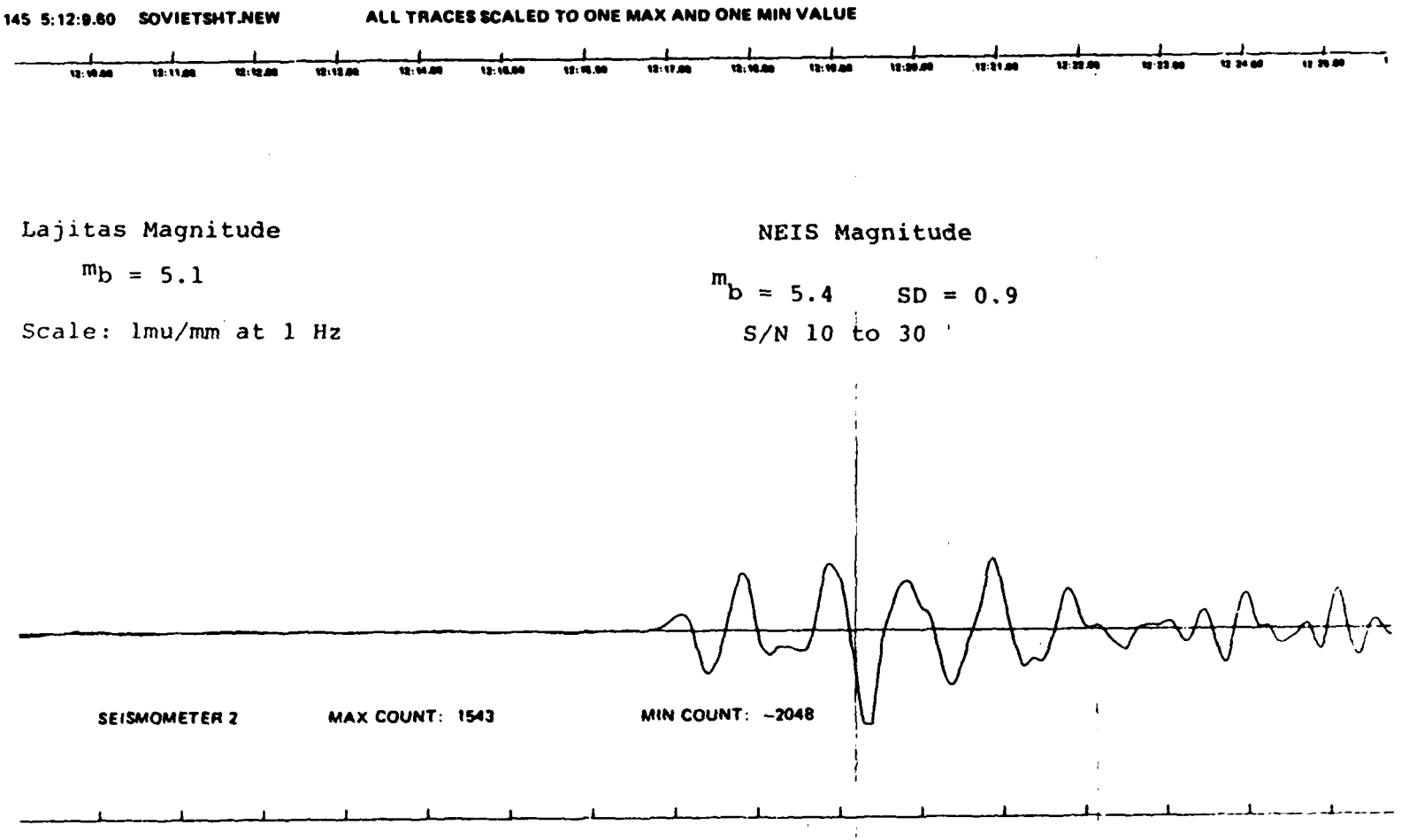


Figure 8. SEISMIC TRACES OF THE USSR NUCLEAR EXPLOSION ON MAY 25, 1981 AT SEISMOMETERS 2 AND 11. THE ORIGIN TIME IS 04:59:57.2 UTC AND THE LOCATION IS SOUTH OF NOVAYA ZEMLYA (68.182N, 053.689E) AT A DISTANCE OF 76°. THE BODY-WAVE MAGNITUDE IS 5.5.

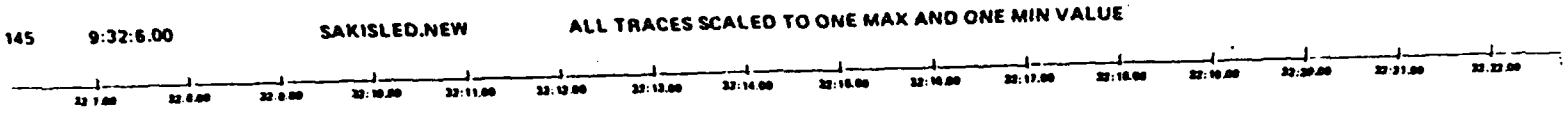


Lajitas Magnitude

$m_b$ = 4.7

Scale: 0.6 mu/mm at 1 Hz

NEIS Magnitude

$m_b$ =5.0 SD =0.9

S/N 5 to 8

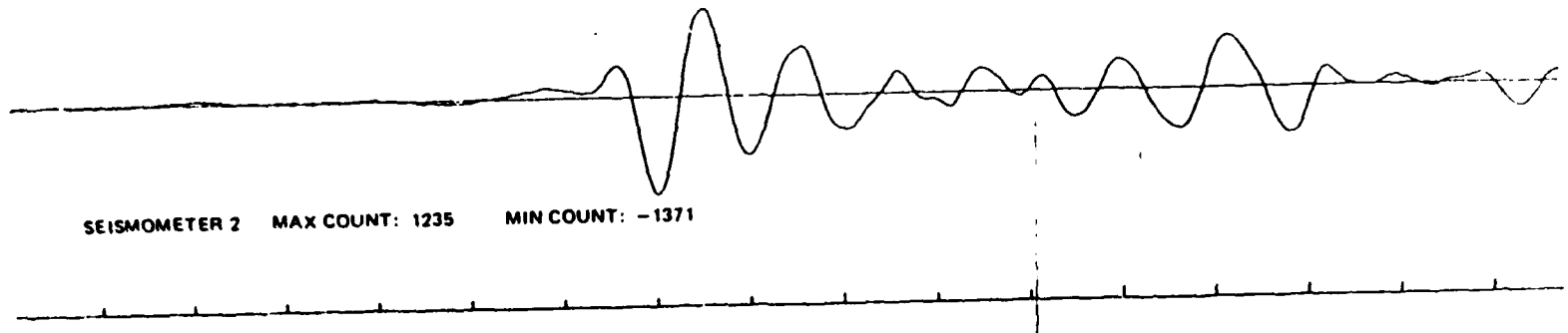


Figure 9. SEISMIC TRACES OF SAKHALIN ISLAND EARTHQUAKE ON MAY 25, 1981 AT SEISMOMETERS 2 AND 11. THE ORIGIN TIME IS 09:19:41.3 UTC. THE EPICENTER IS AT 46.16 N, 141.84 E, A DISTANCE OF 82°. THE DEPTH OF FOCUS IS 33 km AND THE BODY-WAVE MAGNITUDE IS 5.1.

# THE RESOLUTION OF SEISMIC INSTRUMENTS USED IN TREATY VERIFICATION RESEARCH

Eugene Herrin
November 1982

Department of Geological Scienc
Southern Methodist University
Dallas, Texas

## ABSTRACT

The resolution of the seismic sensors discussed in this paper is limited either by the self-noise of the system or the ambient ground noise at the observing site. The resolution limits of a particular system are frequency dependent. A major objective of the designer is to insure that seismic sensors are available which will be limited in resolution only by the ambient background noise at the quietest sites over the frequency band of interest in treaty verification research. This paper presents a review of the data currently available on the limiting resolution of the most advanced instruments used in this research program.

## INTRODUCTION

The seismometer-amplifier combinations discussed in this paper are the "state-of -the-art" systems now in use or in development for use in treaty verification research. Only systems which can be placed in bore-holes with casings of 7 inches or less in diameter fall into this category, because the bore-hole environment has been found to provide the optimum stability and lowest ambient background noise at any given site. All of these instruments are manufactured by Teledyne-Geotech (TG) in Garland, Texas, thus the Teledyne model numbers will be used throughout this paper in the discussions of the properties of the instruments. Systems currently in use are the TG 36000-01 in the Seismic Research Observatories (SRO), the TG 36000-04 and TG 750 in the National Seismic Systems (NSS) and the TG 36000-03 and TG 20171 (23900) used at installations operated by the Air Force Technical Applications Center (AFTAC). The TG 23900 is a version of the TG 20171 designed for operation in deep bore-holes, but the two are essentially the same instrument in so far as the discussions in this paper are concerned.

### Properties of The Instruments

The instrumental characteristics of most importance in treaty verification research can be seperated into four categories: Effective band-width, dynamic range, linearity

at about - 220 dBs as the frequency approaches 10 Hz. Is the apparent resolution limit at about - 220 dBs being set by the ambient ground motion or by the self-noise of the TG 36000-01?

In Figure 3 the noise spectral densities in dBs are shown for two of the quieter SRO's (ANMO in New Mexico and BCAO in the Central African Republic). The BCAO data was taken at night when the background noise at that station is at its lowest level. Note that both spectra fall sharply with increasing frequency through 1 Hz. The "bumps" in the ANMO spectrum at 2 to 3 Hz can be attributed to man-made noise from the nearby town of Albuquerque and from Kirtland Air Force Base. Beyond 4 Hz, however, the two curves approach a minimum value of -210 to -215 dBs. Data such as that shown in Figure 3 and a series of careful tests carried out by Sandia National Laboratory ( H. B. Durham, personal communications, 1982) indicate that the resolution of the TG 36000-01 is set by self-noise at an equivalent ambient noise level of -210 to -220 dBs.

This conclusion means that Peterson's composite noise model (Figure 2) does not represent ambient ground noise at frequencies above 4 Hz because of the limited resolution of the TG 36000. In order to measure the noise levels at sites quieter than -220 dBs, presumably at frequencies above 5 Hz, we must use an instrument with lower self-noise than the TG 36000.

measure of displacement power spectral density decibels relative to 1 $m^2/Hz$. which we call decibels-seismic (dBs).

The effective limit of resolution of seismometer-amplifier combinations can be set by (1) the maximum gain of the system, (2) the self-noise of the system, or (3) the ambient background displacement at the operating site. Clearly for best performance in treaty verificaiton research, the system resolution should be limited by the ambient background noise over the entire frequency band of the system. For the instruments discussed here, the maximum gain is great enough so that the resolution is always set by either the self-noise of the system or the ambient background noise.

## Seismic Background Noise

Peterson (1980) reported on a study of ambient background noise at 12 SRO sites (ANMO, ANTO, BCAO, BOCO, CHTO, GRFO, GUMO, MAIO, NWAO, SHIO, SNZO and TATO). An attempt was made to determine the minimum ambient noise at each site by selecting the "quietest" sample from the digital data available for the study. Using these "quiet samples", displacement power spectral densities in dBs were estimated for each site. The lowest spectral density for each period, as seen at any of the 12 sites, was then selected to form a composite minimum noise model for these sites well distributed over the earth. Figure 1 shows this composite spectral model plotted in dBs vs. period. The individual

points shown in this figure indicate the spectral estimates made by Fix (1972) using data recorded at the Queen Creek mine about 50 km. south of Pheonix, Arizona. Since the mid-1970's, the Queen Creek noise spectrum has been used as a low-noise model in designing seismometer-amplifier combinations. All of the spectral data shown in this paper are for vertical seismic sensors; no data from horizontal sensors are considered here. However, the conclusions reached here concerning the vertical component also apply to horizontal components of the TG 36000 and TG 750 systems. The TG 20171 has only the vertical sensor.

One conclusion which can be reached from Petersons'(1980) study and from Figure 1, is that for periods above 1 sec the resolution of the TG 36000-01 used in the SRO's is limited by the ambient seismic background noise at the site and not by the self-noise of the system. This conclusion also applies to the TG 36000-03 and the TG 36000-04 used in AFTAC and NSS installations respectively, again for periods above 1 sec.

At periods less than 1 sec (frequencies above 1 Hz) the results are less clear. Peterson's composite low-noise spectrum lies below the Queen Creek values as might be expected, because the composite spectrum was intended to represent a lower bound on ambient background noise. This spectral difference can be better seen in Figure 2 where the data from Figure 1 have been replotted as dBs vs. frequency in Hz. Note that both curves in Figure 2 tend to converge

and resolution. All three versions of the TG 36000 are relatively broad-band instruments designed to operate over a frequency band of 0.01 to 20 Hz. The TG 20171 and TG 750 are short-period systems currently being used with an effective band-width of about 0.5 to 40 Hz, although in some installations this band-width, for various reasons, is truncated by low-pass filters.

All of the systems discussed in this paper have demonstrable dynamic range in excess of 120 dB, although because of the configuration and over-all frequence response selected by the user, this dynamic range may not extend over the entire frequency band.

The linearity of systems with such a large dynamic range is very difficult to measure in the laboratory; however, lower bounds can be set. The systems discussed here all have linearity greater than 70 dB (about one part in three thousand).

The last category, resolution, is the primary subject of this paper. Here resolution is taken to be the smallest ground displacement that can be resolved by the instrument. Because resolution may vary with frequency we find that it can best be expressed in terms of displacement power spectral density. These densities are in terms of true ground motion; that is, system outputs must be corrected for the frequency-dependent displacement response of the seismometer-amplifier combination and any subsequent response shaping filters. Following Peterson (1980) we have elected to use as a standard

## A New Low Noise Model

About three years ago the author began a series of noise measurements at a very remote site in the Big Bend region of Texas. The site, located near the small village of Lajitas on the Rio Grande River, is at 29° 20' north latitude and 103° 40' west longitude. A system using the TG 20171 vertical seismometer and an extremely low-noise amplifier (Teledyne-Geotech 43310) was used to measure the ambient background noise levels at the Lajitas site. Figure 4 shows the displacement power spectrum for Lajitas background noise along with the Queen Creek spectrum. Above about 2 Hz the Lajitas spectrum lies about 10 dB below the Queen Creek values, very nearly overlying Peterson's composite low noise spectrum out to about 4 Hz. Beyond that point the Lajitas spectrum continues to drop and finally flattens at about -255 dBs just beyond 20 Hz, where we conclude that the self-noise of the TG 20171/43310 system begins to limit the resolution. The Lajitas noise spectrum is now being used as a low noise model from 0.5 to 20 Hz in the design of new seismometer-amplifier systems.

## Conclusion Regarding Seismometer Resolution

Figure 5 is a diagram prepared by O. D. Starkey (personal communication, 1982) showing the resolution limits of the systems discussed in this paper as set by the calculated self-noise of the seismometer-amplifier combinations. The

line marked "minimum background estimate" is the new low noise model based on the Lajitas noise measurements. The resolution limit for the SRO and AFTAC broad-band instruments (TG 36000-01 and 03) is close to -220 dBs which roughly corresponds to the lowest spectral measurements shown in Figures 2 and 3. The resolution limit for the TG 20171/43310 used to measure the Lajitas noise spectrum is about -255 dBs at 20 Hz. This limit is clearly indicated in the Lajitas noise spectrum shown in Figure 4. Resolution limits for the TG 36000-04 and TG 750 used in the NSS borehole system are also shown in dBs as a function of frequency. Clearly none of the existing systems are capable of resolving the Lajitas ambient background noise at frequencies above 20 Hz.

A new system being developed by Teledyne-Geotech for the Defense Advanced Research Projects Agency has the model number TG 44000. The predicted resolution limit for this system, as shown in Figure 5, is about -270 dBs for frequencies above 2 Hz. If the TG 44000 system now being tested meets the design-goals, it will be the only seismometer-amplifier system which can resolve the ambient ground motion at the quietest known sites over the frequency band from 0.01 Hz to beyond 20 Hz. In treaty verification research we are constantly searching for quieter sites at which to make seismic observations, and we therefore require higher resolution instruments for use at such sites. If ambient noise measurements are made using instruments with resolution limited by

their own self-noise, we can not determine that the ambient noise level is beneath that limit. On the other hand, if we do not have the measurements to indicate that a site is very quiet at certain frequencies, we may lack motivation for developing instruments with greater resolving power. In the verification research program, we are attempting to develop instruments with resolving power capable of operating at the quietest sites, with a resolution limited only by the ambient seismic noise level.

## REFERENCES

Fix, J.E. (1972) Ambient earth motion in the period range from 0.1 to 2560 sec, Bull. Seismol. Soc. Amer., 62, 1753-1760.

Peterson, Jon (1980) Preliminary observations of noise spectra at the SRO and ASRO stations, U.S. Geological Survery open-file Report 80, Albuquerque, New Mexico.

## ACKNOWLEDGEMENTS

The author wishes to thank Jim Durham, O.D. Starkey, John Ferguson, Todd Li and Gordon Sorrells for their contributions of unpublished materials and useful ideas which were incorporated in this review. Preparation of the review was supported by the Defense Research Projects Agency under contract AFOSR F49620-83-C-0021 monitored by the U.S. Air Force Office of Scientific Research.

## FIGURE CAPTIONS

Figure 1. Composite low-noise spectrum obtained by combining low noise points. The X's are for Queen Creek data published by Fix (1972) (After Peterson,1980)

Figure 2. Composite low noise from Figure 1 replotted vs. frequency (dots) and Queen Creek noise spectrum (x's). (After Peterson, 1980, and Fix, 1972)

Figure 3. Minimum noise spectra for the SRO's ANMO (dots) and BCAO (x's) (Modified from Peterson, 1980)

Figure 4. Spectra of Lajitas background noise (dots) and Queen Creek noise (x's).

Figure 5. Limiting displacement resolution of a number of systems based on the calculated self-noise levels (Calculations by O.D. Starkey, 1982).

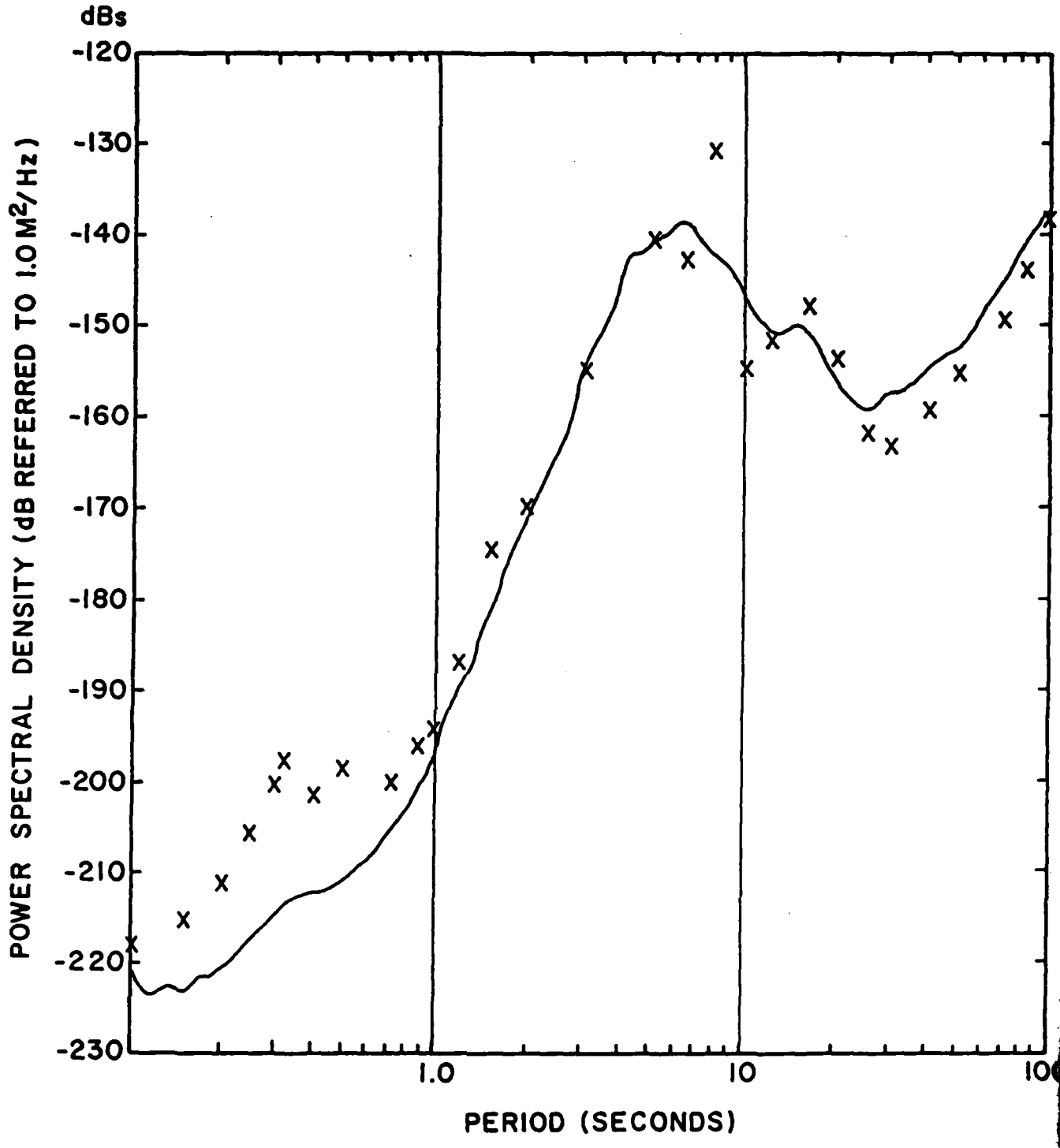
dBs
-120
-130
-140
-150
-160
-170
-180
-190
-200
-210
-220
-230
POWER SPECTRAL DENSITY (dB REFERRED TO 1.0 M²/Hz)
1.0
10
PERIOD (SECONDS)

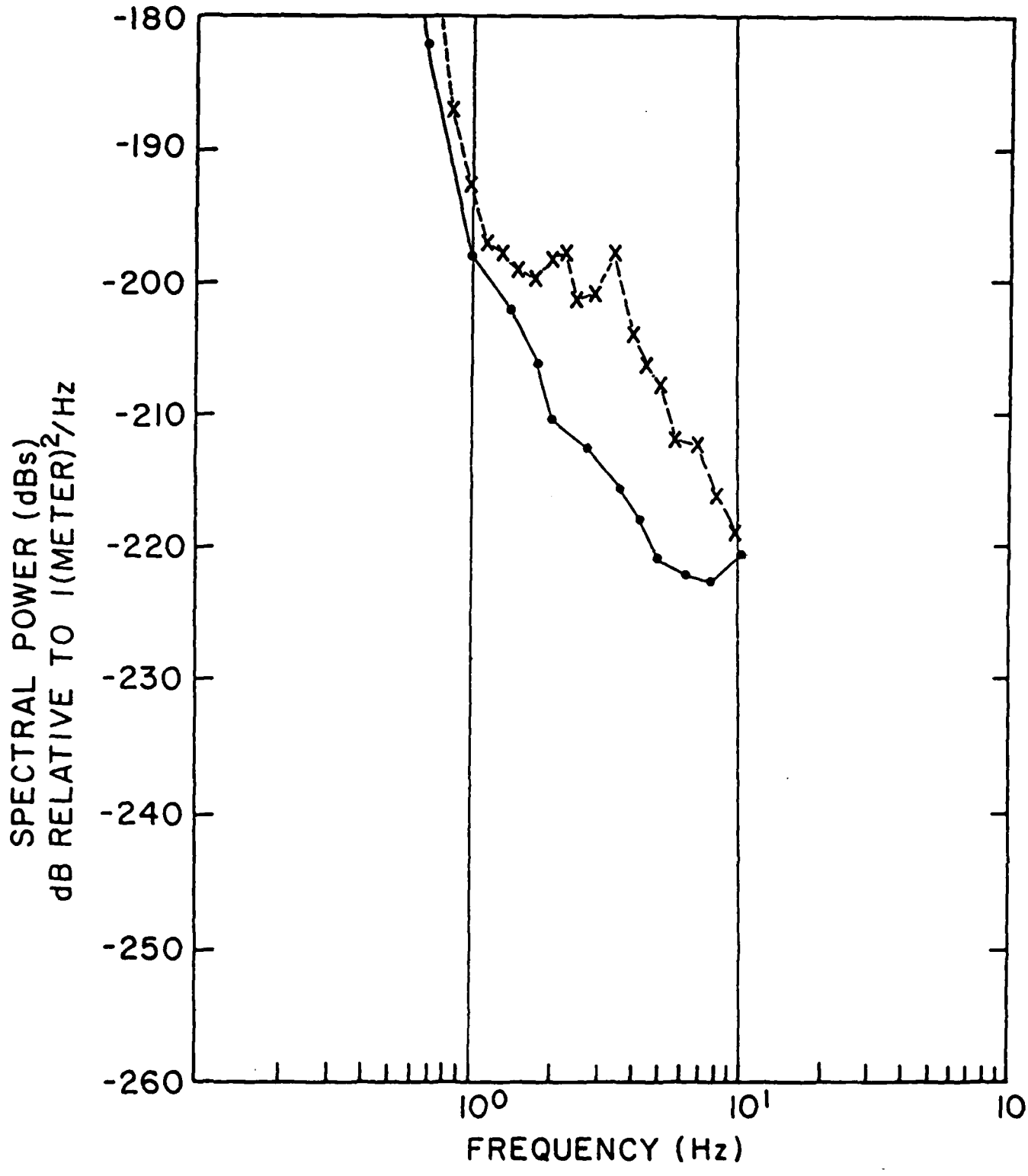
-180
-190
-200
-210
-220
-230
-240
-250
-260
SPECTRAL POWER (dBs)
dB RELATIVE TO 1(METER)²/Hz
10⁰
10¹
FREQUENCY (Hz)

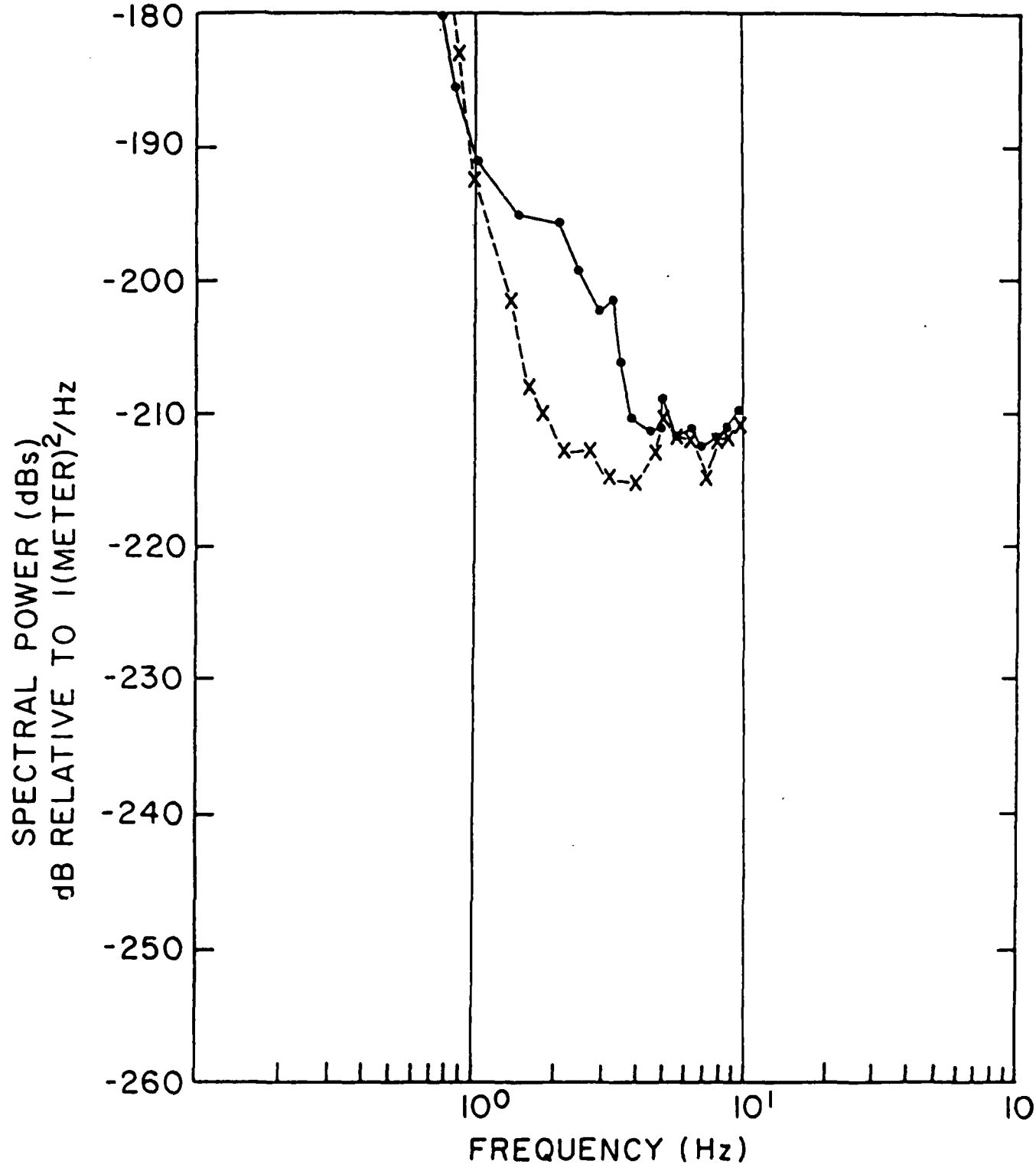
-180
-190
-200
-210
-220
-230
-240
-250
-260
SPECTRAL POWER (dBs)
dB RELATIVE TO 1(METER)²/Hz
10⁰
10¹
FREQUENCY (Hz)

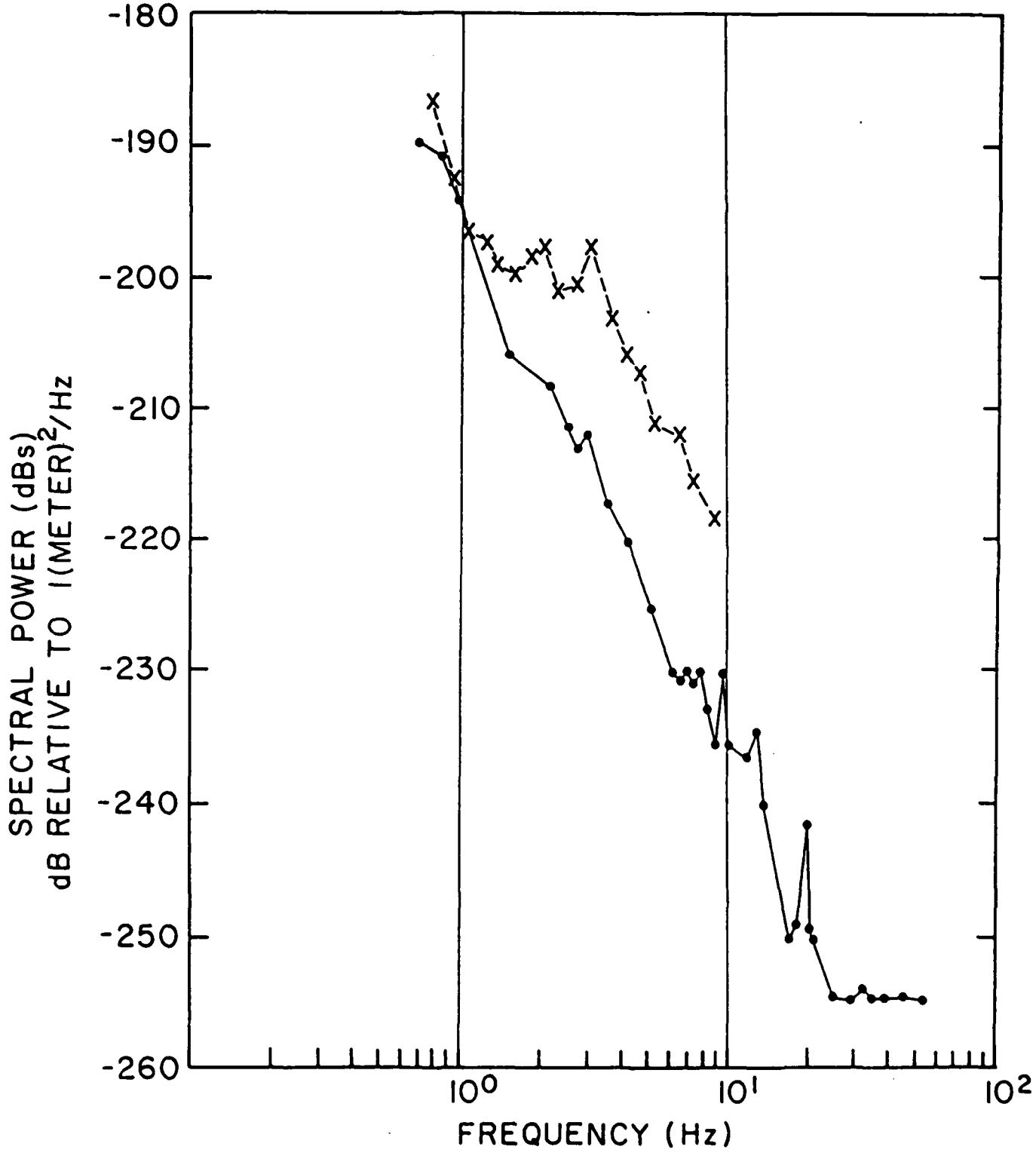
-180
-190
-200
-210
-220
-230
-240
-250
-260
SPECTRAL POWER (dBs)
dB RELATIVE TO 1(METER)$^2$/Hz
$10^0$
$10^1$
$10^2$
FREQUENCY (Hz)

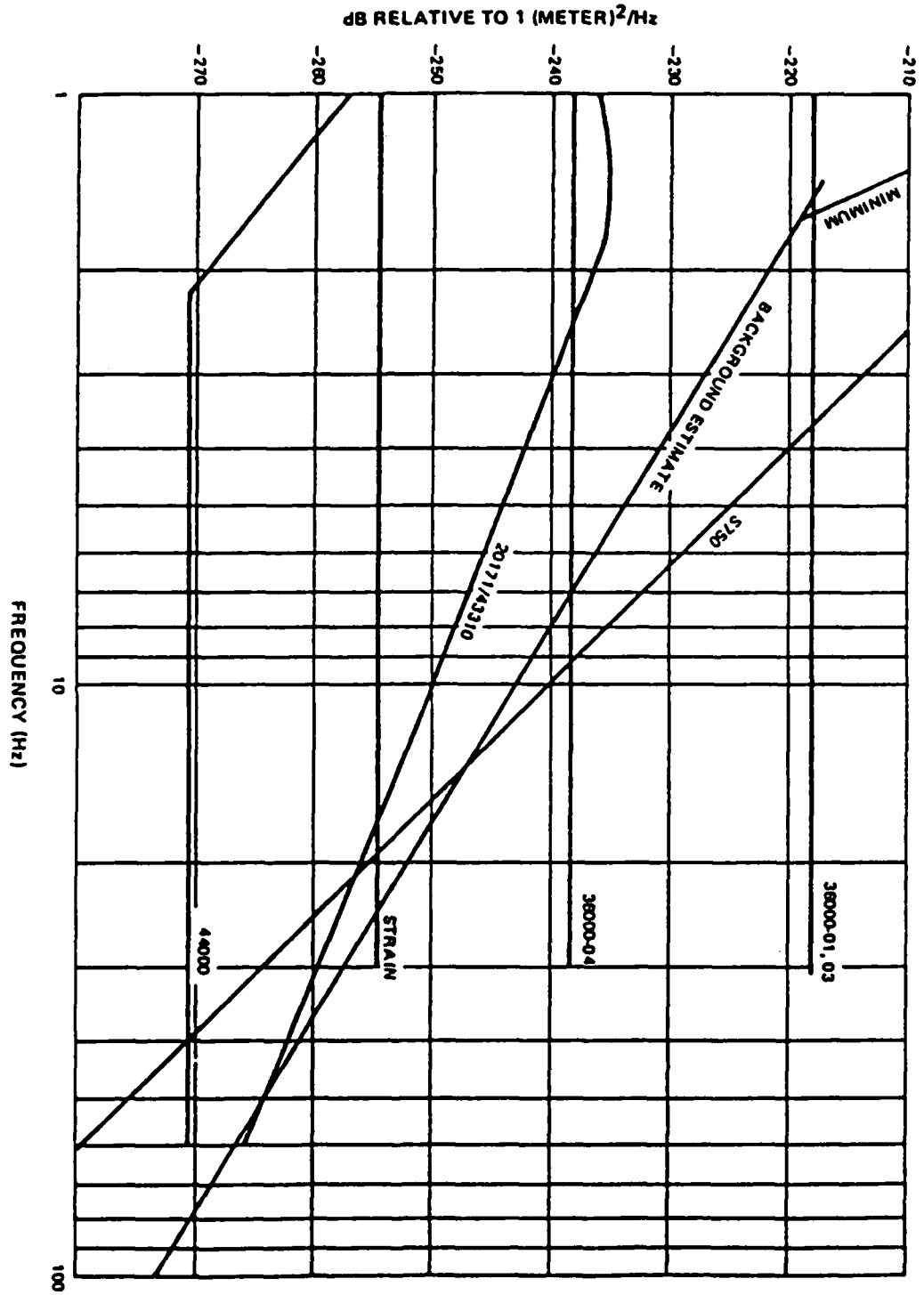
dB RELATIVE TO 1 (METER)$^2$/Hz
-270
-260
-250
-240
-230
-220
-210
1
10
100
FREQUENCY (Hz)
MINIMUM
BACKGROUND ESTIMATE
5750
2017/4331D
STRAIN
4400D
38000-04
38000-01, 03

# Anomalous Rayleigh Waves from Nuclear Explosions at the USSR Shagan River Test Site

by

Tom Goforth, Bijan Rafipour, and Eugene Herrin

## ABSTRACT

A study was made to determine if significant phase differences exist between Rayleigh waves which have traveled almost identical paths from the USSR Shagan River test site. Surface waves from five nuclear explosions recorded at six SRO/ASRO digital stations were used for the analysis. The explosion of 4 August 1979 was selected as a reference, and at each site the spectral phases of the Rayleigh waves from the other five events were compared to the phase of the reference. A technique of phase-matched filtering (Herrin and Goforth, 1979) was used to analyze the signals. This technique reduces the effects of multipathing and removes phase differences due to dispersion along slightly different travel paths.

Each epicenter has been re-located (North and Fitch, 1980) by using calibration data from the cratering shot of 15 January 1965, and remaining errors in location and origin time are considered to be extremely small. Seismograms were analyzed for surface waves recorded at Matsushiro, Japan (MAJO); Shillong, India (SHIO); Kabul, Afghanistan (KAAO); Ankara, Turkey (ANTO); Grafenburg, W. Germany (GRFO); and Alburquerque, N.M. (ANMO).

Results of the study indicate that Rayleigh waves from some Shagan River explosions have undergone large phase shifts relative to Rayleigh waves which have traveled almost identical paths from other Shagan River explosions.

In some cases, the phase shifts can be interpreted as complete phase reversals with associated time delay. In particular, as compared to the explosion of 4 August 1979, Rayleigh waves from the explosion of 7 July 1979 are reversed in polarity at KAAO and ANTO and are reversed in polarity and delayed at GRFO, SHIO, and MAJO.

TABLE OF CONTENTS

ments are made using

END

DATE
FILMED

7-83

DTIC